OVERTOPPING OF COASTAL STRUCTURES

CAUSED BY IRREGULAR WAVES

Stephen Luger, B.Sc (Eng) in Civil Engineering
University of Cape Town

A thesis submitted in partial fulfilment of the requirements for the degree of Master of Science in Engineering

Department of Civil Engineering
University of Cape Town

January 1991

DECLARATION OF CANDIDATE

I, Stephen Luger, hereby declare that this thesis is my own work and that it has not been submitted for a degree to another university.

Signature removed
Stephen Luger
January 1991

SYNOPSIS

This thesis is an experimental investigation into the average rate of overtopping caused by irregular waves. A literature review is given which describes the previous research done in the field of overtopping. This research included a number of model studies using both regular and irregular waves. The literature review emphasises the dimensionless parameters which were developed by the various researchers in order to present their experimental results.

The overtopping experiments were conducted in a 30 m long, 0,75 m wide and 1,0 m deep wave flume equipped with an irregular wave generator. The flume was divided by two walls into three channels and the model structure was placed in the centre channel while the two side channels were used to measure the incident wave conditions. Irregular waves with a Jonswap spectrum were generated and the water which overtopped the model structure was collected in a calibrated tank located behind the structure. A wide range of wave conditions including waves which broke offshore of the structure, at the structure and beyond the structure were tested. The model structures tested were a 100 mm high vertical wall, a 200 mm high vertical wall and a 100 mm high wall with the seaward face inclined at 45°.

It was found that the mechanism of overtopping was different for unbroken and broken waves. In order to model the kinematics of the water particles involved in the overtopping process, the concept of the total energy level or total head associated with the incoming waves was introduced. The total head is defined as

$$H_{tot} = H_{si} + H_{vel}$$

where $H_{vel} = \frac{v^2}{2g}$ is a velocity head associated with the velocity of the water particles in the waves. Expressions were developed for calculating the velocity head for both unbroken and broken waves.

Two dimensionless parameters involving the total head expression, namely $Q/\sqrt{g\ H_{tot}^{3}}$ and F/H_{tot}, were found to consolidate the overtopping data for a particular structure geometry into a single trend. The relation between these two parameters was found to be approximately exponential and equations were fitted to the experimental data for both the structure geometries tested. These equations can be used to predict the rate of overtopping when vertical walls or walls with a 45° slope are subjected to a wide range of wave conditions.

ACKNOWLEDGEMENTS

The author wishes to thank the following :

Professor F.A. Kilner, Head of the Department of Civil Engineering, University of Cape Town, thesis supervisor, for his guidance and expertise.

Mr J. Zwamborn, Programme Manager, Maritime and Hydraulic Structures, EMATEK, CSIR, for the use of the facilities at EMATEK as well as for the technical and financial support provided by EMATEK for the model tests.

The Foundation for Research Development for the award of a post-graduate bursary.

Mr A. van Tonder, EMATEK, CSIR, for his expertise and guidance with the model tests.

Mr F. van Dulm, EMATEK, CSIR, for his valuable assistance with the model tests.

Messrs G. Klix and I. Denyssen, EMATEK, CSIR, for assistance given in constructing the experimental apparatus.

Messrs D. Lackay and R. Gordon, EMATEK, CSIR, for assisting with the model tests.

Mrs P. Jordaan for the efficient typing of this thesis.

TABLE OF CONTENTS

LIST OF FIGURES

LIST OF TABLES

LIST OF PHOTOGRAPHIC PLATES

NOMENCLATURE

Symbol	Description	Dimension
a,b	regression coefficients	-
c, c_1, c_2	empirical coefficients in the velocity head equations	-
C	wave celerity	$L\ T^{-1}$
d	water depth	L
d_b	breaker depth	L
d_s	water depth at structure toe	L
EL	energy level	L
f	frequency	T^{-1}
f_p	spectral peak frequency	T^{-1}
F	freeboard	L
F′	Ahrens' freeboard parameter	-
F_*	Owen's freeboard parameter	-
g	gravitational constant	$L\ T^{-2}$
h_c	height of structure	L
H	regular wave height	L
$\bar{H}$	average wave height	L
H_b	wave height at breaking	L
H_k	characteristic wave height	L
H_s	significant wave height (energy-based)	L
H_{m_0}	significant wave height (energy-based)	L
$H_{1/3}$	significant wave height (statistically-based)	L
H_{tot}	total head	L
H_{vel}	velocity head	L
L	regular wavelength	L
L_p	wavelength based on spectral peak wave period	L
$\bar{L}$	wavelength based on average wave period	L

m_0	area under spectral curve	L^2
p	pressure	$M\ L^{-1}\ T^{-2}$
Q	overtopping rate per unit crest length	$L^3\ T^{-1}\ L^{-1}$
Q_p	spectral peakedness factor	-
R	runup height	L
S	spectral density	$L^2\ T$
SWL	still water level	-
T	regular wave period	T
$\bar{T}$	average wave period	T
T_{gen}	wave period programmed into wave generator	T
T_k	characteristic wave period	T
T_p	spectral peak period	T
$T_{1/3}$	significant wave period	T
v	water particle velocity	$L\ T^{-1}$
w	specific weight of water	$M\ L^{-2}\ T^{-2}$
y	vertical distance above SWL	L
z	elevation above a horizontal datum	L

Greek symbols

θ	structure slope	-
λ	length scale (model dimension : prototype dimension)	-
ϕ	phase angle	-
σ	standard deviation of water surface	L
γ	spectral peak enhancement factor	-
δ	spectral broadness factor	-
ν	kinematic viscosity of water	$L^2\ T^{-1}$

Subscript	Description
i	denotes inshore at the structure toe
o	denotes deep water
t	denotes transitional water
sep	denotes incident wave separated from reflected wave

CHAPTER 1

INTRODUCTION

When waves reach a coastal structure the water rushes up and sometimes over the structure. The discharge of water over the crest of the structure is referred to as the overtopping rate. The instantaneous overtopping rate varies constantly due to the irregular nature of the incident waves and the average overtopping rate which occurs over a number of waves is therefore considered.

The average overtopping rate is an important design parameter for seawalls, breakwaters and tidal pools. Since it is not economically feasible to construct a seawall or breakwater high enough to prevent overtopping completely, the overtopping rate which can be expected for various crest heights and wave conditions is required. The crest of a tidal pool wall should be high enough to provide safe swimming conditions in the pool, but must also be designed to ensure that an adequate volume of fresh water overtops the wall. Plate 1.1 shows overtopping occurring at the St James tidal pool in False Bay.

Although a number of model studies have been conducted to estimate overtopping rates, most of these have been concerned with a particular prototype problem and a general understanding of the overtopping process has therefore not been developed. The objectives of this thesis are therefore :

(a) To review the available literature in the field of overtopping.

(b) To conduct a series of model tests to measure the rate of overtopping which occurs when typical coastal structures are subjected to a wide range of realistic sea states.

(c) To analyse the results obtained in order to develop an understanding of the overtopping process and then to present the results in a form which can be used for the preliminary design of coastal structures.

The thesis begins with some background theory and then reviews the literature published in the field of overtopping. The experimental apparatus and the procedure followed during the tests are then described. The results obtained from the experiments are presented and the analysis of these results leads to a method which can be used to predict overtopping rates.

Plate 1.1 : Overtopping at St James tidal pool

CHAPTER 2

RELEVANT THEORY

2.1 Modelling Laws

The fundamental condition to be satisfied in a model test is that the model must behave in a manner similar to the prototype. Similitude of the model to the prototype is required in the three general categories of geometric shape, kinematics of the various motions, and dynamic forces acting in the model and the prototype. Inertia and gravity are the dominant forces when modelling the process of wave overtopping and overtopping is therefore scaled according to Froude similarity. Froude similarity dictates that the model measurements be scaled as follows :

Measurement	Units	Scale
Dimensions of model	L	λ
Water depth, wavelength, wave height	L	λ
Time, wave period	T	$\lambda^{1/2}$
Overtopping rate per unit crest length	$L^3\ T^{-1}\ L^{-1}$	$\lambda^{3/2}$

2.2 Regular waves

Regular or monochromatic waves refer to a wave train in which each successive wave has the same shape. A regular wave can be described by its length L (the horizontal distance between corresponding points on two successive waves), height H (the vertical distance between the wave crest and the preceding trough), period T (the time for two successive crests to pass a given point) and depth d (the distance from the bed to the stillwater level).

The most elementary theory for describing water waves is referred to as the linear or Airy wave theory. Although this theory is applicable only to 'small' waves (see Figure 2.1), the equations describing the wave characteristics are easy to apply in comparison to other wave theories. For this reason the linear wave theory has been widely used and a brief description of the linear theory which will be used in this thesis is given below. A more complete description of linear wave theory is given in the Shore Protection Manual [1]. (Note: numbers enclosed in square brackets identify the appropriate entry in the List of References.)

The speed at which the wave form propagates is called the wave celerity C and is given by

$$C = \frac{L}{T} \tag{2.1}$$

The wave celerity is linked to the wavelength, wave period and water depth by the following expression

$$C = \frac{g\,T}{2\pi} \tanh\left[\frac{2\pi d}{L}\right] \tag{2.2}$$

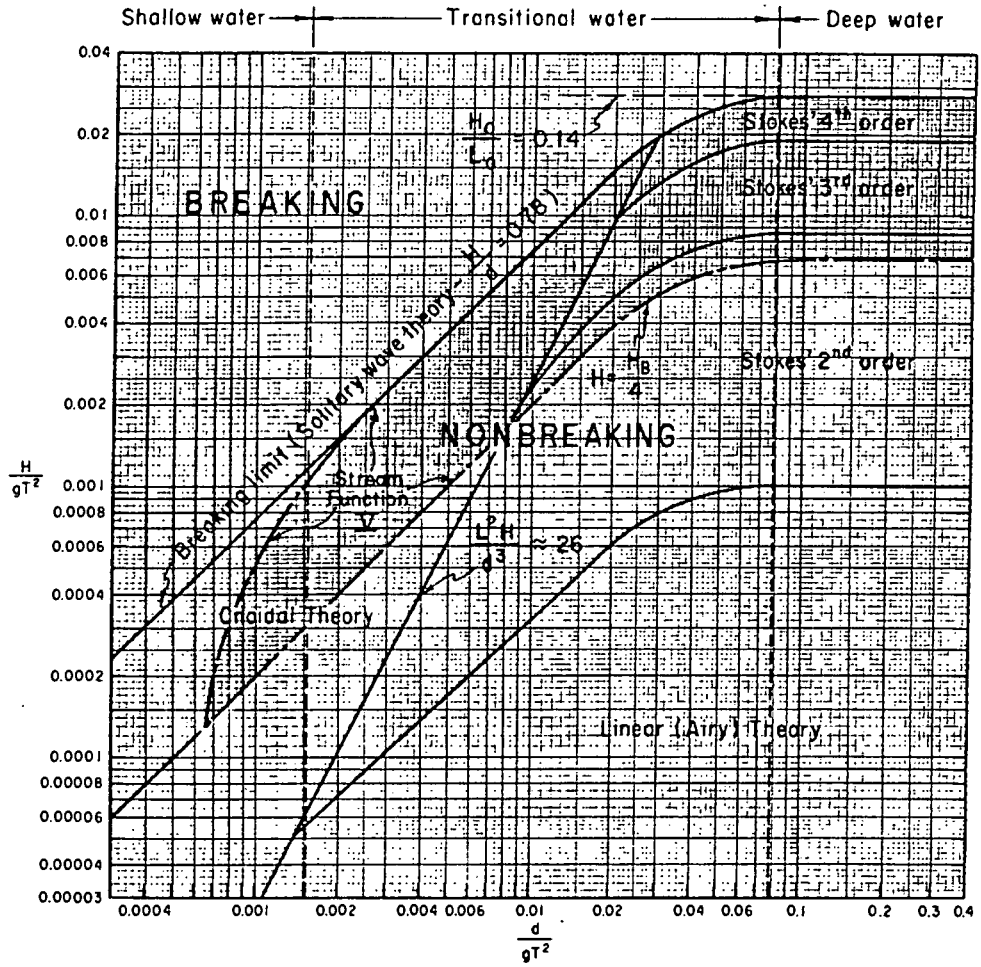

Figure 2.1 : Regions of validity for various wave theories [1]

From eqns. (2.1) and (2.2) the wavelength as a function of the wave period and water depth is given by

$$L = \frac{g\,T^2}{2\pi}\ \tanh\left[\frac{2\pi d}{L}\right] \qquad (2.3)$$

Eqn. (2.3) cannot be solved directly since L appears on both sides of the equation but it can be solved on a computer using an iterative scheme such as Newton's method.

Gravity waves can be classified by the water depth in which they travel as follows:

Deep water	: $d/L > 0{,}5$
Transitional water	: $0{,}04 < d/L < 0{,}5$
Shallow water	: $d/L < 0{,}04$

In deep water tanh $(2\pi d/L)$ approaches unity and the deepwater wavelength is obtained from eqn. (2.3) as

$$L_o = \frac{g\,T^2}{2\pi} \tag{2.4}$$

In shallow water tanh $(2\pi d/L)$ approaches $2\pi d/L$ and the wave celerity in shallow water is obtained from eqn. (2.2) as

$$C = \sqrt{gd} \tag{2.5}$$

If it is assumed that the wave energy flux per unit crest width is conserved as a wave moves from deep water into shoaling water, the relation between the wave height in any depth of water and the wave height in deep water can be shown to be

$$\frac{H}{H_o} = \left[\left[1 + \frac{4\pi d/L}{\sinh\,(4\pi d/L)} \right] \tanh\,\frac{2\pi d}{L} \right]^{-\frac{1}{2}} \tag{2.6}$$

2.3 Irregular waves

Waves in the ocean do not have constant heights and periods and are therefore termed irregular waves. Irregular waves can be represented either by statistical parameters or, more recently, by energy spectra.

2.3.1 Statistically-based wave parameters

Statistically-based wave parameters are obtained from an irregular wave record by either the zero-upcrossing or zero-downcrossing methods. These methods are statistically equivalent and the zero-downcrossing method is described below and illustrated in Figure 2.2.

First, the mean water level is deduced from the wave record and defined as the zero line. Next, the point where the water surface crosses the zero line downwards is found and this point is taken as the start of an individual wave. The next zero-downcrossing point after the surface profile has gone above the zero line is then found and this point defines the end of the wave and the start of the next wave. The distance between two adjacent zero-downcrossing points defines the wave period and the vertical distance between the highest and lowest points between the two zero-downcrossing points defines the wave height.

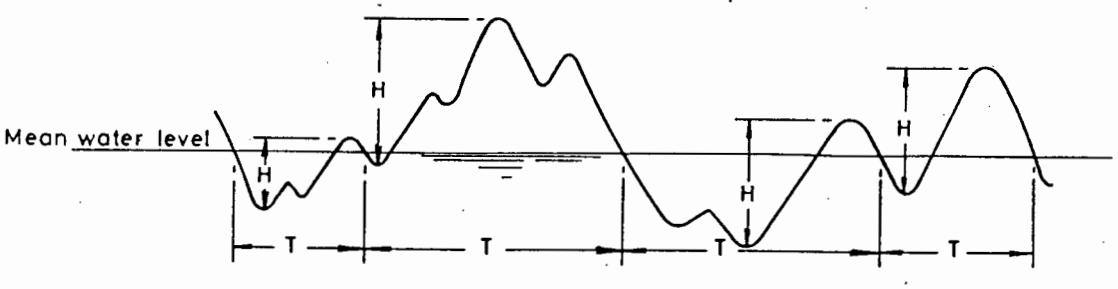

Figure 2.2 : Zero-downcrossing analysis

The wave heights and periods obtained from a zero-downcrossing analysis of a wave record can be used to calculate the following wave parameters :

$H_{1/3}$	The significant wave height calculated as the average wave height of the one-third highest waves in the record.
$T_{1/3}$	The significant wave period calculated as the average wave period of the one-third highest waves in the record.
$\bar{H}$	The average wave height of the waves in the record.
$\bar{T}$	The average wave period of the waves in the record.
H_{max}	The highest wave height in the record.
T_{max}	The period of the highest wave.

The distribution of wave heights obtained from a zero-downcrossing analysis is closely approximated by the Rayleigh distribution in the following form (Goda [2])

$$P(H/\bar{H}) = \exp\left[-\frac{\pi}{4}(H/\bar{H})^2\right] \tag{2.7}$$

where $P(H/\bar{H})$ is the probability that a particular wave height exceeds the prescribed value of $H/\bar{H}$.

2.3.2 Energy spectra of waves

Ocean waves can be described by a sum of sinusoidal terms

$$\eta(t) = \sum_{i=1}^{n} a_i \cos(\omega_i t - \phi_i) \tag{2.8}$$

where

$\eta(t)$ = departure of the water surface from its average position

a_i = the amplitude

ω_i = the frequency

ϕ_i = the phase at the time t = 0

The variation of a_i^2 with frequency can be used to estimate the distribution of wave energy as a function of frequency. This distribution is called the energy spectrum.

Various wave height and period parameters can be estimated from the energy spectrum. These parameters are described below :

The energy-based significant wave height is given by

$$H_{m_0} = 4\sqrt{m_0} \qquad (2.9)$$

where m_0 = area under the spectral curve

An equivalent energy-based significant wave height is given by

$$H_s = 4\sigma \qquad (2.10)$$

where σ = standard deviation of sea surface elevations

H_s and H_{m_0} are equivalent since σ and $\sqrt{m_0}$ are theoretically identical. The distinction between them is due to the different methods used to calculate them. With regard to the relation between the energy-based significant wave heights (H_s and H_{m_0}) and the statistically-based significant wave height ($H_{1/3}$), Thompson [3] found that although they are almost equal in deep water, $H_{1/3}$ can exceed H_s and H_{m_0} by 40 % in shallow water. The energy-based wave heights will be used in this thesis.

With regard to wave period, the main information obtainable from a wave spectrum is the peak period, defined as

$$T_p = \frac{1}{f_p} \tag{2.11}$$

where f_p = the frequency at which the spectral density is a maximum

Various shapes of energy spectra have been proposed based on the analysis of measured wave records. Based on the wave data available in 1964, Pierson and Moskowitz [4] proposed a spectrum for a fully developed sea state of the type

$$S(f) = \alpha\, g^2\, (2\pi)^{-4}\, f^{-5}\, \exp\left[-\frac{5}{4} \left[\frac{f}{f_p}\right]^{-4} \right] \tag{2.12}$$

where

$S(f)$ = spectral density (m^2/Hz)
α = Phillips' constant
f = wave frequency (Hz)
f_p = peak wave frequency (Hz)

More recently, Hasselmann et al [4] arrived at another spectral formulation for fetch-limited, wave-growth conditions during the first Joint North Sea Wave Project (Jonswap). This spectrum was shown to be more sharply peaked than the corresponding Pierson-Moskowitz spectrum. The spectrum obtained is denoted the Jonswap spectrum and is given by

$$S(f) = \alpha\, g^2\, (2\pi)^{-4}\, f^{-5} \exp\left[-\frac{5}{4}\left[\frac{f}{f_p}\right]^{-4}\right] \gamma^{\exp\left[\frac{-(f-f_p)^2}{2\,\delta^2\, f_p^2}\right]} \qquad (2.13)$$

where

γ = peak enhancement factor

δ = broadness of the spectral peak

= δ_a for $f < f_p$

= δ_b for $f > f_p$

The peak enhancement factor was found to have values up to 7 with an average of 3,3. The shape of a typical Jonswap spectrum can be seen in Figure 4.3.

CHAPTER 3

REVIEW OF PRIOR OVERTOPPING STUDIES

3.1 Introduction

This chapter reviews the research in the field of wave overtopping between 1953 and 1989. Research on overtopping derived mainly from the United States, Japan and the Netherlands, although work from Denmark and the United Kingdom is also described. Research originating from Japan has been concerned with overtopping of steep and often vertical walls, while the research in Europe has been concerned with structures having slope gradients of between 1:1 and 1:8. The American research has involved a wide range of structures. The most important parameters used to describe the overtopping process are illustrated in Figure 3.1.

The research is dealt with in chronological order so that the historical development can be traced. The earlier model studies were performed using regular or wind-generated waves and it was not until the introduction of computer-controlled wave generators and data acquisition systems in the 1970's that realistic sea states could be generated in the laboratory.

3.2 Experimental work by Saville & Caldwell (1953) [5], Saville (1955) [6]

A series of overtopping experiments were performed by the Beach Erosion Board (currently the Coastal Engineering Research Centre) in the early 1950's. The experiments were conducted in three different wave flumes all equipped with regular wave generators. A variety of wall configurations all fronted by 1:10 foreshore slopes were tested. Details of the flume dimensions, structures tested and the wave conditions used are given in Table 3.1.

WAVE OVERTOPPING DEFINITION SKETCH

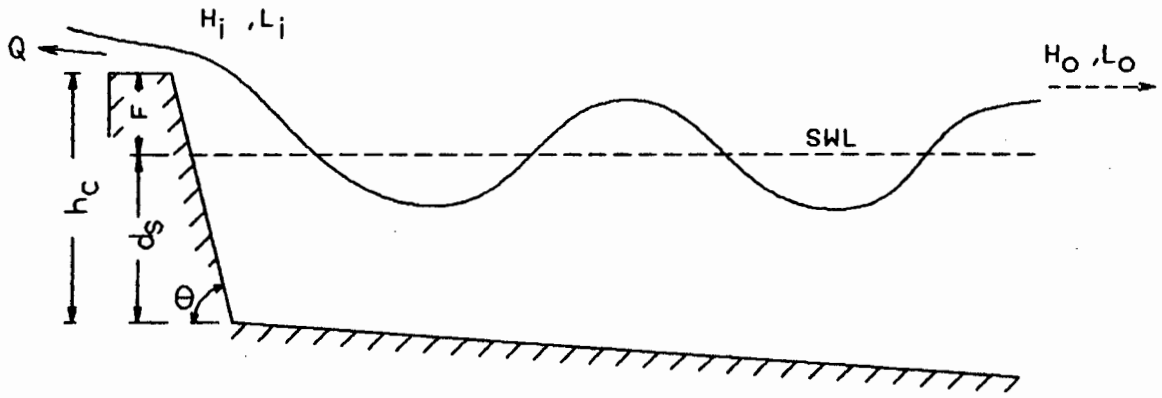

KEY

Q = overtopping rate per unit crest length ($m^3/s/m$)
d_s = water depth at structure toe (m)
h_c = height of structure (m)
F = freeboard (m)
θ = structure slope
H_i = wave height at structure toe (m)
L_i = wavelength at structure toe (m)
H_o = deepwater wave height (m)
L_o = deepwater wavelength (m)

Figure 3.1

Structures Investigated	Flume Dimensions	Type of Generator	Range of Wave Heights (Model Values)	Range of Wave Periods (Model Values)
1 on 3 smooth slope 1 on 6 smooth slope Composite slope Slope with berm	21.3 m long At generator 1.22 m wide 0.88 m deep At test section 0.30 m wide 0.49 m deep	Flap type	4.05 to 12.2 cm	0.822 to 1.28 sec
Smooth vertical wall 1 on 1-1/2 smooth slope 1 on 3 smooth slope 1 on 1-1/2 stepped slope 1 on 1-1/2 riprap faced slope Curved wall Recurved wall	36.6 m long 1.52 m wide 1.52 m deep	Plunger type	5.36 to 21.5 cm	0.717 to 3.64 sec
1 on 3 smooth slope 1 on 6 smooth slope	193.5 m long 4.57 m wide 6.10 m deep	Bulkhead type	48.8 to 140.2 cm	0.386 to 10.12 sec

Table 3.1 : Conditions tested by Saville

The volume of water overtopping the structures was collected in a calibrated container located behind the structure. Measurements were stopped before reflected waves from the structure could reach the wave generator and return to the structure. The wave height was measured in the deep section of the flume and the linear shoaling equation was used to calculate the deepwater wave height. The rates of overtopping measured were presented in both tabular and graphic form. The graphs are of the form shown in Figure 3.2

Although little analysis of the results was presented, this set of overtopping measurements is one of the few which have been published and forms the empirical basis for a number of subsequent studies. The tests involved regular waves only.

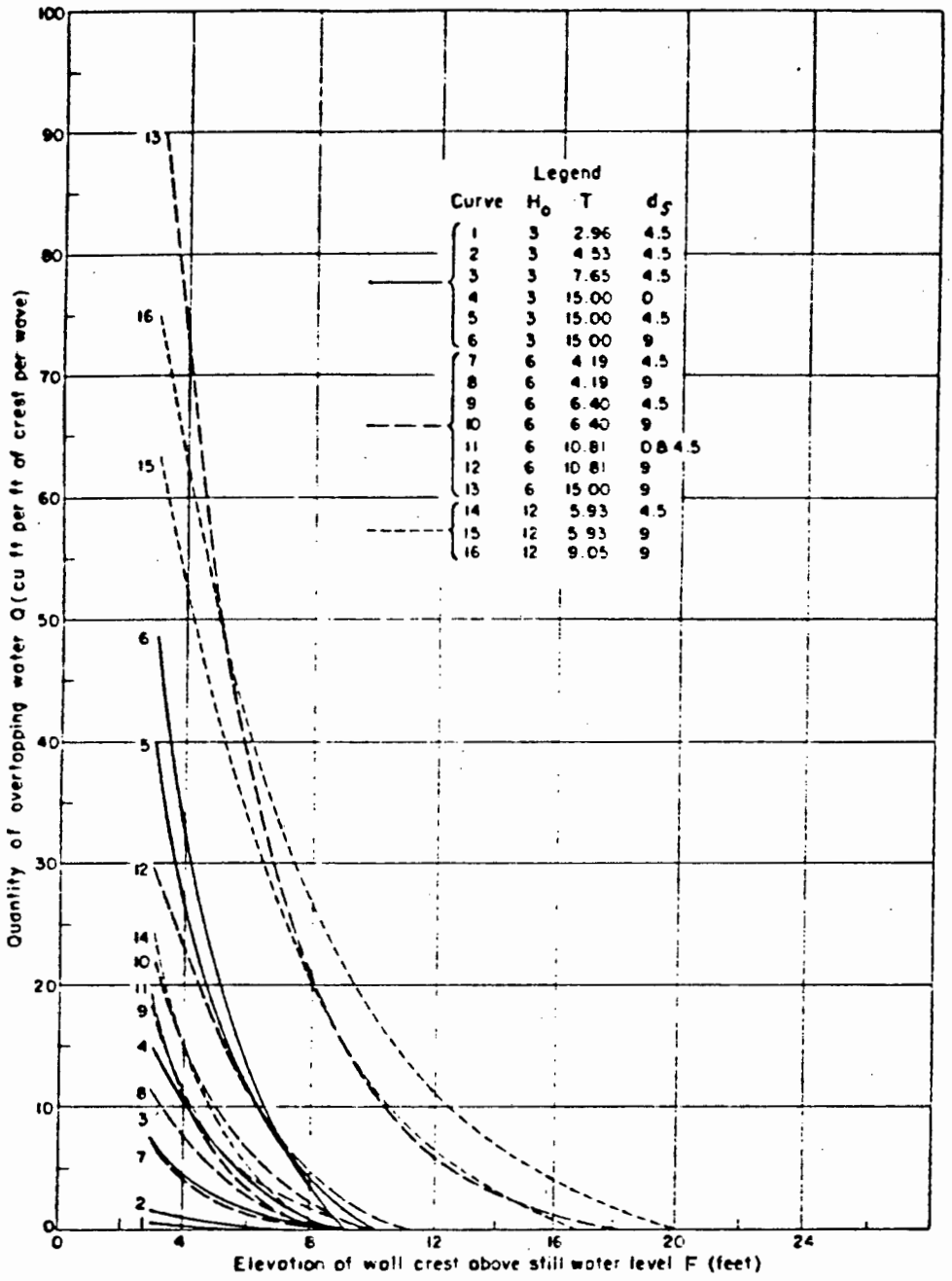

Figure 3.2 : Example of Saville's results for a vertical wall. (Note that the results are presented as prototype equivalents as though the model scale were 1:17)

3.3 Work by Ishihara et al (1960) [7]

An analysis of overtopping results obtained from regular wave tests is presented. The data was obtained from a series of overtopping tests performed by Ishihara and from the results published by Saville. Of importance is the choice of the dimensionless overtopping parameter used in the presentation of the results.

The parameter used is the ratio of the volume of overtopping per wave period (Q.T) to the volume of water moving onshore per wave period. Using small amplitude wave theory the volume of water moving onshore per wave period per unit of wave crest width in deep water is $H_o L_o/2\pi$. The following dimensionless form was used to plot the experimental data.

$$\frac{2\pi QT}{H_o L_o} = fn\left[\frac{H_o}{L_o}, \frac{d_s}{L_o}, \frac{F}{H_o}\right] \qquad (3.1)$$

An example of a dimensionless plot of the results is shown in Figure 3.3.

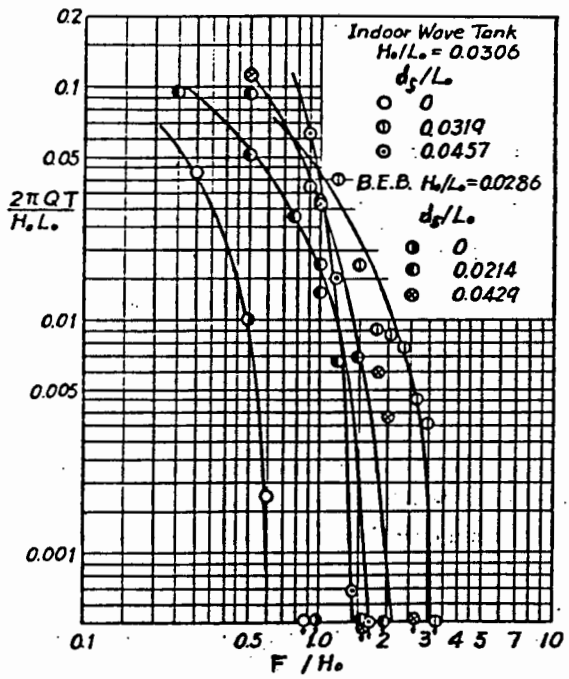

Figure 3.3 : Dimensionless presentation of results by Ishihara

3.4 Experiments by Paape using wind-generated waves (1960) [8]

Experiments were performed to measure the overtopping over dikes by irregular waves generated in a windflume. The structure slopes tested ranged from 1:2 to 1:8 and the structures were fronted by a horizontal foreshore. The water depth in the flume was kept constant at 0,30 m.

The results were presented in the dimensionless form

$$\frac{2\pi Q \bar{T}}{H_{50}\,\bar{L}} = fn\left[\frac{F(\cot\theta)^{3/2}}{H_{50}}\,,\ \tan\theta\,,\ \frac{H_{50}}{\bar{L}}\right] \qquad (3.2)$$

where H_{50} is the wave height exceeded by 50% of the waves.

The results are shown in Figure 3.4. It can be seen that for the slopes between 1:3 and 1:8 the results can be represented by a single line. For a slope of 1:2 the results differ and this was attributed to the decreased wave breaking and increased wave reflection for the steeper slope.

A number of tests were also performed using regular waves and after comparing these with the irregular wave results it is concluded that the overtopping of seawalls depends largely on the irregularity of waves and that the effects cannot be reproduced in a model using regular waves.

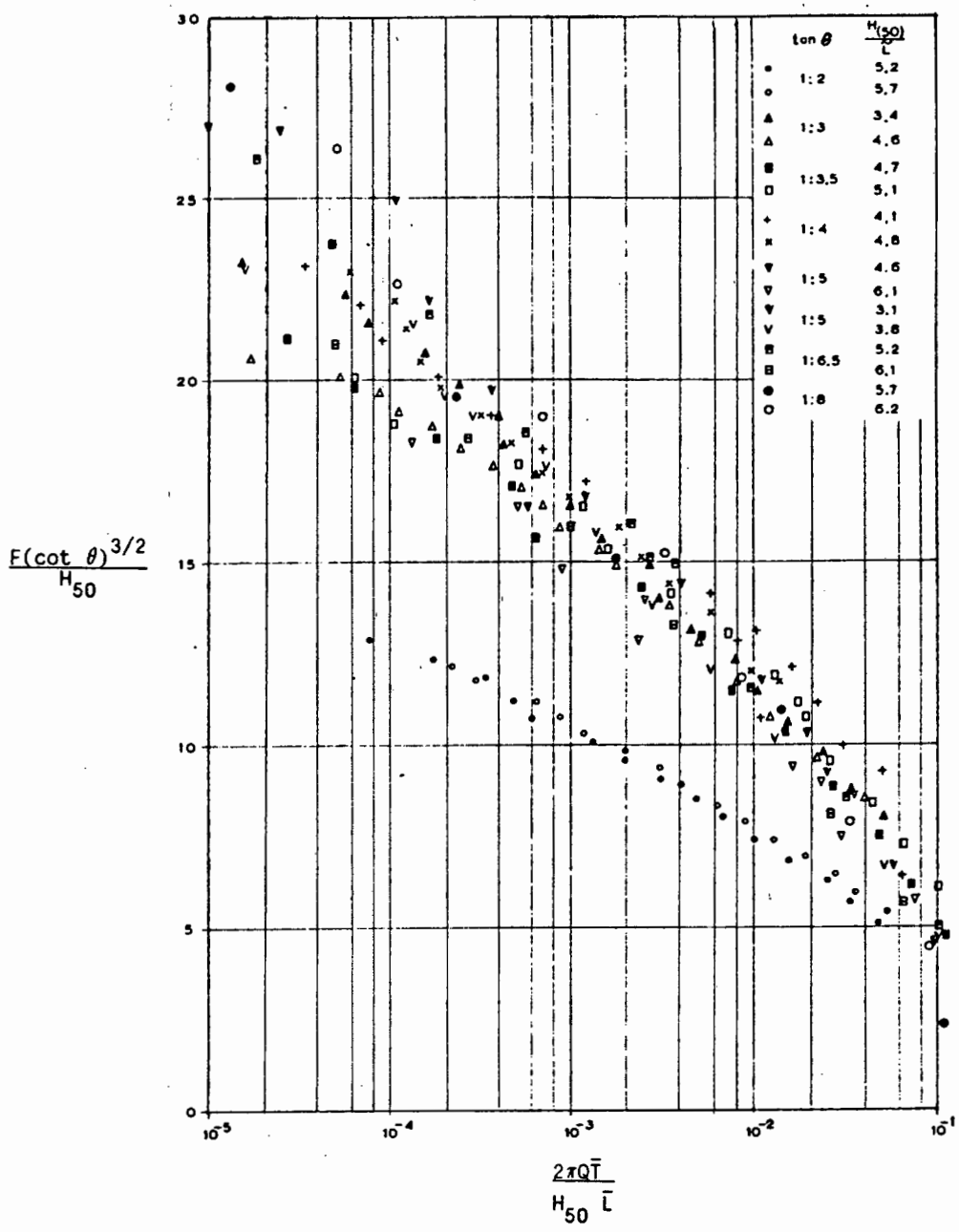

Figure 3.4 : Dimensionless presentation of results by Paape

3.5 Weir-discharge equation used by Kikkawa et al (1968) [9], Shi-igai and Konon (1970) [10]

An analytical approach to the problem of overtopping of regular waves is described by Kikkawa, Shi-igai and Kono. The overtopping is considered as a succession of different states of steady flow so that a weir-discharge formula may be used for the instantaneous discharge over the structure crest :

$$Q = \frac{2}{3} m \sqrt{2g} (y - F)^{3/2} \qquad (3.3)$$

where

y = upstream energy level measured above the mean water level

m = a dimensionless discharge coefficient

The energy level y is written as

$$y(t) = k H_o P(t) \qquad (3.4)$$

where

P(t) = a periodic function of time with period T and a maximum of 1

k = a dimensionless coefficient which may depend on the structure slope and the wave steepness

Substitution of eqn. (3.4) into the weir equation (3.3) and averaging gives

$$Q = \frac{2}{3} m \sqrt{2g} \frac{1}{T} \int_{t_o}^{t_1} (k H_o P(t) - F)^{3/2} dt \qquad (3.5)$$

where t_o and t_1 are the limits of the time interval for which $y(t) \geq F$. For an analytical determination of the integral P(t) is approximated as a triangular waveform and eqn.(3.5) then becomes

$$\frac{Q}{\sqrt{2g H_o^3}} = \frac{2}{15} m k^{3/2} \left[1 - \frac{F}{kH_o}\right]^{5/2} \qquad (3.6)$$

Kikkawa et al choose the value of 0,5 for the discharge coefficient m. There then remains only one unknown coefficient k which was calculated from measurements. For this purpose Kikkawa et al use their own measurements and the results published by Saville [5]. The coefficient k showed little correlation with wave steepness but a close correlation with the structure slope. In Figure 3.5 $Q/(2gH_o^3)^{1/2}$ is plotted against F/H_o according to eqn. (3.6) above for a number of k values. The experimental results are also given for four structure slopes and the trend of the experimental points coincides reasonably well with the calculated curves (k being chosen to maximize the coincidence).

The simplifications introduced in the above derivation are fairly drastic particularly in the use of a discharge formula for steady flows. This is, however, one of the few attempts to approach the overtopping problem analytically. The weir model was also used by Takada [11] who developed an equation similar to the one described above for estimating the rate of overtopping over vertical seawalls.

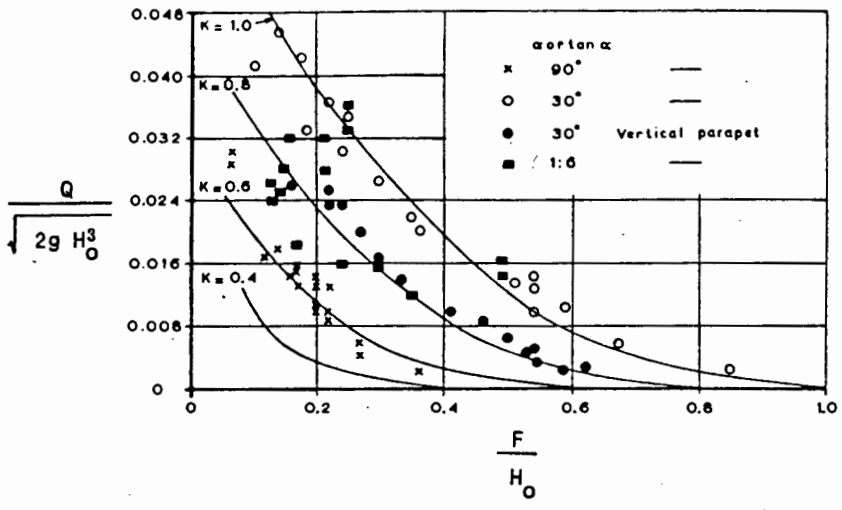

Figure 3.5 : Comparison between weir-discharge equation (lines) and experimental results (points)

3.6 Use of the linear summation principle by Tsuruta and Goda (1968) [12], Goda (1971) [13]

Goda investigated whether the overtopping rate of irregular waves can be estimated from the linear summation of individual wave overtoppings obtained from regular wave overtopping tests.

Experiments using both regular and irregular waves were conducted in a wave flume. The test structure was a vertical wall which was fronted by a 1:20 beach slope. In addition to measuring the average rate of overtopping, the volume of overtopping for individual waves was measured by suspending the container in which the overtopping water was collected from a load cell whose output was recorded during each test.

The irregular waves were generated by an oil pressure pulse motor controlled by ten electric oscillators. Since the measurements were stopped before the waves which were reflected from the test structure re-reflected back from the wave paddle, each irregular wave test consisted of approximately twenty runs with ten waves measured in each run. Five different irregular wave trains were tested. Regular waves with periods of 1,77 s and 1,38 s were also tested.

An example of the regular and irregular wave overtopping rates measured is shown in Figure 3.6. It can be seen that the overtopping due to irregular waves cannot be obtained from regular wave tests by simply using the significant wave height in place of the regular wave height.

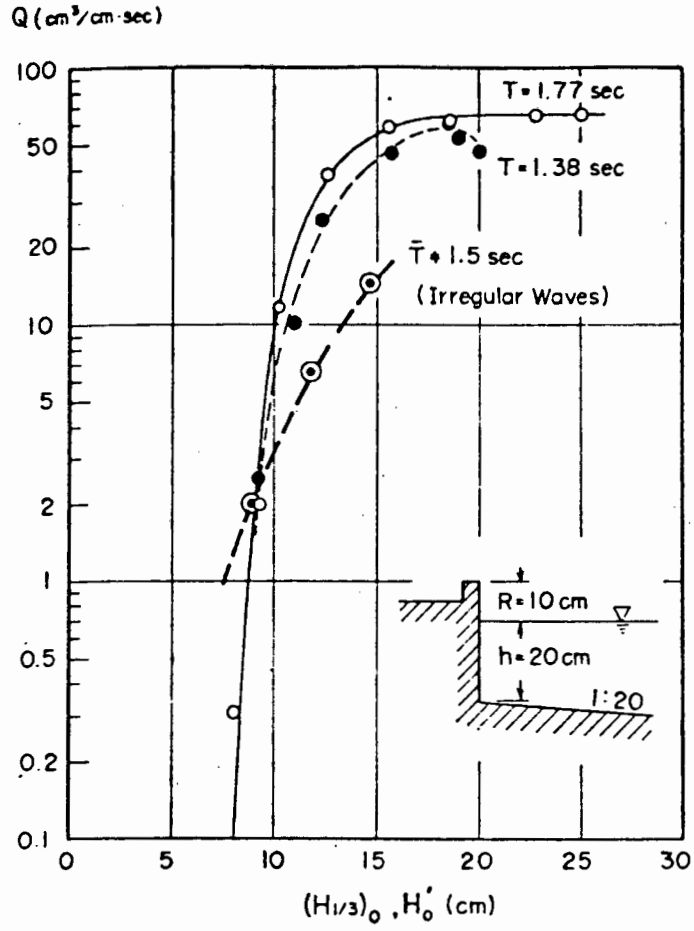

Figure 3.6 : Comparison between regular and irregular overtopping rates

The overtopping discharge of individual waves in an irregular wave train, on the other hand, was found to show a reasonable correlation to the equivalent regular wave discharge The authors therefore suggest that the expected overtopping due to irregular waves can be calculated as

$$Q = \sum_{i=1}^{m} Q(H_i) \frac{n(H_i)}{N} \qquad (3.7)$$

where

Q = expected irregular overtopping rate

$Q(H_i)$ = overtopping rate of regular waves with height H_i

$n(H_i)$ = number of waves in height range H_i

m = number of wave height ranges

N = total number of waves

The effect of wave period is ignored in the above equation. The reasons given are that inclusion of the wave period will increase the complexity of the calculation and that the joint distribution of wave heights and periods will have to be known. It was also found that the period had little effect on the overtopping for deepwater wave steepnesses greater than 0,01.

The overtopping rates which were experimentally measured using regular waves were then used to calculate the expected irregular overtopping rates using eqn. (3.7). The ratio between these calculated rates and the irregular rates measured in the irregular wave experiments was found to be between 0,77 and 1,87.

The authors went on to re-analyse all the overtopping measurements involving regular waves published prior to 1968. By using eqn. (3.7) and assuming a Rayleigh distribution for wave heights the expected rate of irregular overtopping is plotted in the following form

$$\frac{Q}{\sqrt{2g\ H_{so}^{\ 3}}} = fn\left[\frac{H_{so}}{d_s}, \frac{F}{H_{so}}\right] \qquad (3.8)$$

These calculations were performed for vertical seawalls and seawalls fronted by concrete blocks. The plot for vertical seawalls is shown in Figure 3.7.

The linear summation approach which was used by Goda neglects the random process of wave breaking, the presence of surf beat inherent in random waves and the effects of interference by the preceding waves. These effects can only be modelled using irregular waves. One of the reasons for investigating the summation approach was the difficulty in generating and measuring irregular waves in a flume with the apparatus available at the time.

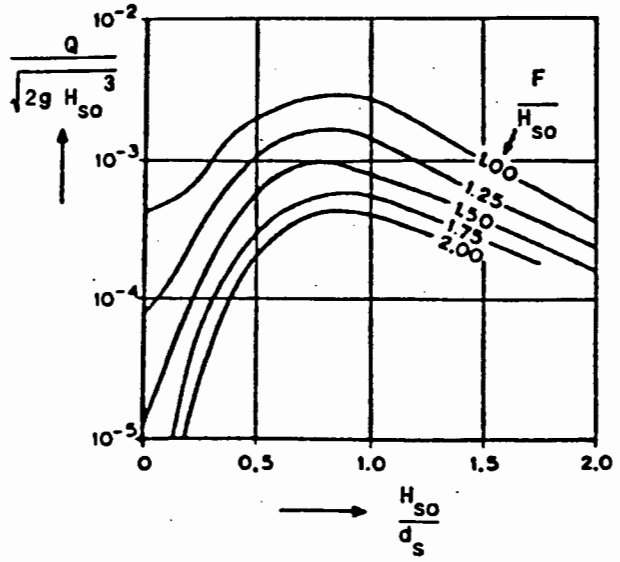

Figure 3.7 : Dimensionless plot for irregular waves by Goda

3.7 Overtopping equation developed by Battjes (1974) [14], Douglass (1986) [15]

Battjes first derives an expression for overtopping caused by regular waves and then accounts for irregular waves by assuming that the deepwater wave height and wavelength are jointly Rayleigh distributed.

An equation is derived which gives the relation between Battjes' dimensionless overtopping parameter, β, and dimensionless freeboard parameter, ζ. These parameters are defined as

$$\beta = \frac{\bar{B}}{(0,1)\,\bar{H}\,\bar{L}_o\sqrt{\tan\theta}} \qquad (3.9)$$

$$\zeta = \frac{F}{\sqrt{\bar{H}\,\bar{L}_o}\,\tan\theta} \qquad (3.10)$$

where $\bar{B}$ is the average overtopping per average wave period (m^3/m).

The relation between β and ζ is shown graphically in Figure 3.8. k is a parameter which depends on the correlation between H and L_o.

The only data with which Battjes could compare his results were those of Paape [8] and it was found that his equation showed the same trend as the experimental data. More experimental data is however required to verify Battjes' equation.

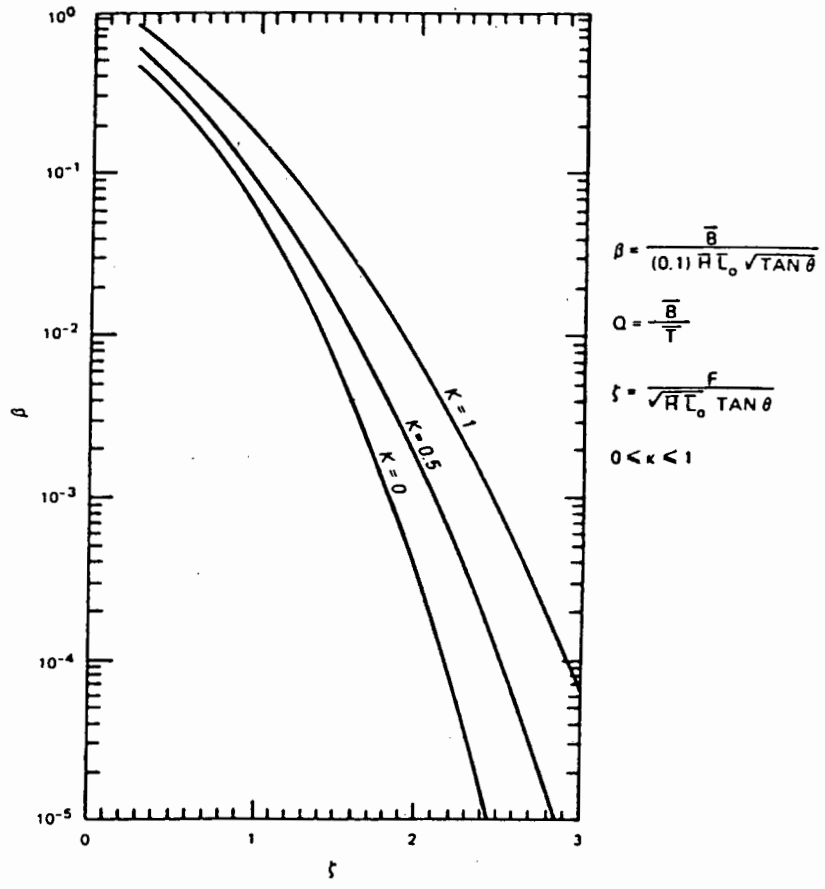

Figure 3.8: Relation between Battjes' dimensionless parameters

3.8 Re-analysis of Saville's results by Weggel (1976) [16]

Weggel re-analysed Saville's [6] results in dimensionless form. By looking at the relations between the relevant dimensionless parameters, Weggel derived the following empirical equation for the regular wave overtopping rate

$$Q = \left[g\, Q_o^*\, H_o^3\right]^{1/2} \exp\left[-\frac{0{,}217}{\alpha} \tanh^{-1}\frac{F}{R}\right] \qquad (3.11)$$

where

Q = rate of overtopping by regular waves

Q_o^* , α = dimensionless empirical coefficients

R = runup

The method given in the Shore Protection Manual [1] for estimating overtopping is based on Weggel's equation. The runup, R, is the vertical distance the regular wave would run up if the structure were high enough to prevent overtopping and is calculated using the design charts given in the Shore Protection Manual. Weggel calculated the empirical coefficients Q_o^* and α as functions of wave steepness (H_o/gT^2) and relative height (d_s/H_o) for each of the situations tested by Saville. These coefficients are presented in the Shore Protection Manual [1] and the Q_o^* - α figure for 1:3 smooth slopes is reproduced in Figure 3.9.

The inclusion of the potential runup, R, in an overtopping equation is questionable as it introduces another independent variable to the problem and because design charts must be used to obtain the value of R. It would be preferable to involve only the independent variables relating to the structure dimensions and the wave conditions in an overtopping equation. An examination of Figure 3.9 shows that a general relation between Weggel's parameters Q_o^* and α and the dimensionless variables d_s/H_o and H_o/gT^2 does not exist. This is apparent when an attempt is made to interpolate between points on this graph and makes it difficult to apply this equation to situations which were not precisely modelled by Saville.

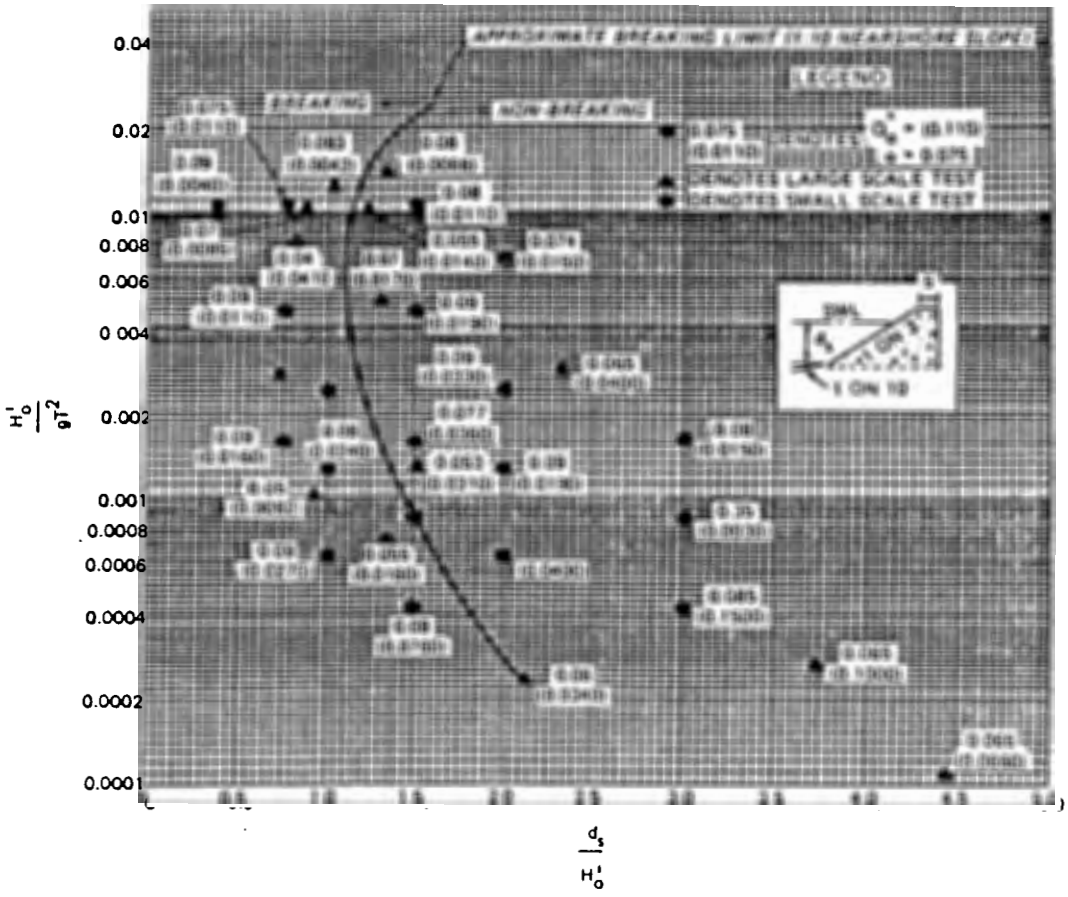

Figure 3.9 : Weggel's empirical coefficients Q_o^* and α

3.9 Extension of Weggel's equation to irregular waves by Ahrens (1977) [17], [18]

To apply Weggel's equation to a sea of irregular waves, Ahrens assumed that the distribution of runups caused by an irregular sea will follow a Rayleigh distribution. Ahrens estimated the overtopping rate by summing the overtopping contributions from the individual runups

$$Q_{IRR} = \frac{1}{199} \sum_{j=1}^{199} Q_j \qquad (3.12)$$

where

Q_{IRR} = overtopping caused by irregular waves

Q_j = overtopping caused by one runup in the runup distribution

$$= \left[g\, Q_o^*\, H_{so}^3 \right]^{1/2} \exp\left[\frac{-0,217}{\alpha} \tanh^{-1} \frac{F}{R_P} \right] \qquad (3.13)$$

H_{so} = deepwater significant wave height

R_P = runup of probability of exceedance p

$$= \left[\frac{\ln 1/p}{2} \right]^{1/2} R_s \qquad (3.14)$$

$p = 0.005 \times i$, $i = 1, 2, 3, \ldots, 199$

R_s = runup of regular wave with the significant wave height and period

Ahrens' equation can be considered to correct Weggel's regular wave results for the effect of irregular waves and is the method described in the Shore Protection Manual [1] for estimating irregular wave overtopping rates.

More recent results by Ahrens [19] have shown runup to fit a Weibull distribution and not a Rayleigh distribution as was assumed above. Ahrens' assumptions that α and Q_o^* remain constant as the overtopping contributions of the individual runups are summed and that the H_o term in Weggel's equation can be replaced by H_{so} have not been verified.

3.10 Tests by Jensen and Sorensen using irregular waves (1979) [20], 1987 [21]

A series of model tests were performed to measure overtopping of rubblemound structures due to irregular waves. The significant wave height was measured in front of the the structure and the wave height was compensated for the effect of wave reflection and re-reflection. The water depth at the structure toe was such that the waves were not limited by depth.

The results are given in the following dimensionless form

$$\frac{Q\,\bar{T}}{(B^*)^2} = fn\left[\frac{H_{si}}{F}, \frac{U}{\sqrt{gB^*}}\right] \qquad (3.15)$$

where

B* = horizontal distance from where the front of the structure intersects SWL to the rear side of the structure

U = wind speed

The logarithm of $\frac{Q\,\bar{T}}{(B^*)^2}$ was found to be proportional to H_{si}/F as shown in Figure 3.10. The wind effect was found to most pronounced for low overtopping rates and had little influence at high rates of overtopping.

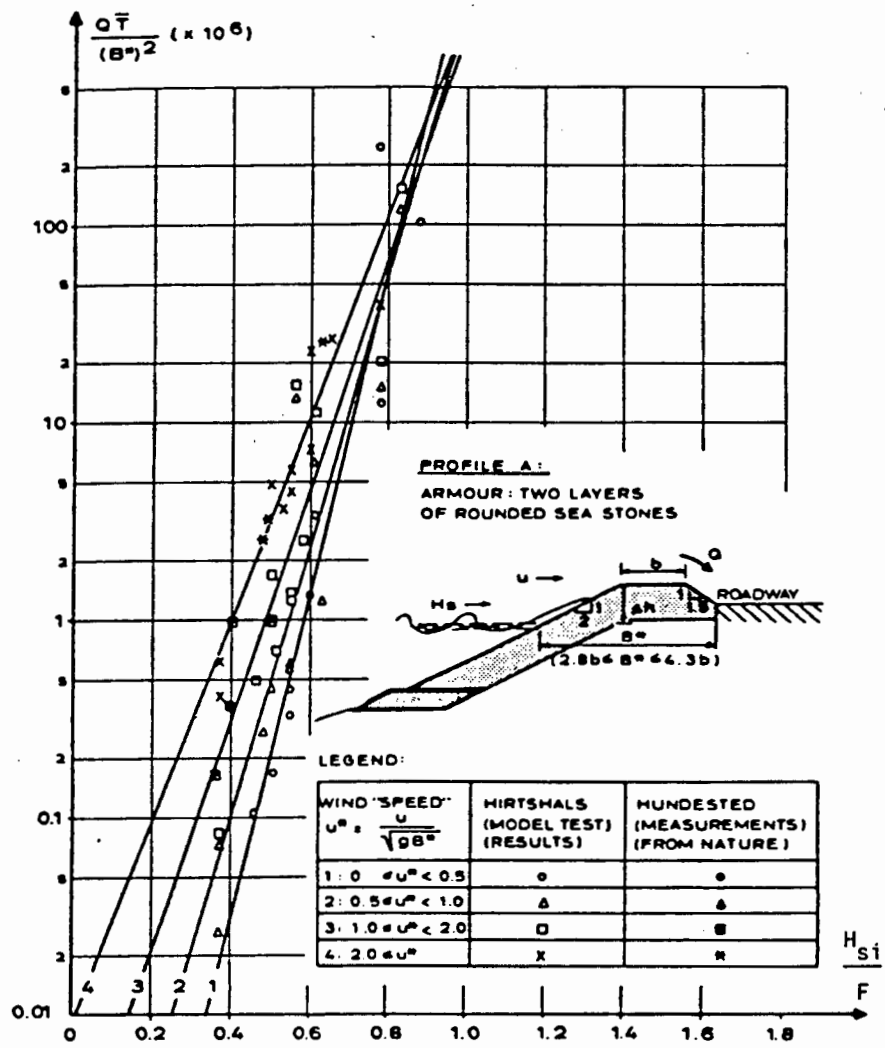

Figure 3.10 : Dimensionless presentation of results by Jensen

3.11 Owen's empirical equation (1982) [22], 1980 [23]

Model tests were carried out in a wave basin equipped with an electrically controlled irregular wave generator. A Jonswap type spectrum was used and the water depth at the toe of the structure was kept constant at 160 mm. The test structures had seaward slopes of between 1:1 and 1:4 and included both plane sloped and bermed structures. The structures were fronted by a 1:20 beach slope.

Owen found that for seawalls having identical underwater geometry the relative effects of different crest elevations under attack by waves of differing height and period are taken into account by an expression of the form

$$Q_* = A.\exp(-B.F_*) \tag{3.16}$$

where

Q_* = Owen's dimensionless overtopping parameter

$$= \frac{Q}{\bar{T}\, g\, H_{si}} \tag{3.17}$$

F_* = Owen's dimensionless freeboard parameter

$$= \frac{F}{\bar{T}\sqrt{gH_{si}}} \tag{3.18}$$

H_{si} = significant wave height at structure

A,B = dimensionless empirical coefficients for the particular structure calculated using linear regression

An example of a dimensionless graph of Owen's results is shown in Figure 3.11. The correlation coefficients were found to be greater than 0,91 provided that H_{si} was adjusted for wave breaking if this occurred. Owen cautions against applying his method to situations other than those he tested. His experimental parameter ranges were as follows :

$$0{,}05 < F_* < 0{,}30$$
$$10^{-6} < Q_* < 10^{-2}$$
$$1{,}5 < d_s/H_{si} < 5{,}5$$
$$0{,}035 < H_{si}/\bar{L}_o < 0{,}055$$

This is an important study as it is based on experiments with irregular waves and because it introduces the idea of a simple exponential relation to predict overtopping. The range of conditions tested was limited and the wave height of waves which break before the structure must first be replaced by an equivalent wave height which can then be used in the overtopping equation. Note that the water depth at the structure toe was kept constant during the tests and is not included in the overtopping equation.

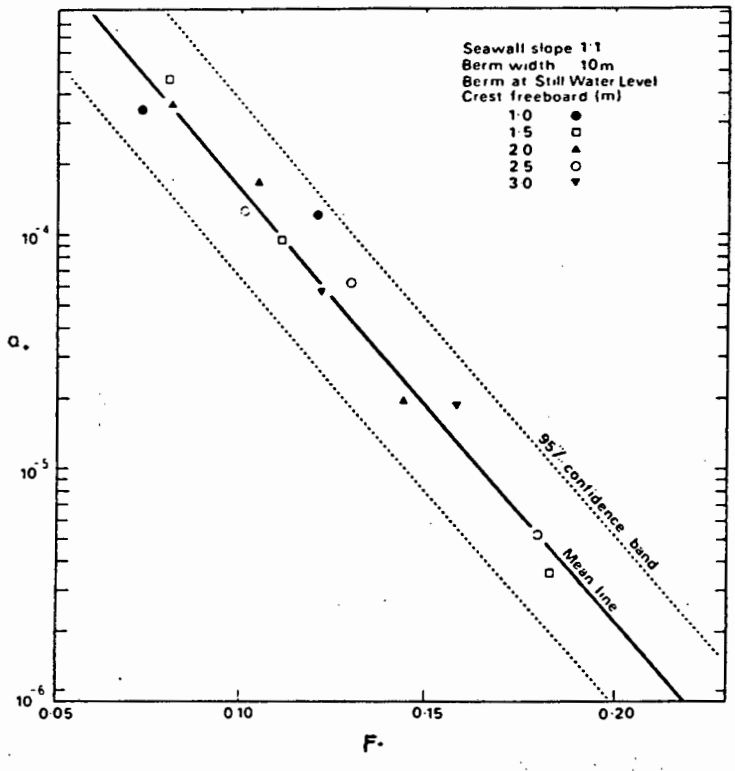

Figure 3.11 : Relation between Owen's dimensionless parameters

3.12 Analytical models by Kobayashi (1983) [24], (1989) [25]

An analytical method was developed by Kobayashi and Reece [24] for estimating the overtopping around the circumference of man-made islands. The method is derived using an approach similar to that used by Battjes [14]. In this case a regular wave runup equation developed by Ahrens is used to determine the runup term in Weggel's regular wave overtopping equation (see Section 3.8). An assumed joint wave height and period distribution is then used to determine the irregular overtopping rate using the principle of linear summation. The equation obtained is specific to circular islands and has not been verified using irregular wave results.

A later publication by Kobayashi [25] describes an analytical approach to calculating regular wave overtopping using a numerical model which predicts the temporal variations of the velocity and depth of flow over the crest of the structure. The model was compared to the regular wave overtopping rates measured by Saville [6] and the model was shown to predict the experimental data to a similar degree of accuracy as the empirical equation developed by Weggel (see Section 3.8). The model was not extended to irregular waves.

3.13 Irregular overtopping tests by Goda (1985) [2]

A more recent publication by Goda is a set of diagrams for estimating overtopping based directly on irregular wave overtopping tests. Trains of approximately 200 irregular waves were generated and applied to a vertical seawall and a seawall fronted by concrete blocks. The model structures were fronted by beach slopes of 1:10 and 1:30. Since the incident waves arriving at the structure are contaminated by the multi-reflection of waves between the test structure and the wave paddle Goda measured the waves at two positions in the deep portion of the flume and was then able to separate the deepwater incident wave train from the reflected wave train using a fast Fourier transform technique.

The results for each structure geometry tested are presented in the following form :

$$\frac{Q}{\sqrt{2g\ H_{so}^{\ 3}}} = fn\left[\frac{d_s}{H_{so}}, \frac{F}{H_{so}}, \frac{H_{so}}{L_{po}}\right] \qquad (3.19)$$

Separate diagrams have been drawn for deepwater steepnesses of 0,012, 0,017 and 0,036. The diagram for a vertical wall with a 1:10 foreshore slope and a steepness of 0,012 is shown in Figure 3.12. The wave height parameter used is the deepwater significant wave height. The diagrams described in this section, and which are based on irregular wave results, are expected to be more accurate than those obtained using the linear summation principle used previously by Goda and described in Section 3.6.

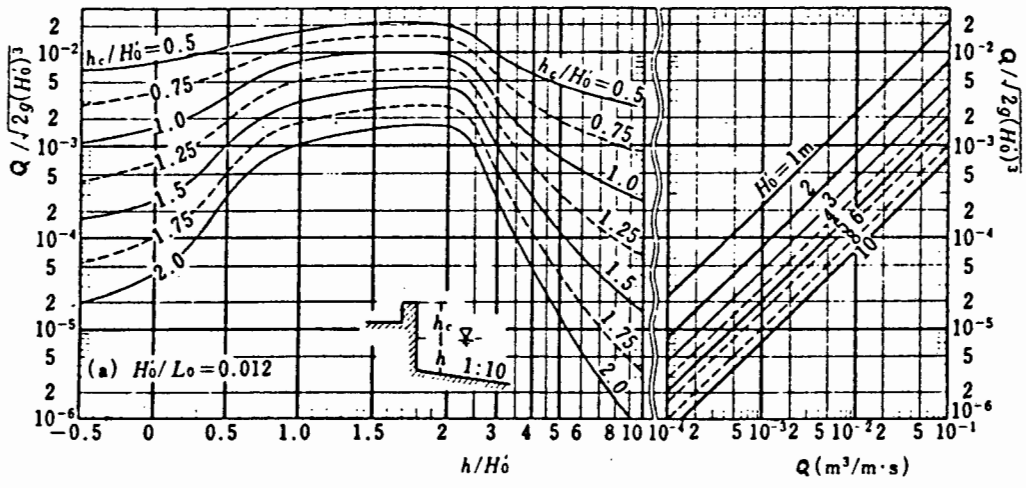

Figure 3.12 : Presentation of results by Goda

3.14 Seawall overtopping model by Ahrens & Heimbaugh (1988) [26]

An overtopping model is developed based on three separate studies performed at the Coastal Engineering Research Centre (CERC). The structures tested included vertical and recurved seawalls as well as seawalls with toe protection and fronting revetments. All the tests used irregular waves generated by computer controlled wave generators. The incident wave conditions were measured in a side channel of the flume.

Overtopping rates were found to be strongly dependent on a dimensionless relative freeboard parameter, F′, which was found to consolidate all the overtopping data for similar structures into a well defined trend. F′ is defined as

$$F' = \frac{F}{(H_{si}^{\ 2} L_{pi})^{1/3}} \qquad (3.20)$$

The parameter F′ can be described as the ratio of the freeboard to the severity of the local wave conditions. The depth at the structure toe, d_s, and the peak wave period, T_p, are included in F′ through the local wave length, L_{pi}. Three models involving F′ were used to estimate the overtopping rate. The models in order of increasing complexity are :

Model 1 : $Q = Q_o \exp (C_1 F')$

Model 2 : $Q' = Q_o' \exp (C_1 F')$

Model 3 : $Q' = Q_o' \exp (C_1 F' + C_2 X_2)$

where

Q' = dimensionless overtopping rate

$$= \frac{Q}{\sqrt{g\ H_{si}^3}}$$

Q_o = overtopping coefficient

Q_o', C_1, C_2 = dimensionless overtopping coefficients

X_2 = dimensionless secondary variable

Different dimensionless secondary variables, X_2, were found to be applicable to different structures. Examples of the secondary variables used for X_2 included F/d_s and the deepwater wave steepness, H_{so}/L_{po}. The values of the overtopping coefficients were found using regression analysis.

A comparison between the overtopping rates predicted using the three models and the experimental values is shown in Figure 3.13. Model 3 was found to give the best results and the correlation coefficients between the predicted and experimental overtopping rates using Model 3 were greater than 0,8.

The form of the overtopping model described above is similar to the model proposed by Owen (Section 3.11). Both models provide a means of consolidating the overtopping measurements for one structure geometry into a single, dimensionless trend. An advantage of the overtopping parameter used by Ahrens is that the water depth at the structure is included in the model. It should be noted that the studies which led to these models were all related to specific prototype structures and did therefore not cover the full range of wave conditions possible.

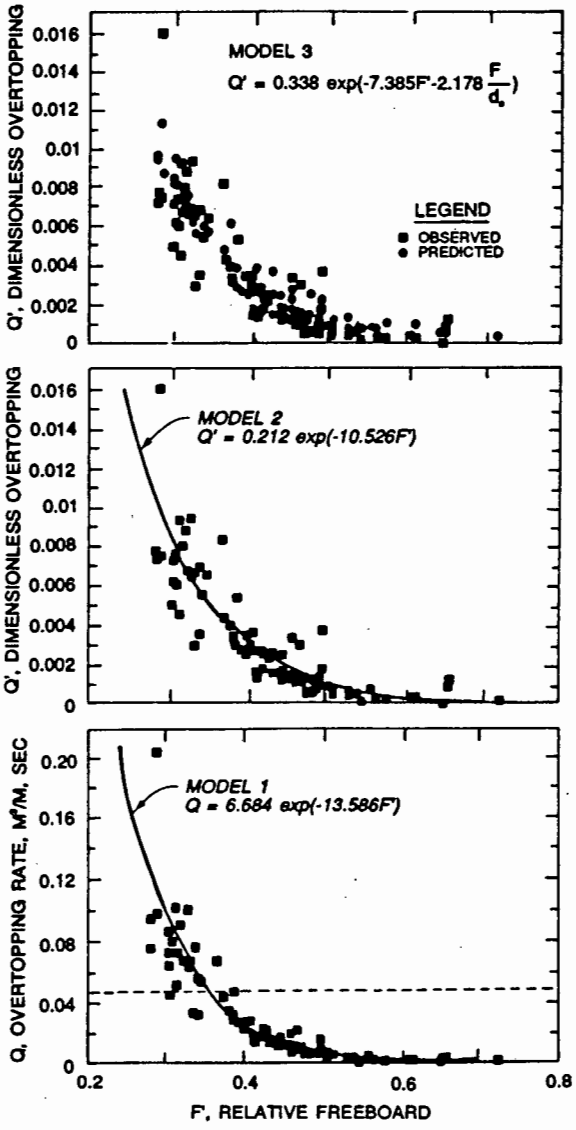

Figure 3.13 : Comparison between Ahrens' overtopping models and the experimental results

3.15 Discussion

The overtopping studies described in the previous sections can be grouped into three categories which are discussed below :

1. Empirical equations or dimensionless presentations of results based on overtopping tests using regular waves.

   The dimensionless form used by Ishihara to plot his overtopping measurements (Section 3.3) and the overtopping equation developed by Weggel (Section 3.8) fall into this category. Goda (Section 3.6) and Ahrens (Section 3.9) used the linear summation principle to apply these regular wave results to irregular waves. The linear summation approach has, however, not been sufficiently verified and experiments using irregular waves are therefore preferable.

2. Development of analytical equations to estimate regular wave overtopping rates and in some cases extending these results to irregular waves using the principle of linear summation.

   This category includes the weir-discharge equation for regular wave overtopping presented by Kikkawa and others (Section 3.5), the irregular overtopping equation developed by Battjes (Section 3.7), and the two analytical models proposed by Kobayashi (Section 3.12). Wave overtopping is a complex phenomenon and involves both the process of wave transformations in shallow water and the process of wave runup on structures. The overtopping process is further complicated when irregular waves are considered. No analytical method which has been shown to accurately predict irregular wave overtopping has been developed as yet.

3. **Empirical equations or dimensionless presentations of results based on overtopping tests using irregular waves.**

This category includes the windflume experiments conducted by Paape (Section 3.4), the dimensionless presentations of results by Jensen (Section 3.10) and Goda (Section 3.13), and the exponential overtopping equations developed by Owen (Section 3.11) and Ahrens (Section 3.14). These studies have consisted of measuring the overtopping rates due to realistic wave conditions and then plotting the relevant variables in a dimensionless form. Owen and Ahrens have then developed simple empirical equations relating the dimensionless parameters. The approach which will be followed in this thesis will also fall into this category.

CHAPTER 4

EXPERIMENTAL APPARATUS

4.1 Introduction

The experiments performed by Owen (Section 3.11) and Ahrens (Section 3.14) which led to the development of simple empirical models to predict irregular overtopping rates were performed using a limited range of wave conditions. In particular, these tests did not include very shallow water depths at the structure toe which cause the incident waves to break some distance offshore from the structure. It is therefore not known whether a simple empirical model can be developed to predict irregular overtopping rates over the full range of incident wave conditions including broken, breaking and unbroken waves. The objective of the experiments was therefore to measure the rate of overtopping which occurred when a model structure was subjected to a full range of realistic sea states.

The experimental work was conducted at the EMATEK division of the CSIR in Stellenbosch using a 30 m long wave flume equipped with an irregular wave generator. The flume was divided into three channels and the model structure was placed in the centre channel while the two side channels were used to measure the incident wave conditions. A train of irregular waves was generated and the water which overtopped the model structure was collected in a calibrated tank, located behind the structure.

The design, construction and operation of the experimental apparatus is described in the following sections.

4.2 The wave flume

The tests were conducted in a 0,75 m wide, 1,0 m deep and 30 m long glass flume equipped with a Seasim wave generator capable of generating irregular waves. The flume is shown in Plate 4.1.

Plate 4.1 : The wave flume

4.2.1 Foreshore slope

Coastal structures are typically fronted by a sloping foreshore and a foreshore slope was therefore built into the flume. It would have been preferable to test a number of different foreshore slopes. However, the slope was built into the flume using bricks and mortar and the glass panes used to divide the flume into three channels were cut to match the foreshore slope. It would therefore have been both time consuming and costly to change the foreshore slope and the tests were limited to one foreshore slope. The foreshore slopes used in prior overtopping tests are listed in Table 4.1.

Author	Year	Foreshore slope
Saville	1953	1 : 10
Ishihara	1960	1 : 10
Owen	1982	1 : 20
Goda	1985	1 : 10 and 1 : 30
Ahrens	1986	1 : 100

Table 4.1 : Foreshore slopes used in prior overtopping studies

A foreshore slope of 1 : 20 was used for this thesis. The slope was started 13,0 m in front of the wave generator and extended to near the end of the flume. The slope was constructed of packed loose bricks and was finished off with a layer of weak mortar. Strips of softboard were placed between the mortar and the glass sides of the flume to prevent the glass from being cracked due to expansion of the mortar. The foreshore slope can be seen in Plate 4.2.

Plate 4.2 : Foreshore slope built into flume

4.2.2 Partitioning of flume

4.2.2.1 Introduction

The overtopping studies by Goda (Section 3.13) and the Shore Protection Manual (Section 3.8) make use of the wave parameters measured in deep water offshore while Ahrens (Section 3.14) and others use the wave parameters measured inshore at the structure toe. For this thesis it was decided to measure both the offshore and inshore incident wave characteristics to ensure that as much information about the wave conditions as possible was available for analysis.

Since the tests involved irregular waves it was necessary to generate at least 150 waves to ensure that the complete wave spectrum was produced. The problem of multi-reflection between the model structure and wave paddle was therefore expected. The Seasim wave generators are equipped with a wave absorption unit which makes it possible to absorb the reflections from the model structure, thus minimizing unwanted re-reflections off the wave generator paddle. The waves measured in the flume therefore consist of two wave trains; the incident wave train from the wave generator and the wave train reflected from the model structure. A method was required to allow the pure incident wave train to be measured, both in deep water offshore and at the position of the model structure.

One of the methods considered was to first measure the inshore and offshore wave characteristics with the 1:20 foreshore slope built into the flume but without the model structure installed. The relation between the wave heights in the flume and the gain setting of the wave generator could be established for each of the wave periods and water depths to be tested. This method was not used due the large number of calibrations which would be necessary and due to the possibility of drift in the analog gain setting of the wave generator between the calibration and the testing.

Another approach considered was to remove the model structure prior to each test in order to perform the calibration and then to replace the model and proceed with the test. The problem with this approach was that the large collecting tank located behind the model structure would also have to be removed each time.

A third approach considered was to measure the waves at three positions in the flume and then to separate the incident wave train from the reflected wave train using the method described by Mansard and Funke (see Section 4.7.4). One constraint with this procedure is that the wave probes should be more than one wavelength away from both the model structure and the wave paddle and this approach could

therefore not be used to measure the incident wave at the structure toe. The technique could, however, be used to measure the deepwater incident wave in the deep section of the flume. A method was therefore sought to measure the incident waves at the structure toe directly.

4.2.2.2 Final layout of flume

The method adopted was to divide the flume into three equal channels each 0,242 m wide by constructing two dividing walls. The partitioning was started 11,4 m in front of the wave generator and extended up to the model structure. The two dividing walls were constructed using 8 mm laminated glass panes which were cut to match the 1 : 20 foreshore slope. The bottom edges of the glass were located by aluminium channels embedded in the mortar finish of the foreshore slope. The top edges were located by aluminium channels which were held in position with steel bars spanning the top of the flume at 1,5 m intervals. The joints between adjacent panes of glass were sealed with silicon.

The model structure was placed in the centre channel at a distance of 23,5 m from the wave generator and a steel collecting tank was located directly behind the model. The width of the tank was equal to the width of the centre channel and this allowed the 1 : 20 foreshore slope to be continued on either side of the collecting tank in the two side channels. The waves in the two side channels were therefore the pure incident waves free from any reflections from the model structure. The final layout of the flume is shown in Figure 4.1.

A less complicated alternative would have been to use two channels only with the model structure placed in one and the other used to measure the incident waves. This was not used because of the possibility of cross-waves occurring in the flume due to the different reflection characteristics of the two channels. The symmetry of the three channel system with the model structure placed in the centre channel reduced the probability of cross-waves occurring.

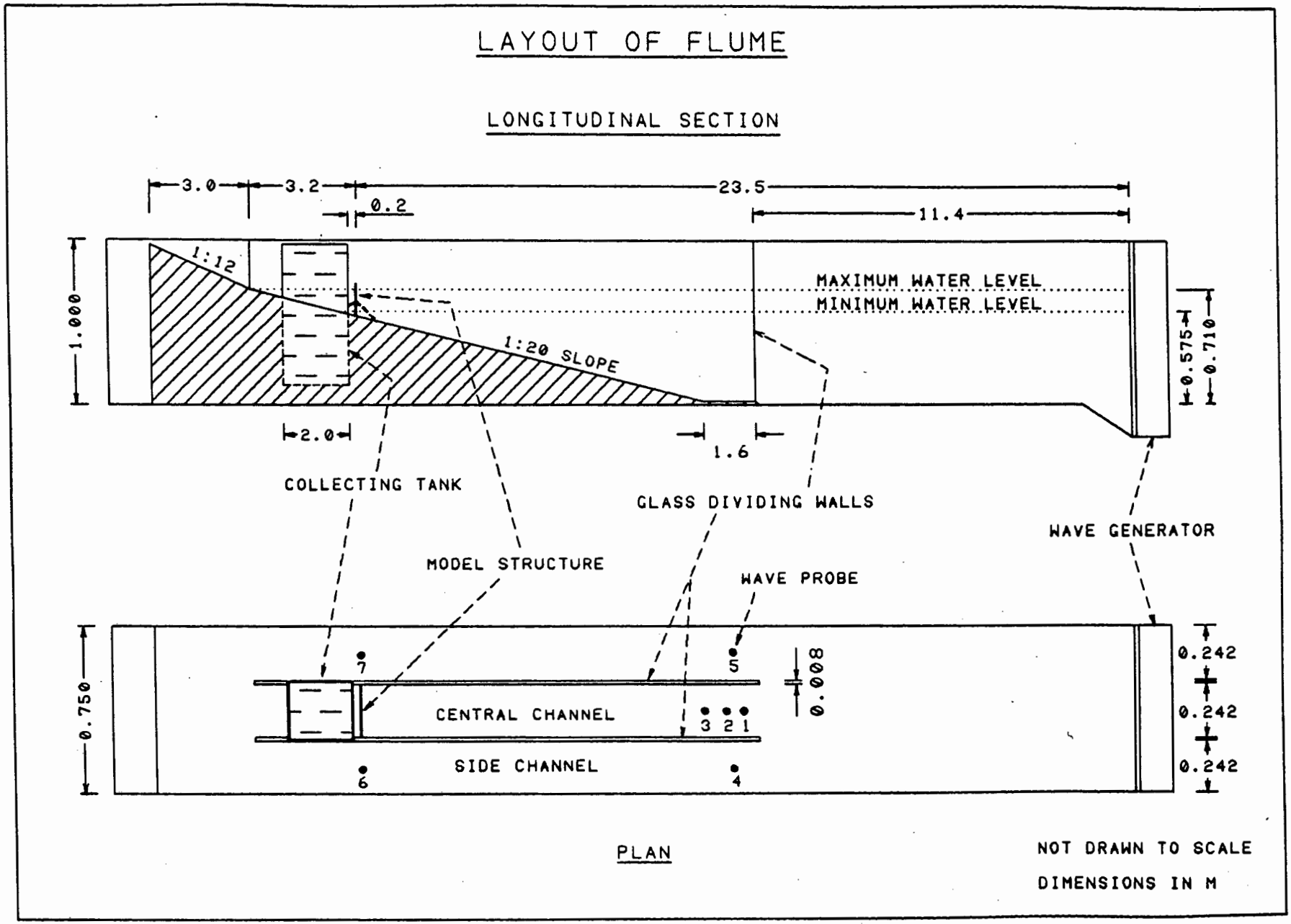
LAYOUT OF FLUME
LONGITUDINAL SECTION
3.0
3.2
0.2
23.5
11.4
1:12
1:20 SLOPE
MAXIMUM WATER LEVEL
MINIMUM WATER LEVEL
1.000
0.575
0.710
2.0
1.6
COLLECTING TANK
GLASS DIVIDING WALLS
WAVE GENERATOR
MODEL STRUCTURE
WAVE PROBE
0.750
7
5
CENTRAL CHANNEL
3 2 1
SIDE CHANNEL
6
4
0.800
0.242
0.242
0.242
PLAN
NOT DRAWN TO SCALE
DIMENSIONS IN M

Figure 4.1

4.3 The model structures

The coastal structures where overtopping is an important design parameter are tidal pools, seawalls and breakwaters. The geometric shapes of these structures show a large variation. Tidal pool walls, for example, often have an inclined face to increase the amount of overtopping. Seawalls, on the other hand, may have a recurved face to reduce overtopping and breakwaters may have protective dolosse in front of the wall.

It was therefore decided to limit the model structures to two geometric shapes and to test each over a wide range of wave conditions instead of trying to model a large number of specific prototype structures. The structures tested were

(a) 100 mm high vertical wall
(b) 100 mm high wall with a 45° slope on the seaward face
(c) 200 mm high vertical wall

All three structures had a horizontal crest 30 mm wide and were constructed of marine plywood which was sanded to a smooth finish and then varnished. The model structures are shown in Figure 5.1.

4.4 The collecting tank

In order to measure the average rate of overtopping the volume of water overtopping the model structure in a certain period of time had to be measured. A special steel collecting tank was constructed for this purpose.

4.4.1 Design of tank

The tank volume required was calculated as the maximum overtopping rate expected multiplied by the length of a test. Based on this calculation a rectangular tank 2,0 m long, 0,245 m wide and 0,88 m high was used. The tank was constructed of 5 mm thick steel plates

which were welded together and then zinc plated. The tank was placed directly behind the model structure in the centre channel and a chute directed the water which overtopped the structure into the collecting tank. The width of the tank was equal to the width of the centre channel and this allowed the foreshore slope to be continued on either side of the tank in the two side channels. The bottom plate of the tank protruded by 155 mm along either side to allow the tank to be built into the foreshore slope and thereby prevent the tank from floating due to the positive buoyancy of the tank when the flume was filled with water.

The volume of water collected was obtained by measuring the water level in the tank before and after each test using manometers. The error in the measurement for small water volumes would have been unacceptably high because the manometers could only be read accurately to the nearest 0,5 mm. For example, if the volume collected was 1 litre the rise in water level in the tank would be only 1,9 mm and the error in the reading would be 26 %.

This problem was overcome by dividing the tank into three compartments using two plywood bulkheads. The first compartment was 0,1 m long, the second 0,4 m long and the third 1,46 m long. The collecting tank is shown in Figure 4.2 and Plate 4.3. The water overtopping the model structure fell into the first compartment. When the first compartment was full the water flowed over the bulkhead into the second and then the third compartments. The water level in each compartment was measured using separate manometers. The accuracy of the volume measurement using this system was greater than 1 % for all the volumes measured. Each compartment could be emptied by unscrewing a plug in the bottom of the compartment.

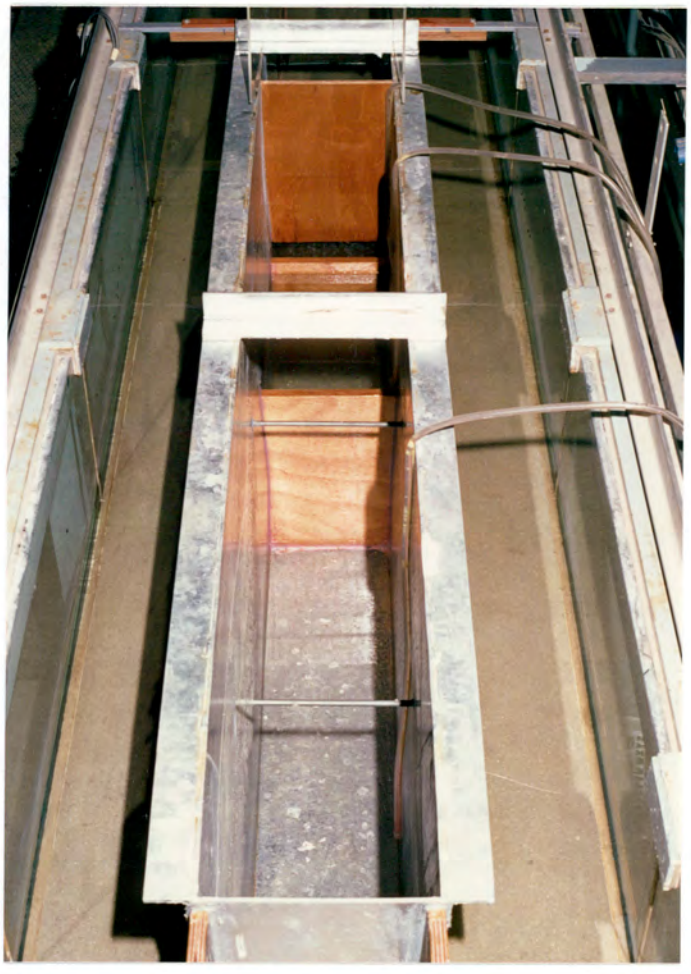

Plate 4.3 : Collecting tank installed in the flume

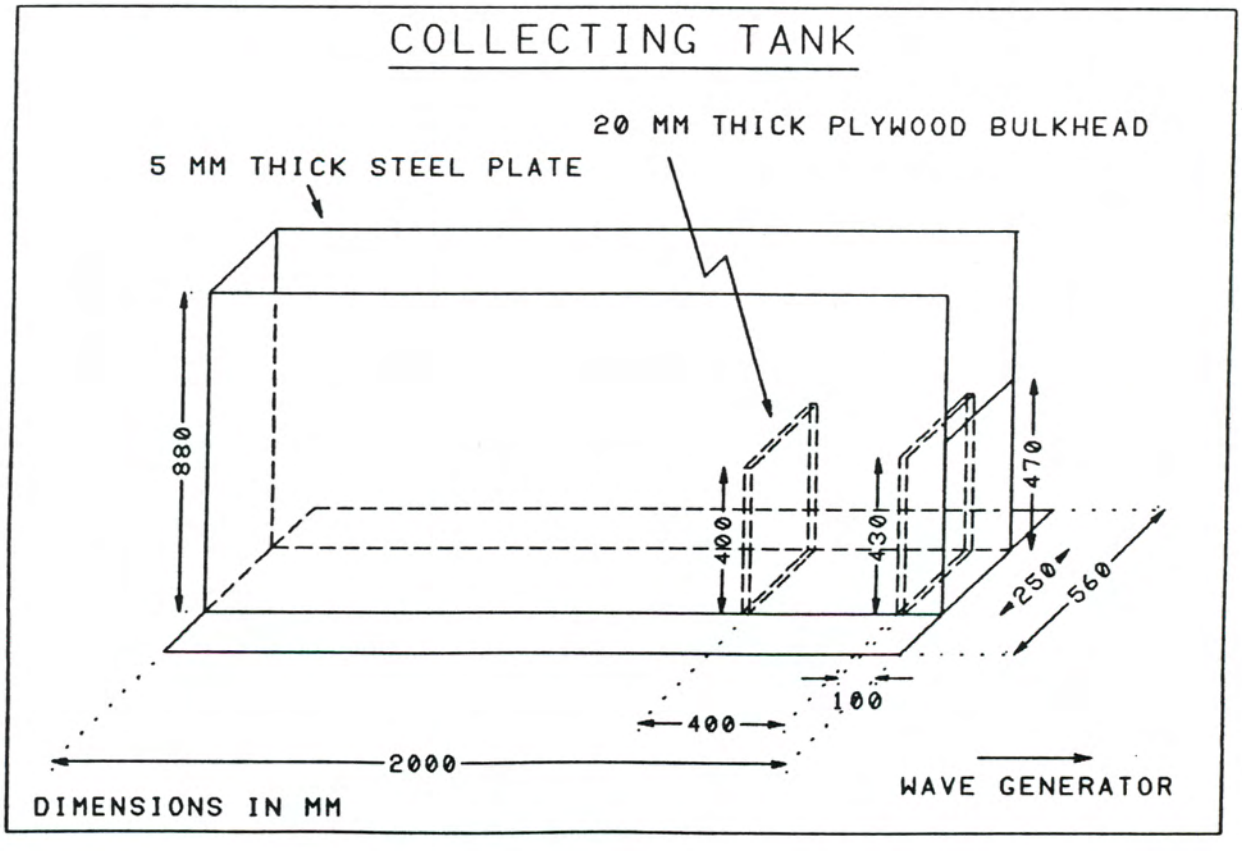

Figure 4.2

The manometers were located on a wooden board attached to the side of the flume as shown in Plate 4.4. One manometer was used for each of the three compartments of the collecting tank and a fourth one to measure the water level in the flume. Each manometer consisted of a clear plastic tube running from the bottom of the collecting tank to the bottom of a 30 mm diameter clear PVC tube attached to the manometer board. The water level in the tube was measured by sliding the perspex box shown in Plate 4.5 along the tube until the marks on the front and back of the box lined up with the bottom of the meniscus. The water level was then read on the measuring tape hanging next to each manometer.

Plate 4.4 : Manometer board

Plate 4.5 : Measurement of water level in manometer

4.4.2 Calibration of tank

The collecting tank was calibrated by pouring known volumes of water into the tank and noting the relevant manometer readings. The data from the calibration were used to write a computer program to calculate the average overtopping rate during each test.

The input to the program were the water levels in all three compartments both before and after a test, and the length of the test. For each water level entered the program calculates the volume by performing a linear interpolation between the nearest two levels found in the calibration data. The total volume obtained in this way is then divided by the test length and the crest length of the structure to obtain the average overtopping rate in $m^3/s/m$.

4.5 Replacement of lost water

If the rate of overtopping during a test were sufficient to fill the collecting tank then the water level in the flume would drop by 10,5 mm. This drop was undesirable because overtopping is very sensitive to the water level. A number of methods were considered to maintain a constant water level in the flume during a test.

The method selected was to allow water to flow into the flume from a constant head tank through a calibrated valve. The apparatus used is shown in Plate 4.6. A 167 litre drum located 1,6 m above the flume was used for the constant head tank. Water was supplied to the drum through a hosepipe and a 55 mm diameter pipe connected near the top of the drum was used as an overflow. Water was run into the flume through a 55 mm diameter pipe connected near the base of the drum. A calibrated valve was used to control the flow of water into the flume.

In order to ensure that the flow rate of water back into the flume was the same as the rate of water lost due to overtopping the procedure described below was followed. A range of overtopping rates were chosen and for each rate the level to which the water would rise in

the first compartment of the collecting tank after one minute of testing was calculated. These levels were marked on the manometer board. When the tests were performed the water level in the first compartment was read on the manometer board exactly one minute after starting the test and the calibrated valve was opened by the required amount to allow water to flow into the flume at the correct rate. This method proved to be accurate and the water level measured after a test never varied by more than 0,5 mm from that measured before the test.

Plate 4.6 : Constant head tank

4.6 The wave generator

4.6.1 Description of wave generator

The Seasim irregular wave generator has two paddles hinged at the bottom. These are driven by two low inertial D.C. servo-motors through an intermediate transmission and an adjustable pneumatic compensation unit balances the paddles against hydrostatic pressure. The Seasim wave generators are equipped with a wave absorption unit which detects the water level in front of the paddle using two resistance wires located on the face of each wave paddle and then determines how the movement of the paddle should be modified in order to absorb any reflected wave which is detected. The wave generator is shown in Plate 4.7.

The wave generator was driven by the programmable spectrum signal generator (PSSG) shown in Plate 4.8. This device numerically filters digital white noise generated by a shift register sequence into a required spectral shape and sends the required analog time series to the wave generator. The information required to program the PSSG are the spectrum shape, the peak wave period and the required cycle length of the time series. The wave height is controlled by adjusting the gain setting of the PSSG.

The cycle length of the time series depends on the number of data points used for each cycle and the clock interval between each point. It was decided to use 2048 data points for each cycle and to vary the clock interval between each point depending on the peak wave period being generated. The clock intervals were chosen so that 12 data points were used to describe the waveform during each time interval corresponding to the peak wave period. The clock intervals and cycle lengths for the three peak wave periods tested are given in Table 4.2.

T_p (s)	Clock Interval (ms)	Cycle Length (minutes:seconds)
1,2	100	3:24
2,1	175	5:58
3,0	250	8:32

Table 4.2 : Cycle lengths used to generate spectra

Since the length of each test was 10 minutes at least one complete cycle of waves was generated during each test. The wave generator automatically repeats the cycle after the end of a cycle is reached.

4.6.2 Wave spectrum shape

Various theoretical spectral shapes were discussed in Section 2.3.2. The Jonswap spectrum has been shown to correspond closely to storm spectra recorded at Slangkop, Cape Town, during the May 1984 storm [27] and was also the spectrum selected by Ahrens (Section 3.14) and Owen (Section 3.11) for their overtopping tests. The Jonswap spectrum was therefore selected for this thesis. The shape of Jonswap spectrum is given by eqn. (2.13). The peak enhancement factor, γ, was set to 3,3 and the values of δ_A and δ_B were 0,07 and 0,09 respectively.

Plate 4.7 : Seasim wave generator

Plate 4.8 : Programmable spectrum signal generator

4.7 Measurement of waves

Waves were measured by means of twin-wire resistance type probes (see Plate 4.9). The probes were connected by means of cables to an amplifier unit located in the instrumentation cabin. The amplifier unit was connected to an analog-to-digital converter and a data

acquisition unit. An Olivetti personal computer which could interface with the data acquisition unit as well as the CSIR mainframe computer was also used. The interior of the instrumentation cabin is shown in Plate 4.10.

Seven wave probes were used and were located at the positions indicated in Figure 4.1. Probes 6 and 7 were used to measure the incident wave spectrum at the structure toe. Probes 4 and 5 were used to measure the incident wave spectrum in transitional water. Probes 1, 2 and 3 were located in the central channel and were used to measure the incident spectrum in transitional water by separating the incident wave train from the reflected wave train. The linear wave shoaling equation (eqn. (2.6)) was used to calculate the deepwater wave height from the measurements made in transitional water.

4.7.1 Calibration of wave probes

Resistance wave probes work on the principle that the electrical resistance between the twin wires of the probe is inversely proportional to the water depth between the wires. The wave probes were calibrated each morning prior to testing to determine the calibration coefficients to be used in the wave analysis programs.

The calibration procedure was to lower each of the seven probes into the water in five 40 mm steps. The analog-to-digital converter was programmed to take 100 samples at each step at a sampling interval of 100 ms. The calibration data were then transferred to the personal computer and a linear regression analysis of the data was performed. The output of the analysis was the calibration coefficients for each wave probe as well as the correlation coefficients and a graphical display of the data. The calibration coefficients have the form 'x digital units per mm of water'. The correlation coefficients obtained in the regression analyses were 0,998 or better.

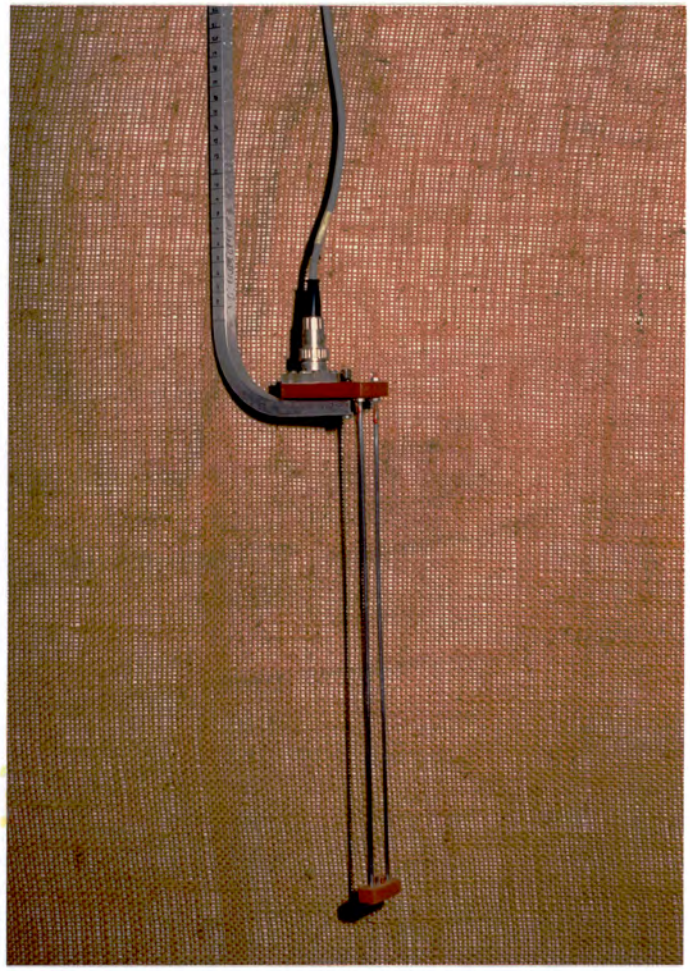

Plate 4.9 : Resistance wave probe

Plate 4.10 : Instrumentation cabin

4.7.2 Sampling of wave data during testing

In order to measure the exact wave spectrum generated the waves were measured over exactly one cycle of waves produced by the wave generator. This was done by programming the analog-to-digital converter to sample the water surface 2048 times at the same sampling rate as the clock interval used to generate the waves. The waves were therefore not measured for the full 10 minute test period but rather over the appropriate cycle length for the peak wave period being generated (see Table 4.2). The time during the test in which the waves were measured is indicated in Table 4.3. This time was chosen to be approximately in the middle of the 10 minute test period. During the remaining test time the same cycle is repeated by the wave generator.

T_p (s)	Time during which waves measured (minutes:seconds)
1,2	3:00 to 6:24
2,1	2:00 to 7:58
3,0	0:30 to 9:02

Table 4.3 : Sampling of wave data during testing

4.7.3 Single wave probe analysis

The wave data measured using probes 4, 5, 6 and 7 were analysed on the CSIR mainframe computer using a fast Fourier transform spectral analysis program developed by the CSIR. The program analyses the data in both the time and the frequency domain and extracts the relevant statistical parameters.

Typical graphic output of the program is shown in Figure 4.3. The measured wave spectrum is shown together with the target spectrum. Also shown graphically are the measured wave record, the distribution of wave height compared to the Rayleigh distribution and the wave steepness distribution. The wave parameters of direct interest for this thesis were the significant wave height, H_s, the peak wave period, T_p, and the ETA parameter which gives the goodness-of-fit between the target and measured spectra. A detailed explanation of the wave parameters calculated by this program is included in Appendix A.

In addition to the spectral analysis program described above a second program was also used. This program was run on the personal computer and was used to calculate the significant wave height at each wave probe based on the standard deviation of the water surface measurements. The measured wave record was also shown graphically on the computer monitor. Although neither the spectral shape nor peak wave period were calculated, this program was useful in identifying any errors in the wave data and was run directly after each test.

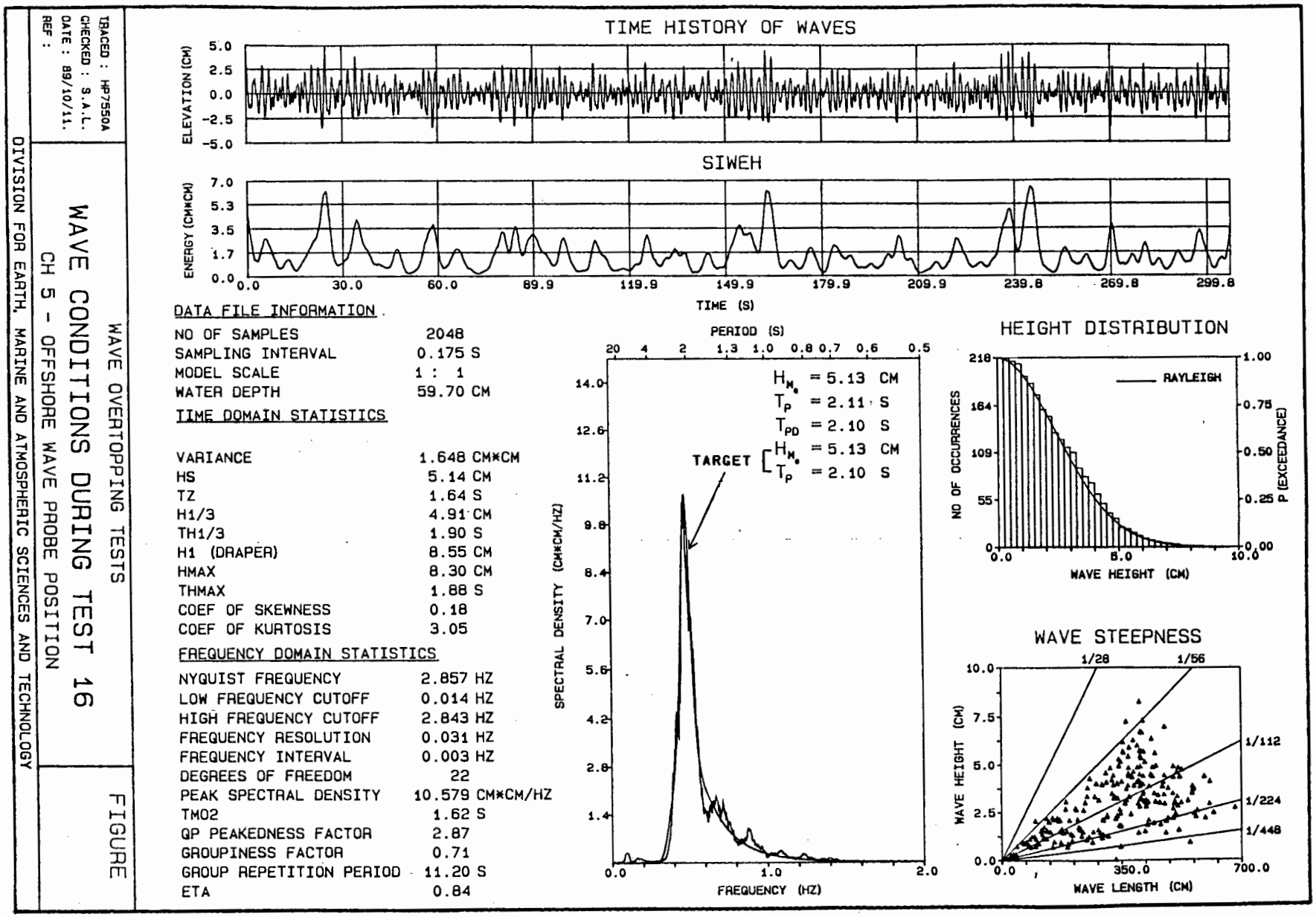

IRACED : HP7550A
CHECKED : S.A.L.
DATE : 89/10/11.
REF :

WAVE OVERTOPPING TESTS

WAVE CONDITIONS DURING TEST 16

CH 5 - OFFSHORE WAVE PROBE POSITION

FIGURE

DIVISION FOR EARTH, MARINE AND ATMOSPHERIC SCIENCES AND TECHNOLOGY

Figure 4.3

4.7.4 Separation of incident and reflected spectra

The wave data measured using probes 1, 2 and 3 were analysed on the personal computer and the incident spectrum from the wave generator was separated from the spectrum reflected from the model structure using a computer program developed by the CSIR. The method used by Mansard and Funke [28] is employed. This method uses a least squares technique to decompose the spectra from three simultaneous wave probe recordings into an incident and reflected spectrum.

The output of the program includes the significant wave height and peak wave period of both the incident and reflected spectra, the incident wave spectrum, and the reflection coefficient. The incident wave spectrum obtained in this way served to confirm the spectrum obtained using the single probe analysis of the data measured using probes 4 and 5.

The spacing between the three wave probes used were chosen according to the recommendations of Mansard and Funke [28] and are dependent on the wavelength associated with the peak wave period. The spacings which were used are given in Table 4.4.

T_p (s)	Distance between probes 1 and 2 (m)	Distance between probes 1 and 3 (m)
1,2	0,207	0,685
2,1	0,466	1,197
3,0	0,710	1,197

Table 4.4 : Spacings between probes 1, 2 and 3

CHAPTER 5

EXPERIMENTAL PROCEDURE

5.1 Test conditions

The model structures and water levels which were tested are given in Table 5.1 and illustrated in Figure 5.1.

Model structure	Water levels (mm)
100 mm vertical wall	25 ; 50 ; 75
100 mm wall with 45^0 slope	25 ; 50 ; 75
200 mm vertical wall	120 ; 160

Table 5.1 : Model structures and water levels tested

The wave conditions which were tested are given in Table 5.2. Approximately four different wave heights were generated for each water level and wave period. The wave heights were chosen so that the smallest height just overtopped the structure while the largest caused severe overtopping. The test conditions detailed above resulted in 111 different tests.

Spectrum type	T_p (s)	H_{so} (mm)
Jonswap	1,2 ; 2,1 ; 3,0	15 to 125

Table 5.2 : Wave conditions tested

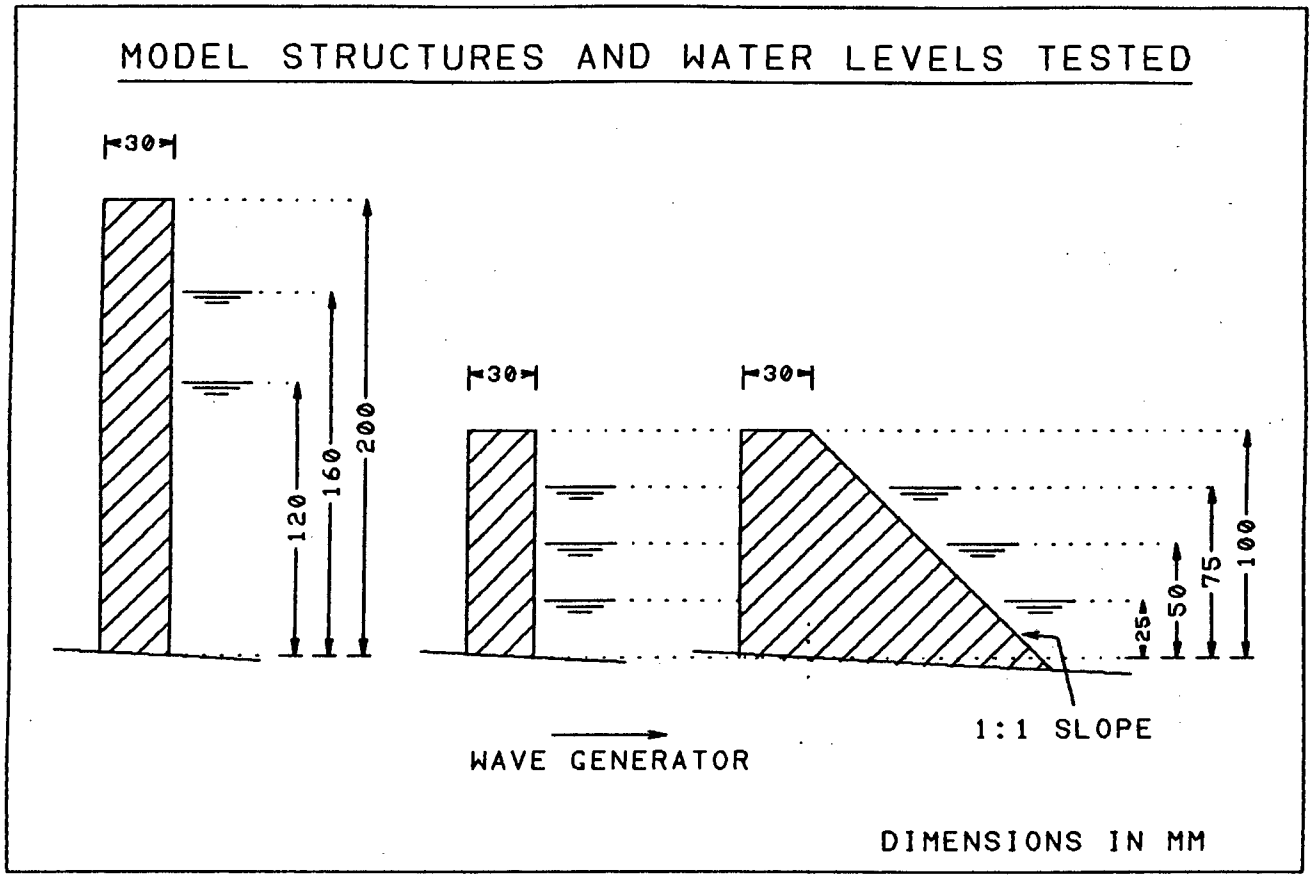

Figure 5.1

The dimensions of the model structures, as well as the wave characteristics and water depths tested were selected so that the results of the model tests could be scaled up to realistic prototype conditions using Froude modelling laws. Table 5.3 below illustrates how the model tests could be scaled up to typical prototype structures.

	h_c (m)	T_p (s)	H_{so} (m)
Model	0,1 or 0,2	1,2 to 3,0	0,015 to 0,125
Prototype (scale 1:20)	2,0	5,4 to 13,4	0,3 to 2,5
Prototype (scale 1:50)	10,0	8,5 to 21,2	0,75 to 6,3

Table 5.3 : Model and prototype test conditions

When the 100 mm high wall is considered at a scale of 1:20 the conditions obtained are typical of a tidal pool situation where sufficient overtopping must be obtained from relatively small waves. When the 200 mm high wall is considered at a scale of 1:50 the conditions are more typical of a larger structure such as seawall or breakwater subjected to storm waves. The test conditions were therefore thought to be realistic and could be applied to a wide range of prototype structures.

5.2 Description of test procedure

The experimental data from each test was entered in a worksheet. An example of the worksheet used is given in Figure 5.2.

WAVE OVERTOPPING WORKSHEET

TEST NUMBER : .....

DATE : .....

MODEL HEIGHT (mm) : .....

WAVE GENERATOR SETTINGS : T_P (s) : .....
Gain : .....

DEPTH AT STRUCTURE (mm) : Before : .....
After : .....
Average : .....

LEVELS IN COLLECTING TANK (mm) :

	Before Test	After Test
Compartment A :	.....	.....
Compartment B :	.....	.....
Compartment C :	.....	.....

TEST LENGTH (min) : .....

WAVE MEASUREMENTS :

	H_s (mm)	T_P (s)
Probes 6 and 7 (average) :	.....	.....
Probes 4 and 5 (average) :	.....	.....
Probes 1,2,3 (incident wave):	.....	.....

REFLECTION COEFFICIENT (%) : .....

AVERAGE BREAKER DEPTH (mm) : .....

BREAKER TYPE : .....

COMMENTS ON WAVE SPECTRUM : .....
.....
.....

OVERTOPPING RATE ($dm^3/s/m$) : .....

COMMENTS ON OVERTOPPING: .....
.....
.....
.....

Figure 5.2

5.2.1 Procedure followed prior to a test

The seven wave probes were calibrated each day prior to testing. The calibration procedure was described in Section 4.7.1. Before each test or calibration the water in the flume was thoroughly mixed using a paddle and by switching on the wave generator. This ensured that the water did not form horizontal layers of differing electrical conductivity which would influence the wave probe measurements.

The water level in the flume was then adjusted to the required level. Water was drained from the collecting tank and the initial water levels in each of the three compartments of the collecting tank were read on the manometers and noted in the worksheet.

The pneumatic compensation unit of the wave generator was adjusted to correspond with the water level in the flume. The programmable spectrum signal generator was then programmed to generate a Jonswap spectrum with the required peak period. The gain setting on the PSSG was adjusted to obtain the approximate wave height required. The memory of the data acquisition unit was cleared and the analog-to-digital converter was programmed to sample the signal from the wave probes at the required rate corresponding to the wave period to be tested (see Section 4.7.2).

Finally, the water supply to the constant head tank was turned on.

5.2.2 Procedure followed during a test

The wave generator was started and the test was timed from the moment when the first wave arrived at the model structure. The wave measurement system was then started at the appropriate time listed in Table 4.3. The wave measurement proceeded automatically until 2048 water levels had been sampled at each probe position.

After one minute of testing the water level in the collecting tank was noted and the valve from the constant head tank was opened by the required amount in order to replace the water lost from the flume due to the overtopping (see Section 4.5).

The position at which the waves broke in the two side channels of the flume was also recorded during each test. The breaker position was defined as the position at which the wave crest first became vertical. Vertical lines were drawn on the side of the flume at 0,4 m intervals and each zone defined in this way was numbered. As each wave broke the number of the zone where the breaking occurred was written down. Approximately 100 waves were observed for this purpose. Waves which were not large enough to be clearly defined were ignored. The type of wave breaking (spilling, plunging or surging) as well as the type of overtopping which occurred were also noted in the worksheet.

At the end of the 10 minute test a hinged wooden flap was lowered across the central channel in front of the model structure to prevent any further overtopping. The wave generator was then switched off. The valve between the constant head tank and the flume was closed and the water supply to the constant head tank stopped.

Approximately one quarter of the tests were later repeated to allow the tests to be recorded on video. A number of tests were also repeated to allow photographs of the overtopping process to be taken. For these tests a purple dye was placed in the central channel so that the waves in the central channel could be easily differentiated from those in the side channels.

5.2.3 Procedure followed after a test

When the water surface in the flume had settled the water level in the flume as well the water levels in the three compartments of the collecting tank were measured and recorded in the worksheet.

The wave data from the acquisition unit were transferred to the personal computer and a preliminary check on the data was performed using the computer program described in Section 4.7.3. If no errors were identified the next test was then proceeded with.

At a later stage the wave data measured using probes 4, 5, 6 and 7 were transferred to the CSIR mainframe computer where the spectral analysis program described in Section 4.7.3 was used to determine the significant wave height and peak wave period. The average of the wave heights and periods calculated at probes 4 and 5, and at probes 6 and 7 were entered in the worksheet. The wave data measured at probes 1, 2 and 3 were analysed to separate the incident spectrum from the reflected spectrum using the program described in Section 4.7.4. The significant wave height and peak wave period of the incident wave train as well as the reflection coefficient were entered in the worksheet.

The average breaker depth was then calculated from the observations of the zones in which the breaking occurred. The overtopping rate was determined using the program described in Section 4.4.2 and was entered in the worksheet. The experimental results which were obtained using the procedure described above are given in the following chapter.

CHAPTER 6

EXPERIMENTAL RESULTS

6.1 Tabulated results

The experimental results were transferred from the overtopping work-sheets into a LOTUS 123 spreadsheet. Tables 6.1, 6.2 and 6.3 show the experimental results for the 100 mm vertical wall, the 200 mm vertical wall and the 100 mm wall with a 45° slope.

The methods used to calculate the parameters in Tables 6.1, 6.2 and 6.3 are described below :

d_s = average of the water depth measured at the structure toe before and after the test

F = average freeboard measured

T_{gen} = peak wave period programmed into wave generator

T_p = peak wave period calculated as the average of the peak wave periods measured at wave probes 4 and 5 (refer to Figure 4.1 for the probe locations)

$(T_p)_{sep}$ = peak wave period calculated by separating the incident and reflected wave trains measured using probes 1, 2 and 3

H_{st} = significant wave height in transitional water calculated as the average of the significant wave heights measured at probes 4 and 5

$(H_{st})_{sep}$ = significant wave height in transitional water calculated by separating the incident and reflected spectra measured using probes 1, 2 and 3

H_{so} = deepwater significant wave height calculated using H_{st} and the linear wave shoaling equation (eqn. (2.6))

H_{si} = significant wave height at the structure toe calculated as the average of the significant wave heights measured at probes 6 and 7

L_{po} = deepwater wavelength calculated using eqn. (2.4) and T_p

L_{pi} = wavelength at structure toe calculated using eqn. (2.3) and T_p

Refl = reflection coefficient measured using probes 1, 2 and 3

d_b = average breaker depth observed in the side channels of the flume

Q = overtopping rate measured

The wave parameters calculated by separating the incident and reflected spectra measured in the central channel, namely $(T_p)_{sep}$ and $(H_{st})_{sep}$, were found to be within 15 % of those obtained by measuring the incident spectrum directly in the side channel of the flume, namely T_p and H_{st}. The reasons for the differences are thought to be due to the assumptions upon which the method for separating the incident and reflected spectra is based (Mansard and Funke [28]). These assumptions are that irregular waves can be described as a linear superposition of discrete components and that each component travels at its own phase velocity as described by the dispersion relation. For the analysis of the experimental results the parameters measured in the side channel of the flume will be used as these are considered to be more accurate than those measured in the central channel.

Ref. no.	d_s (mm)	F (mm)	T_{gen} (s)	T_p (s)	$(T_p)_{sep}$ (s)	H_{st} (mm)	$(H_{st})_{sep}$ (mm)	H_{so} (mm)	H_{s1} (mm)	L_{po} (mm)	L_{p1} (mm)	Refl (%)	d_b (mm)	Q ($dm^3/s/m$)
1	25.0	75.0	1.20	1.17	1.16	60.5	60.1	64.7	29.7	2137	572	12.0	52	0.0215
2	25.0	75.0	1.20	1.17	1.16	85.7	84.9	91.7	33.8	2137	572	12.2	78	0.0313
3	25.0	75.0	1.20	1.17	1.14	98.6	96.7	105.5	36.4	2137	572	10.3	82	0.0397
4	25.0	75.0	1.20	1.17	1.14	119.9	117.4	128.3	38.6	2137	572	12.6	101	0.0552
5	25.0	75.0	2.10	2.09	2.13	29.1	29.6	30.5	31.2	6820	1031	36.1	38	0.0094
6	25.0	75.0	2.10	2.08	2.08	43.0	43.4	45.1	38.1	6755	1026	20.9	49	0.0153
7	25.0	75.0	2.10	2.11	2.08	70.4	71.7	73.6	51.4	6951	1041	16.2	72	0.0599
8	25.0	75.0	2.10	2.08	1.99	95.4	96.4	100.1	62.0	6755	1026	13.2	87	0.1615
9	25.0	75.0	2.10	2.08	2.04	102.9	102.7	108.0	65.5	6755	1026	13.7	93	0.1931
10	25.0	75.0	3.00	2.97	2.98	38.7	38.8	36.3	33.5	13772	1468	34.1	48	0.0091
11	25.0	75.0	3.00	3.14	2.98	50.7	50.4	46.6	38.6	15394	1552	19.4	62	0.0193
12	25.0	75.0	3.00	3.04	2.91	64.0	63.8	59.6	43.0	14429	1503	19.5	74	0.0366
13	25.5	74.5	3.00	2.98	2.91	75.1	74.3	70.4	46.5	13865	1488	17.4	84	0.0694
14	25.0	75.0	3.00	2.97	2.84	90.7	89.7	85.1	53.4	13772	1468	14.0	99	0.1223
15	50.0	50.0	1.20	1.19	1.19	25.3	29.2	27.0	28.6	2211	814	50.1	27	0.0372
16	50.0	50.0	1.20	1.19	1.22	49.8	53.1	53.2	43.0	2211	814	34.0	47	0.2114
17	50.0	50.0	1.20	1.20	1.16	102.8	104.2	110.1	48.6	2248	821	16.0	93	0.4700
18	50.0	50.0	1.20	1.18	1.19	124.2	126.9	132.6	51.8	2174	806	15.3	108	0.6426
19	50.0	50.0	2.10	2.10	2.08	16.5	18.8	17.4	24.2	6885	1460	78.6	24	0.0145
20	50.0	50.0	2.10	2.10	2.13	19.6	21.2	20.6	26.8	6885	1460	79.5	28	0.0262
21	50.0	50.0	2.10	2.14	2.09	23.9	25.2	25.0	31.9	7150	1488	79.0	32	0.0572
22	50.0	50.0	2.10	2.10	2.04	47.6	49.2	50.1	43.3	6885	1460	42.9	57	0.2774
23	49.5	50.5	2.10	2.08	2.04	78.2	76.5	82.5	52.5	6755	1438	24.6	78	0.5514
24	49.5	50.5	2.10	2.10	2.04	104.9	102.2	110.4	59.5	6885	1452	17.5	98	0.9384
25	50.0	50.0	2.10	2.08	2.11	106.2	104.1	111.9	62.3	6755	1445	19.6	105	1.0250
26	50.0	50.0	3.00	3.08	2.84	22.0	25.9	20.5	32.2	14811	2149	80.9	34	0.0583
27	49.8	50.2	3.00	3.09	2.84	32.1	30.6	29.9	38.9	14908	2152	70.0	41	0.1033
28	50.0	50.0	3.00	3.04	2.84	43.8	41.2	41.1	44.8	14429	2121	57.4	53	0.2135
29	50.0	50.0	3.00	3.04	2.72	62.1	66.0	58.3	50.2	14429	2121	38.7	76	0.4861
30	49.8	50.2	3.00	3.02	2.98	83.7	88.0	78.7	56.5	14240	2103	20.1	94	0.7278
31	75.0	25.0	1.20	1.17	1.25	21.0	24.2	22.3	22.9	2137	967	46.9	25	0.0274
32	75.0	25.0	1.20	1.17	1.16	25.7	29.1	27.3	27.9	2137	967	49.2	29	0.0825
33	75.0	25.0	1.20	1.19	1.19	42.3	46.6	45.0	44.5	2211	984	38.4	42	0.5701
34	75.2	24.8	1.20	1.20	1.22	51.0	57.8	54.4	49.3	2248	994	31.7	50	0.8653
35	75.5	24.5	1.20	1.20	1.16	57.0	60.2	60.8	53.9	2248	996	29.7	53	1.1207
36	75.0	25.0	1.20	1.20	1.22	65.3	68.1	69.6	58.4	2248	993	26.6	61	1.4514
37	75.0	25.0	2.10	2.10	2.04	17.3	19.6	18.3	21.7	6885	1781	79.0	25	0.0397
38	75.0	25.0	2.10	2.10	2.04	25.9	27.8	27.4	32.4	6885	1781	78.9	32	0.2158
39	75.0	25.0	2.10	2.11	1.99	35.0	38.0	37.0	42.9	6951	1789	64.0	41	0.5148
40	75.0	25.0	2.10	2.11	2.04	42.0	44.7	44.4	48.1	6951	1789	57.9	46	0.8347
41	74.8	25.2	2.10	2.09	1.99	50.9	55.4	53.9	53.5	6820	1770	46.4	56	1.1804
42	73.8	26.2	2.10	2.10	2.04	51.3	54.4	54.2	53.9	6885	1767	47.4	55	1.1377
43	75.0	25.0	3.00	3.02	2.67	23.7	25.5	22.5	34.3	14240	2576	83.0	35	0.2193
44	75.0	25.0	3.00	2.98	2.67	33.0	33.5	31.4	44.7	13865	2542	74.7	41	0.5239
45	75.3	24.7	3.00	2.96	2.67	38.3	41.1	36.6	50.2	13680	2529	66.9	50	0.8379
46	75.3	24.7	3.00	2.98	2.67	47.7	48.9	45.4	55.4	13865	2547	60.9	57	1.2196

Table 6.1 : Experimental results for 100 mm vertical wall

Ref. no.	d_s (mm)	F (mm)	T_{gen} (s)	T_p (s)	$(T_p)_{sep}$ (s)	H_{st} (mm)	$(H_{st})_{sep}$ (mm)	H_{so} (mm)	H_{si} (mm)	L_{po} (mm)	L_{pi} (mm)	Refl (%)	d_b (mm)	Q ($dm^3/s/m$)
47	120.0	80.0	1.20	1.16	1.19	43.3	48.9	45.5	46.4	2101	1183	53.3	41	0.0166
48	119.8	80.2	1.20	1.19	1.19	58.1	65.7	61.4	59.8	2211	1217	50.4	54	0.1202
49	120.0	80.0	1.20	1.11	1.19	73.9	77.8	77.0	71.3	1924	1125	48.8	67	0.3103
50	120.0	80.0	1.20	1.09	1.11	89.7	98.3	93.1	78.9	1855	1102	38.2	78	0.4695
51	120.0	80.0	1.20	1.20	1.16	112.0	125.2	118.6	84.2	2248	1229	33.3	105	0.8885
52	120.0	80.0	2.10	2.10	2.13	36.2	41.5	38.6	48.8	6885	2237	81.9	46	0.0343
53	120.0	80.0	2.10	1.99	2.13	43.7	48.4	47.0	58.0	6183	2115	78.4	50	0.0958
54	120.0	80.0	2.10	1.99	2.13	61.1	67.1	65.7	73.5	6183	2115	73.1	71	0.4539
55	119.5	80.5	2.10	2.10	2.13	73.2	79.4	78.0	81.2	6885	2232	66.0	75	0.7754
56	119.5	80.5	2.10	2.10	2.13	88.7	93.3	94.5	89.0	6885	2232	57.3	96	1.2458
57	120.0	80.0	3.00	3.00	2.98	34.0	37.5	32.7	45.8	14052	3226	93.5	50	0.0480
58	120.0	80.0	3.00	3.00	2.98	40.4	43.8	38.9	55.5	14052	3226	94.3	52	0.1429
59	119.8	80.2	3.00	3.00	2.91	52.9	56.9	50.9	69.4	14052	3223	86.9	68	0.4017
60	119.5	80.5	3.00	3.00	2.91	65.1	68.9	62.7	78.9	14052	3219	77.9	77	0.6326
61	119.8	80.2	3.00	3.00	3.05	89.6	89.8	86.3	90.6	14052	3223	63.7	92	1.3052
62	160.0	40.0	1.20	1.18	1.16	39.2	42.6	41.1	33.4	2174	1364	51.2	36	0.0250
63	160.0	40.0	1.20	1.16	1.22	41.6	46.9	43.5	35.6	2101	1337	49.1	37	0.0477
64	159.8	40.2	1.20	1.16	1.16	63.5	70.3	66.4	53.7	2101	1336	44.4	58	0.4089
65	160.0	40.0	1.20	1.17	1.19	71.3	75.7	74.6	61.3	2137	1350	45.1	67	0.6371
66	160.0	40.0	1.20	1.11	1.16	81.9	87.4	84.8	69.2	1924	1269	45.3	80	1.0541
67	160.0	40.0	2.10	2.10	2.04	25.3	27.0	27.1	31.5	6885	2567	80.5	31	0.0095
68	160.0	40.0	2.10	2.19	2.04	31.0	35.3	32.9	38.4	7488	2682	79.6	41	0.0697
69	159.5	40.5	2.10	2.10	2.04	42.0	46.0	45.0	47.7	6885	2563	79.4	55	0.3233
70	160.0	40.0	2.10	2.10	2.04	48.1	51.7	51.5	54.6	6885	2567	73.1	57	0.5747
71	160.0	40.0	2.10	2.17	2.04	60.9	66.3	64.8	66.7	7352	2657	66.7	74	1.2472
72	160.0	40.0	3.00	3.09	2.84	24.3	24.9	23.4	30.4	14908	3828	88.7	30	0.0251
73	160.0	40.0	3.00	3.09	2.84	26.5	28.9	25.5	33.2	14908	3828	86.8	35	0.0502
74	160.2	39.8	3.00	3.00	2.84	39.3	40.9	38.2	51.8	14052	3716	85.2	46	0.3232
75	159.8	40.2	3.00	3.07	2.78	54.4	56.9	52.5	64.1	14715	3800	81.2	68	0.9471
76	160.0	40.0	3.00	3.09	2.78	60.0	61.9	57.8	71.0	14908	3828	79.1	78	1.3065

Table 6.2 : Experimental results for 200 mm vertical wall

Ref. no.	d_s (mm)	F (mm)	T_{gen} (s)	T_p (s)	$(T_p)_{sep}$ (s)	H_{st} (mm)	$(H_{st})_{sep}$ (mm)	H_{so} (mm)	H_{s1} (mm)	L_{po} (mm)	L_{p1} (mm)	Refl (%)	d_b (mm)	Q ($dm^3/s/m$)
77	25.0	75.0	1.20	1.16	1.16	29.3	32.0	31.3	21.9	2101	567	33.1	29	0.0358
78	25.0	75.0	1.20	1.16	1.19	51.4	55.2	54.9	26.9	2101	567	19.0	47	0.0739
79	25.0	75.0	1.20	1.17	1.16	96.0	98.5	102.7	34.5	2137	572	12.2	86	0.1512
80	25.0	75.0	1.20	1.17	1.19	118.0	121.0	126.3	37.0	2137	572	10.7	110	0.1689
81	25.0	75.0	2.10	2.08	2.19	16.7	17.9	17.5	19.8	6755	1026	69.6	25	0.0164
82	25.0	75.0	2.10	2.07	2.13	35.7	36.1	37.5	26.9	6690	1021	40.1	44	0.0568
83	25.0	75.0	2.10	2.13	2.19	67.2	70.8	70.1	40.6	7084	1051	19.3	74	0.2076
84	25.2	74.8	2.10	2.10	2.08	99.4	102.7	104.0	51.3	6885	1036	15.8	100	0.4557
85	25.0	75.0	3.00	3.00	2.98	17.2	18.0	16.1	22.9	14052	1483	72.1	25	0.0113
86	25.0	75.0	3.00	2.97	2.91	45.2	45.7	42.4	36.3	13772	1468	36.4	56	0.0983
87	25.0	75.0	3.00	3.00	2.84	64.5	64.6	60.3	43.1	14052	1483	25.4	77	0.1930
88	25.2	74.8	3.00	2.98	2.98	86.7	86.0	81.3	50.4	13865	1479	20.0	93	0.3353
89	50.0	50.0	1.20	1.15	1.22	23.8	27.3	25.3	26.2	2065	785	43.4	25	0.0463
90	49.5	50.5	1.20	1.19	1.22	30.7	34.5	32.8	32.9	2211	810	41.4	33	0.1379
91	49.8	50.2	1.20	1.17	1.22	77.4	81.4	82.5	46.4	2137	798	19.5	65	0.7561
92	50.0	50.0	1.20	1.20	1.16	111.3	114.6	119.2	48.5	2248	821	13.9	98	1.0541
93	50.0	50.0	2.10	2.10	2.08	14.7	15.9	15.5	21.1	6885	1460	86.5	24	0.0090
94	50.0	50.0	2.10	2.10	2.08	20.6	22.3	21.7	28.0	6885	1460	78.7	28	0.0698
95	50.0	50.0	2.10	2.10	2.13	30.4	31.7	32.0	36.2	6885	1460	68.0	42	0.2683
96	50.2	49.8	2.10	2.10	2.04	66.5	68.0	70.0	50.6	6885	1462	32.6	70	0.9550
97	50.0	50.0	3.00	3.08	2.78	15.0	15.6	14.0	21.5	14811	2149	92.9	24	0.0065
98	50.0	50.0	3.00	3.09	2.78	22.0	23.4	20.5	31.6	14908	2156	88.7	32	0.1023
99	50.0	50.0	3.00	3.03	3.20	56.4	57.7	53.0	51.2	14334	2114	48.5	71	0.7966
100	50.2	49.8	3.00	3.03	2.72	82.1	80.6	77.1	59.4	14334	2119	32.6	81	1.3878
101	75.0	25.0	1.20	1.18	1.25	17.1	19.1	18.2	17.3	2174	975	51.1	23	0.0147
102	75.0	25.0	1.20	1.20	1.16	26.7	30.9	28.5	27.0	2248	993	39.7	29	0.1674
103	74.0	26.0	1.20	1.19	1.19	44.0	49.3	46.9	43.5	2211	978	30.9	41	0.8232
104	75.0	25.0	1.20	1.20	1.19	59.4	63.0	63.4	53.5	2248	993	26.3	56	1.5292
105	75.0	25.0	2.10	2.10	2.24	13.3	14.8	14.1	16.7	6885	1781	78.8	23	0.0170
106	75.0	25.0	2.10	2.12	2.24	20.9	22.6	22.1	27.0	7017	1798	74.4	33	0.1861
107	75.5	24.5	2.10	2.09	2.04	32.6	35.0	34.5	41.0	6820	1778	57.7	42	0.7146
108	75.0	25.0	2.10	2.10	1.99	49.3	51.2	52.1	53.1	6885	1781	43.4	57	1.4094
109	75.0	25.0	3.00	3.00	2.67	19.9	22.4	18.9	29.1	14052	2559	81.9	33	0.1746
110	75.0	25.0	3.00	3.00	2.67	31.2	33.7	29.7	42.7	14052	2559	72.3	45	0.6763
111	75.5	24.5	3.00	3.03	2.72	39.2	39.3	37.1	49.9	14334	2593	66.1	48	1.0606

Table 6.3 : Experimental results for 100 mm wall with 45° slope

6.2 Graphical presentation

The influence of the significant wave height, peak wave period and water depth at the structure toe on the rate of overtopping is illustrated in Figures 6.1 to 6.6.

In Figures 6.1, 6.2 and 6.3 the overtopping rate is graphed against the deepwater significant wave height. It can be seen that the overtopping increases as the wave height increases and as the water depth increases. For a particular wave height and depth at the toe of the structure the overtopping increases with increasing wave period.

In Figures 6.4, 6.5 and 6.6 the overtopping is graphed against the significant wave height measured at the structure toe. The overtopping again increases as the wave height increases and as the water depth increases. In these graphs the curves representing the three different wave periods for a particular water depth lie closer together than was the case for deepwater wave height. There is no obvious relation between the overtopping and the wave period.

The reason for these curves lying closer together is due to the influence of the deepwater wave steepness on the wave shoaling and breaking which occurred between deep water and the structure toe. Figure 6.7 shows a graph developed by Goda [2] to estimate wave heights in shallow water. It can be seen that for two waves having equal deepwater wave heights the wave with the lower deepwater wave steepness (or longer wave period) will have a larger wave height when the waves reach shallow water. This causes the curves for the three different periods to lie closer together in Figures 6.4 to 6.6 compared to Figures 6.1 to 6.3 and is the primary reason why a deepwater wave with a longer wave period causes more overtopping than one with a shorter period.

OVERTOPPING RATE vs DEEPWATER SIGNIFICANT WAVE HEIGHT

Vertical Wall h_c = 100 mm

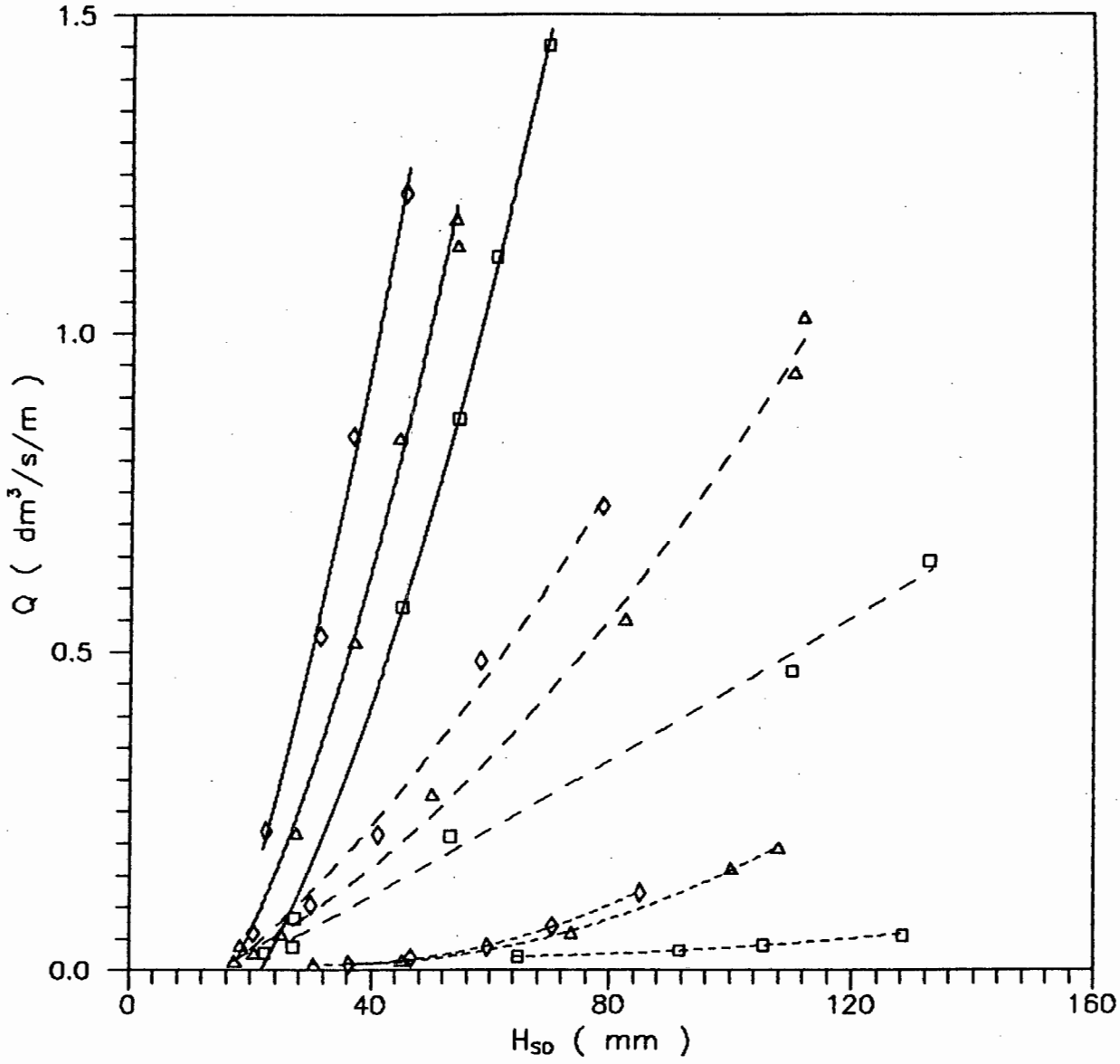

□□□□□ T_P = 1,2 s
△△△△△ T_P = 2,1 s
◇◇◇◇◇ T_P = 3,0 s
] d_s = 25 mm

□□□□□ T_P = 1,2 s
△△△△△ T_P = 2,1 s
◇◇◇◇◇ T_P = 3,0 s
] d_s = 50 mm

□□□□□ T_P = 1,2 s
△△△△△ T_P = 2,1 s
◇◇◇◇◇ T_P = 3,0 s
] d_s = 75 mm

Figure 6.1

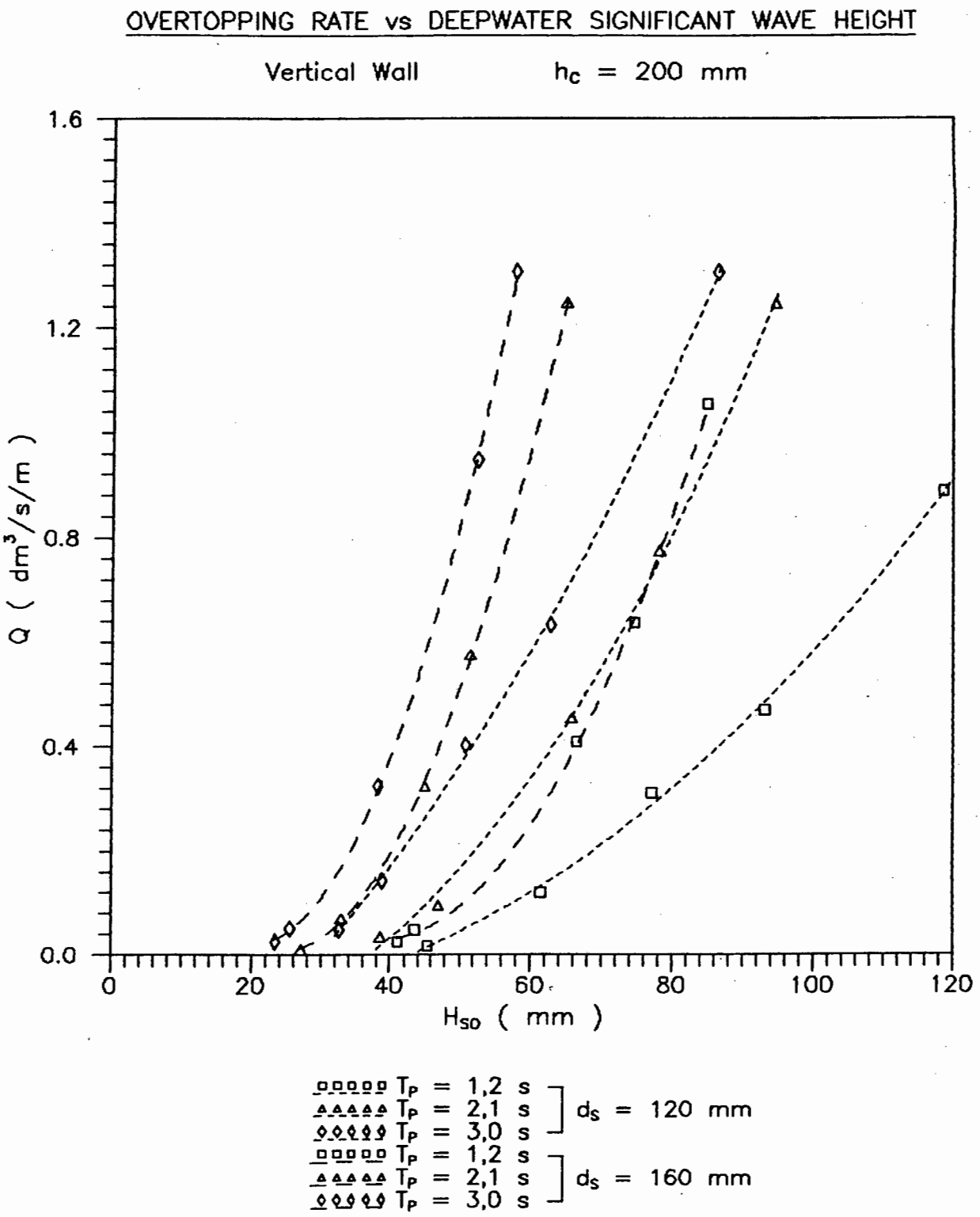
OVERTOPPING RATE vs DEEPWATER SIGNIFICANT WAVE HEIGHT
Vertical Wall
h_c = 200 mm
Q ($dm^3/s/m$)
1.6
1.2
0.8
0.4
0.0
0
20
40
60
80
100
120
H_{so} (mm)
T_p = 1,2 s
T_p = 2,1 s
T_p = 3,0 s
d_s = 120 mm
T_p = 1,2 s
T_p = 2,1 s
T_p = 3,0 s
d_s = 160 mm

Figure 6.2

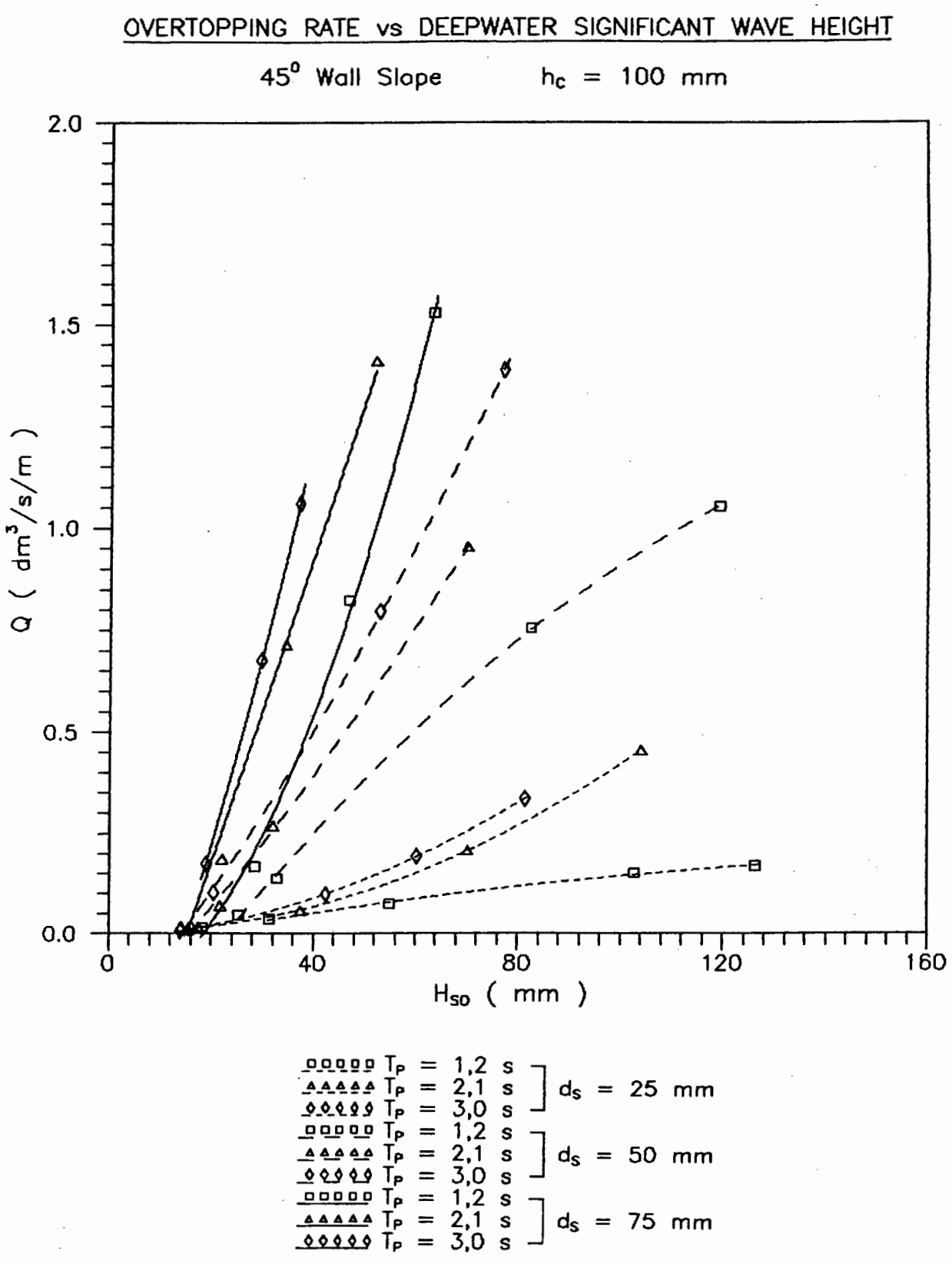
OVERTOPPING RATE vs DEEPWATER SIGNIFICANT WAVE HEIGHT
45° Wall Slope
h_c = 100 mm
Q ($dm^3/s/m$)
2.0
1.5
1.0
0.5
0.0
0
40
80
120
160
H_{so} (mm)
T_P = 1,2 s
T_P = 2,1 s
T_P = 3,0 s
d_s = 25 mm
T_P = 1,2 s
T_P = 2,1 s
T_P = 3,0 s
d_s = 50 mm
T_P = 1,2 s
T_P = 2,1 s
T_P = 3,0 s
d_s = 75 mm

Figure 6.3

OVERTOPPING RATE vs SIGNIFICANT WAVE HEIGHT AT STRUCTURE

Vertical Wall h_c = 100 mm

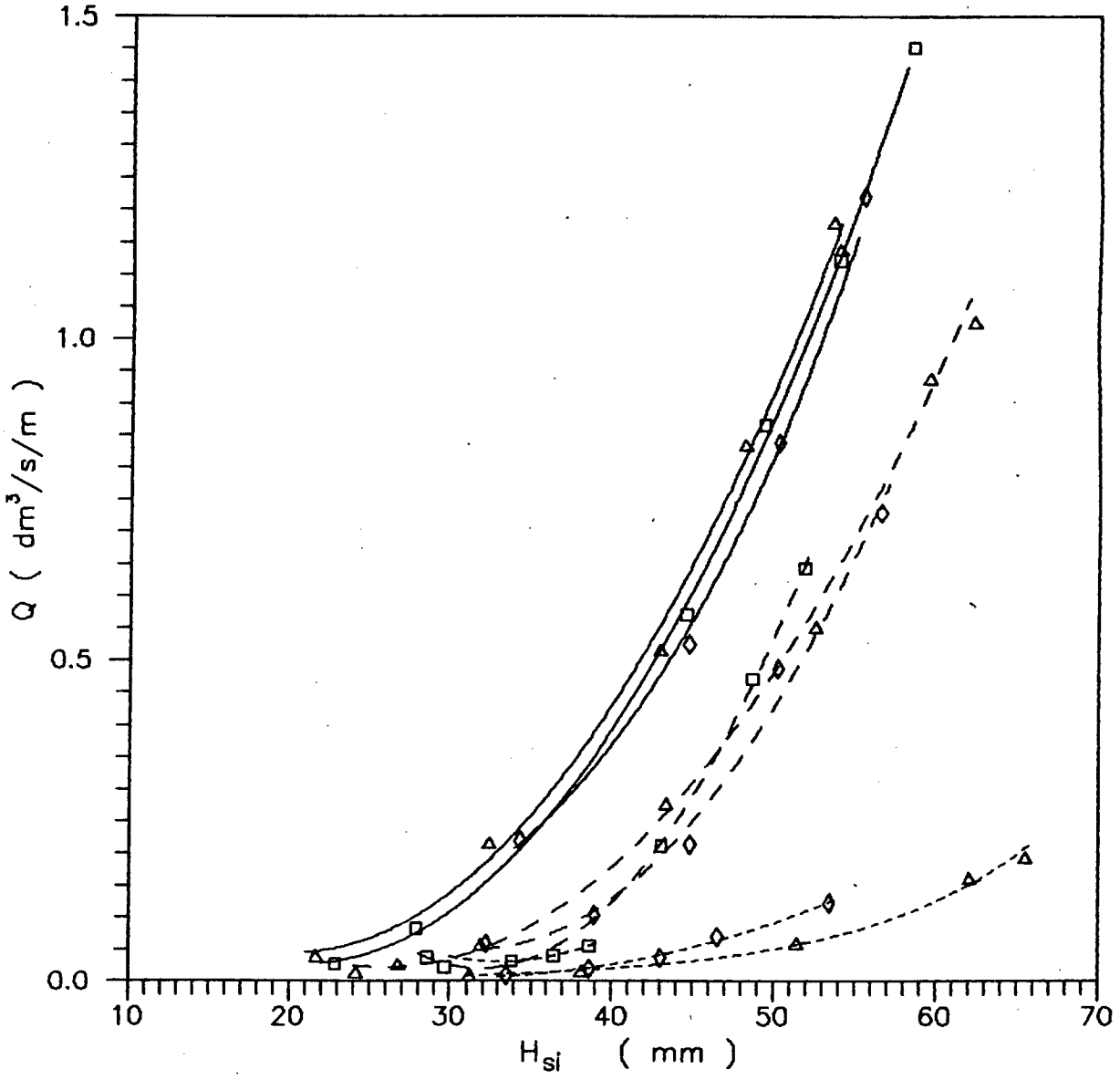

□□□□□ T_P = 1,2 s
△△△△△ T_P = 2,1 s
◇◇◇◇◇ T_P = 3,0 s
] d_s = 25 mm

□□□□□ T_P = 1,2 s
△△△△△ T_P = 2,1 s
◇◇◇◇◇ T_P = 3,0 s
] d_s = 50 mm

□□□□□ T_P = 1,2 s
△△△△△ T_P = 2,1 s
◇◇◇◇◇ T_P = 3,0 s
] d_s = 75 mm

Figure 6.4

OVERTOPPING RATE vs SIGNIFICANT WAVE HEIGHT AT STRUCTURE

Vertical Wall h_c = 200 mm

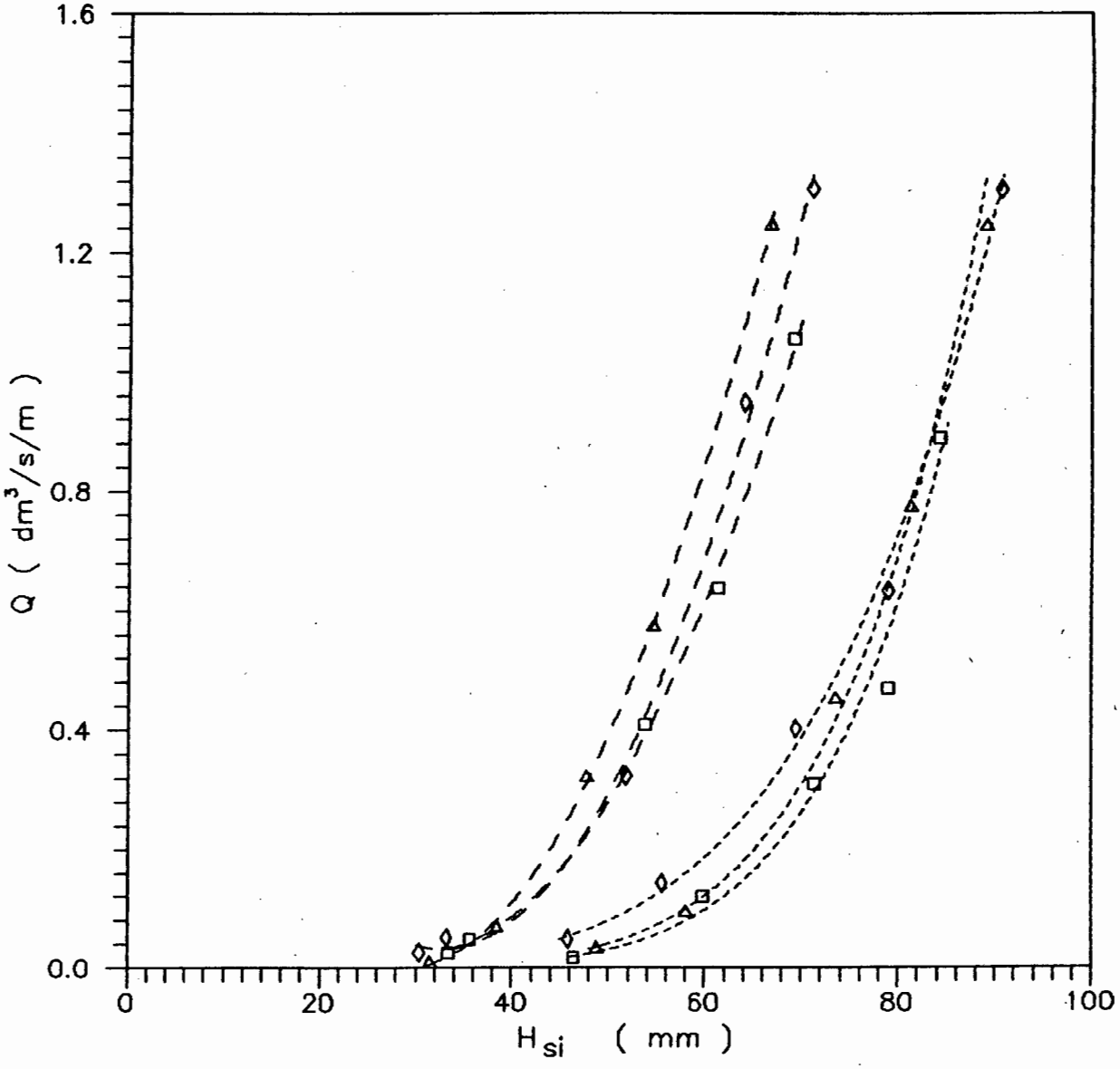

□□□□□ T_P = 1,2 s
△△△△△ T_P = 2,1 s
◇◇◇◇◇ T_P = 3,0 s
] d_s = 120 mm

□□□□□ T_P = 1,2 s
△△△△△ T_P = 2,1 s
◇◇◇◇◇ T_P = 3,0 s
] d_s = 160 mm

Figure 6.5

OVERTOPPING RATE vs SIGNIFICANT WAVE HEIGHT AT STRUCTURE

45° Wall Slope h_c = 100 mm

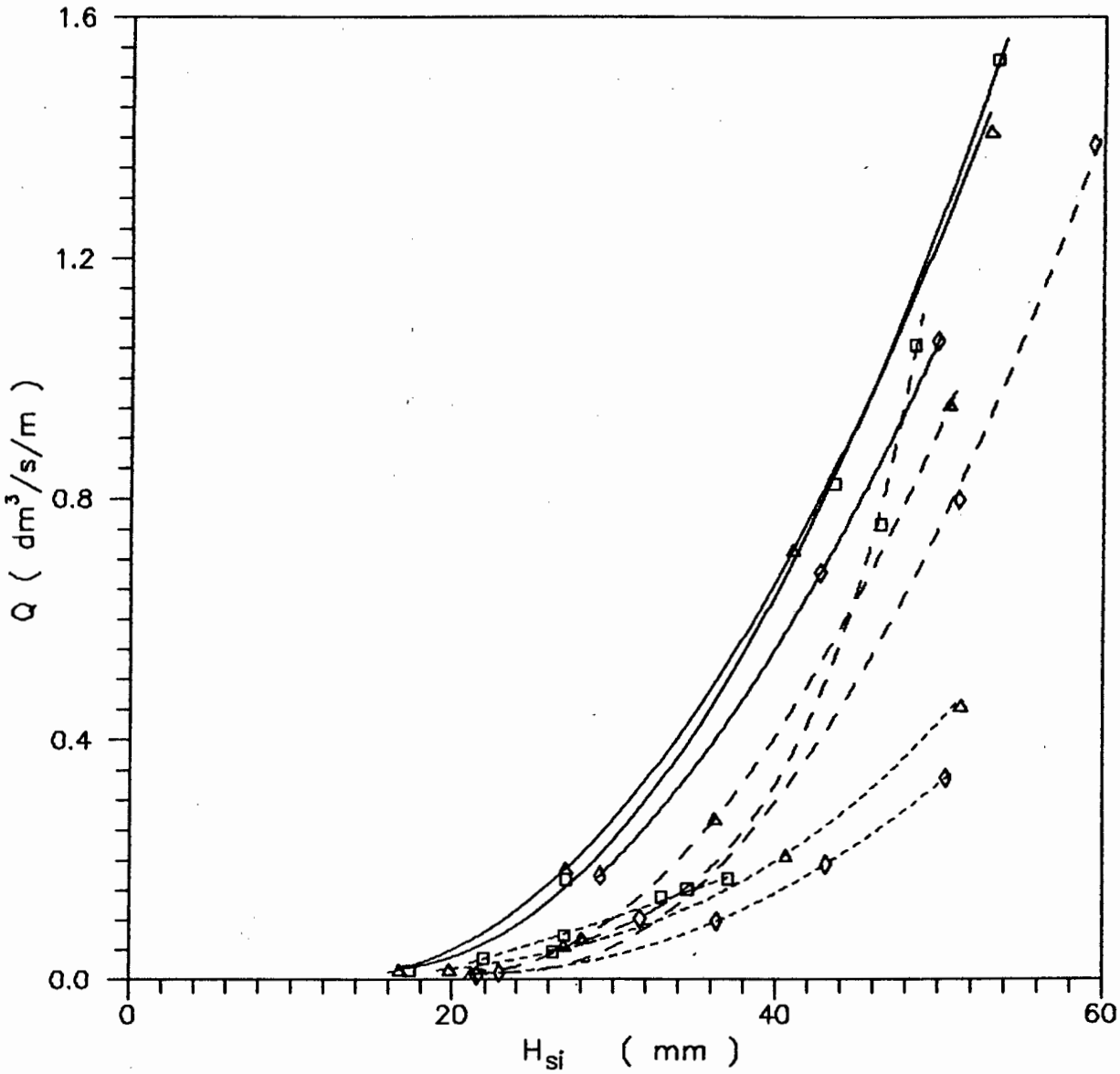

□□□□□ T_P = 1,2 s
△△△△△ T_P = 2,1 s
◇◇◇◇◇ T_P = 3,0 s
} d_s = 25 mm

□□□□□ T_P = 1,2 s
△△△△△ T_P = 2,1 s
◇◇◇◇◇ T_P = 3,0 s
} d_s = 50 mm

□□□□□ T_P = 1,2 s
△△△△△ T_P = 2,1 s
◇◇◇◇◇ T_P = 3,0 s
} d_s = 75 mm

Figure 6.6

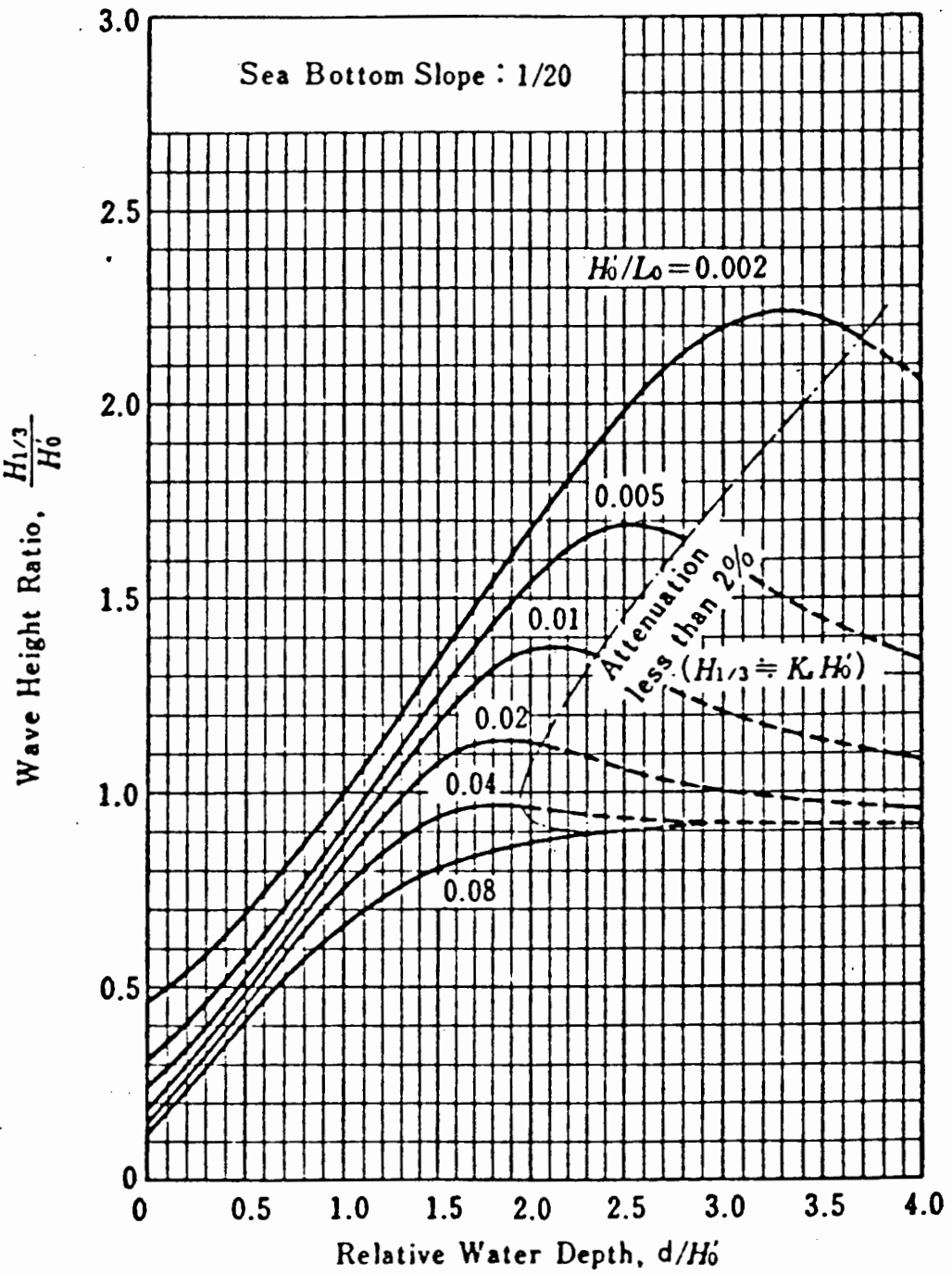

Figure 6.7 : Influence of deepwater wave steepness on the significant wave height [2]

6.3 Wave shoaling and breaking

6.3.1 Introduction

The experiments were performed over a wide range of conditions and included waves which broke offshore of the structure, at the structure and landward of the structure (in the side channels). The wave conditions in the central channel differed from those in the side channels due to the influence of wave reflection from the model structure. This can be seen in Plate 6.1 which shows a wave in the central channel breaking ahead of the waves in the side channels. During the same test the wave in the central channel also broke behind the waves in the side channels and this is illustrated in Plate 6.2. Note that a purple dye was placed in the centre channel of the flume while the two side channels contained clear water.

Figure 6.8 shows how the breaker depth which was measured depended on the deepwater wave steepness.

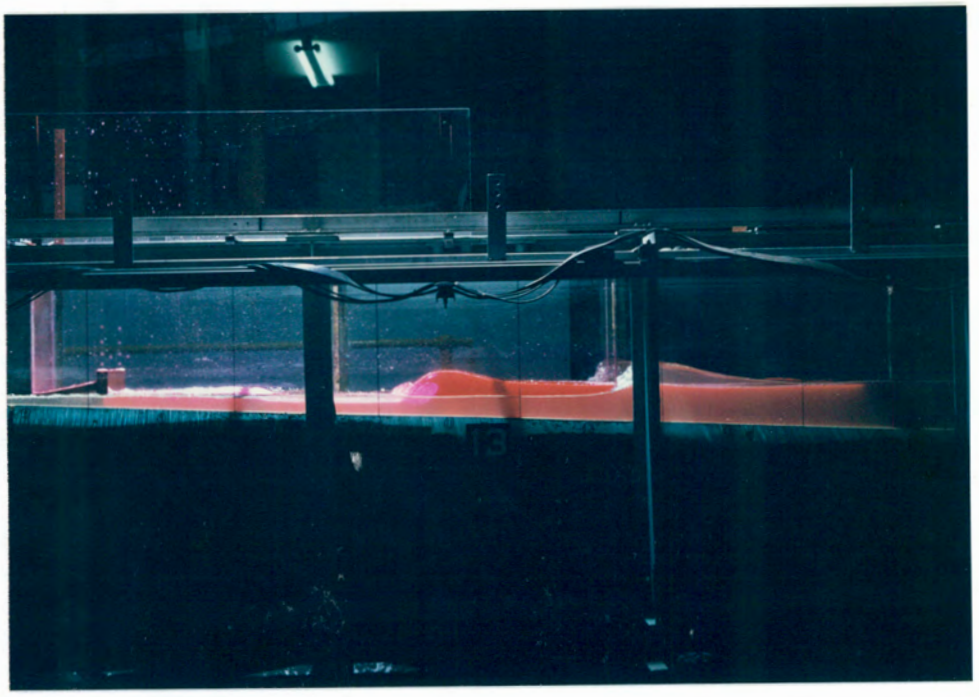

Plate 6.1 : Wave in central channel breaking ahead of waves in side channel

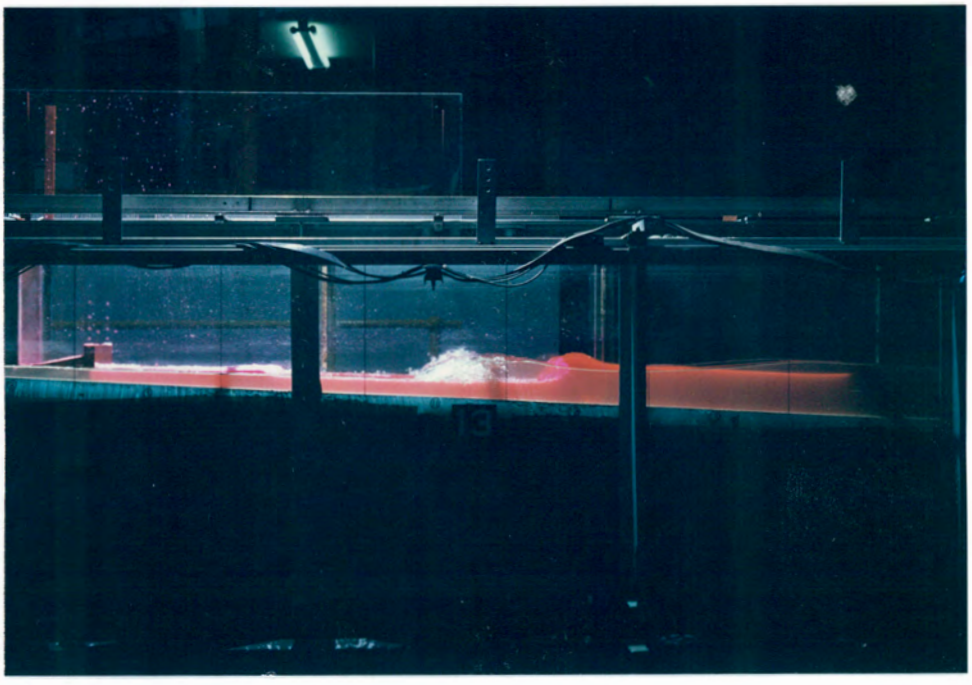

Plate 6.2 : Wave in central channel breaking behind waves in side channel

INFLUENCE OF DEEPWATER WAVE STEEPNESS ON BREAKER DEPTH INDEX

Foreshore slope = 1 : 20

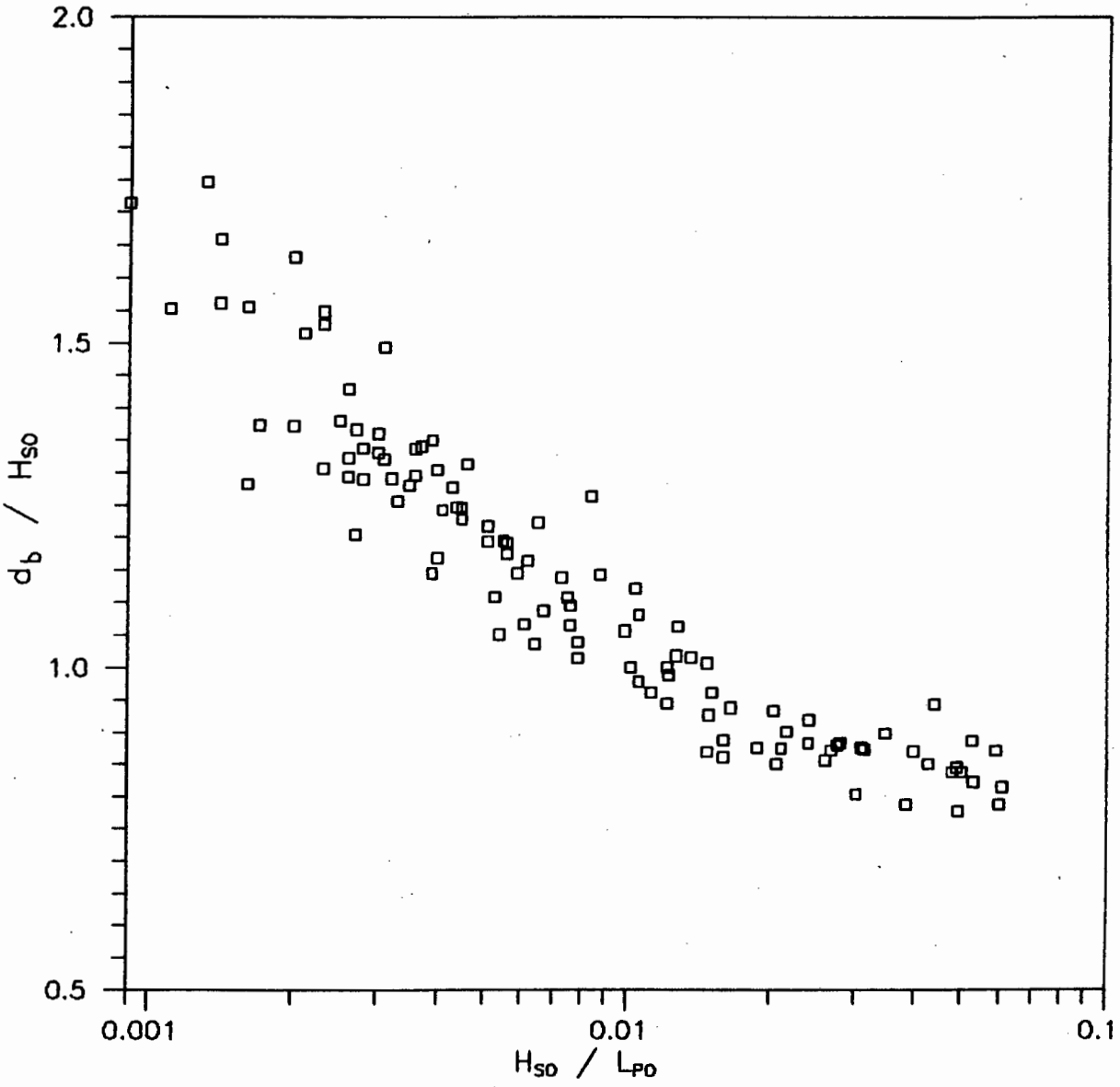

Figure 6.8

6.3.2 Characteristics of broken waves

The wave analysis plots for a test in which waves broke offshore of the structure is shown in Figures 6.9 and 6.10. Figure 6.9 shows the wave characteristics measured at probe 4 in transitional water while Figure 6.10 shows the waves measured at probe 6 at the structure toe. The wave spectrum shown in Figure 6.9 is similar to the target Jonswap spectrum and the wave height distribution closely resembles the Rayleigh distribution. The effect of wave breaking can be seen in Figure 6.10. The wave spectrum shows that the wave energy has shifted to the longer periods. This longer period wave energy causes the phenomenon of surf beat which can be seen in the plotted time history of the waves as the irregular fluctuation in the mean water level with a period of approximately 20 s. The wave height distribution shows a deficit of large waves compared to the Rayleigh distribution and the significant wave height is reduced by half.

6.3.3 Characteristics of unbroken waves

The wave analysis plots for a test which involved unbroken waves is shown in Figures 6.11 and 6.12. Figure 6.11 shows the wave characteristics measured at probe 5 in transitional water while Figure 6.12 shows the waves measured at probe 7 at the structure toe. The wave spectrum in transitional water is similar to the target Jonswap spectrum and the wave height distribution follows the Rayleigh distribution. The shape of the spectrum measured at the structure toe is similar to the spectrum offshore but the wave height has increased due to wave shoaling. The wave height distribution at the structure toe remains similar to the Rayleigh distribution but the wave steepness has increased due to the increase in wave height and the decrease in wavelength.

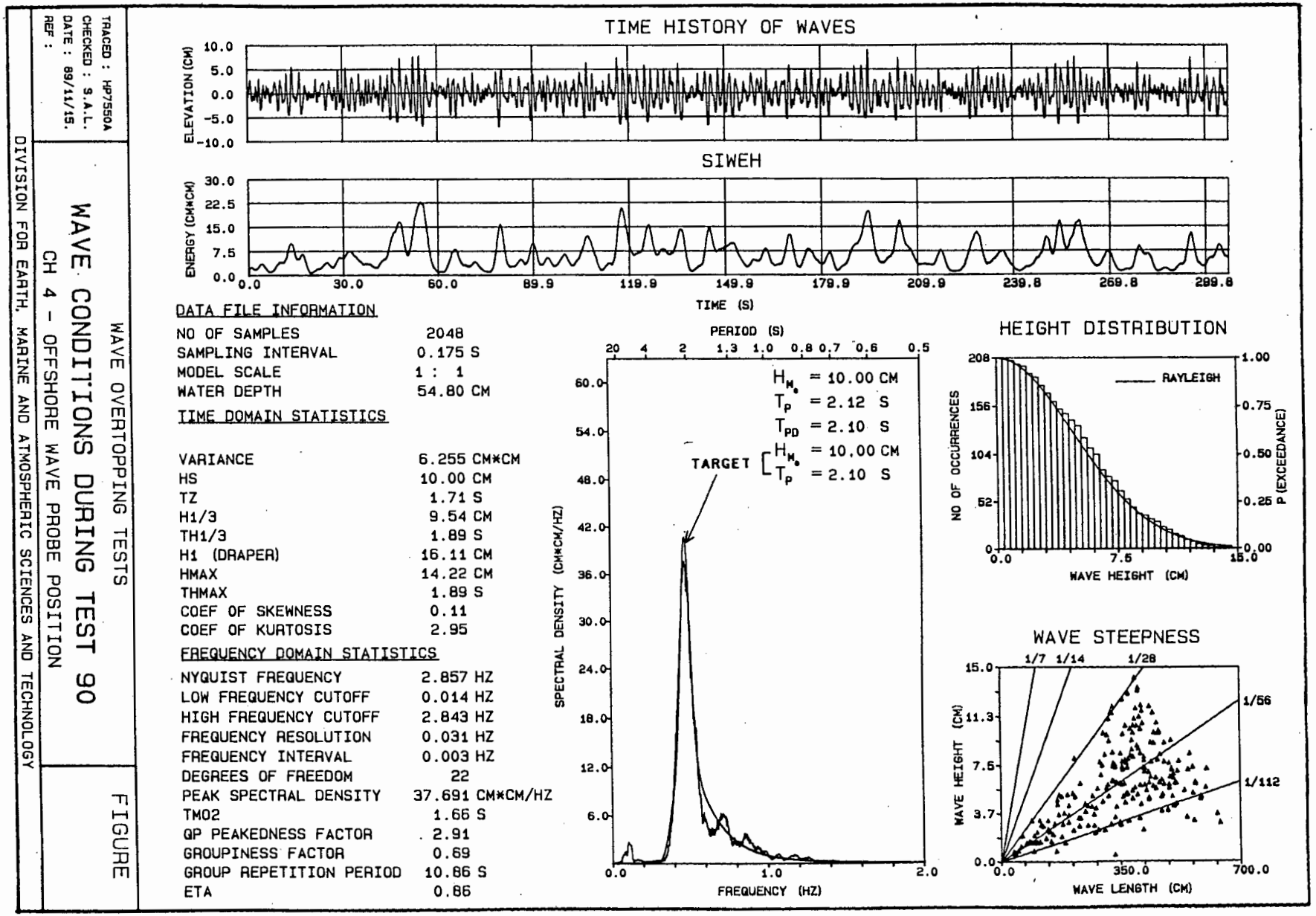
TIME HISTORY OF WAVES
ELEVATION (CM)
10.0
5.0
0.0
-5.0
-10.0
SIWEH
ENERGY (CM*CM)
30.0
22.5
15.0
7.5
0.0
0.0
30.0
60.0
89.9
119.9
149.9
179.9
209.9
239.8
269.8
299.8
TIME (S)
DATA FILE INFORMATION
NO OF SAMPLES 2048
SAMPLING INTERVAL 0.175 S
MODEL SCALE 1 : 1
WATER DEPTH 54.80 CM
TIME DOMAIN STATISTICS
VARIANCE 6.255 CM*CM
HS 10.00 CM
TZ 1.71 S
H1/3 9.54 CM
TH1/3 1.89 S
H1 (DRAPER) 16.11 CM
HMAX 14.22 CM
THMAX 1.89 S
COEF OF SKEWNESS 0.11
COEF OF KURTOSIS 2.95
FREQUENCY DOMAIN STATISTICS
NYQUIST FREQUENCY 2.857 HZ
LOW FREQUENCY CUTOFF 0.014 HZ
HIGH FREQUENCY CUTOFF 2.843 HZ
FREQUENCY RESOLUTION 0.031 HZ
FREQUENCY INTERVAL 0.003 HZ
DEGREES OF FREEDOM 22
PEAK SPECTRAL DENSITY 37.691 CM*CM/HZ
TM02 1.66 S
QP PEAKEDNESS FACTOR 2.91
GROUPINESS FACTOR 0.69
GROUP REPETITION PERIOD 10.86 S
ETA 0.86
PERIOD (S)
20 4 2 1.3 1.0 0.8 0.7 0.6 0.5
60.0
54.0
48.0
42.0
36.0
30.0
24.0
18.0
12.0
6.0
SPECTRAL DENSITY (CM*CM/HZ)
H_{M_o} = 10.00 CM
T_P = 2.12 S
T_{PD} = 2.10 S
TARGET
H_{M_o} = 10.00 CM
T_P = 2.10 S
0.0
1.0
2.0
FREQUENCY (HZ)
HEIGHT DISTRIBUTION
208
156
104
52
0
NO OF OCCURRENCES
RAYLEIGH
1.00
0.75
0.50
0.25
0.00
P (EXCEEDANCE)
0.0
7.5
15.0
WAVE HEIGHT (CM)
WAVE STEEPNESS
1/7 1/14 1/28
15.0
11.3
7.5
3.7
0.0
WAVE HEIGHT (CM)
1/56
1/112
0.0
350.0
700.0
WAVE LENGTH (CM)
TRACED : HP7550A
CHECKED : S.A.L.
DATE : 89/11/15.
REF :
WAVE OVERTOPPING TESTS
WAVE CONDITIONS DURING TEST 90
CH 4 - OFFSHORE WAVE PROBE POSITION
FIGURE
DIVISION FOR EARTH, MARINE AND ATMOSPHERIC SCIENCES AND TECHNOLOGY

Figure 6.9

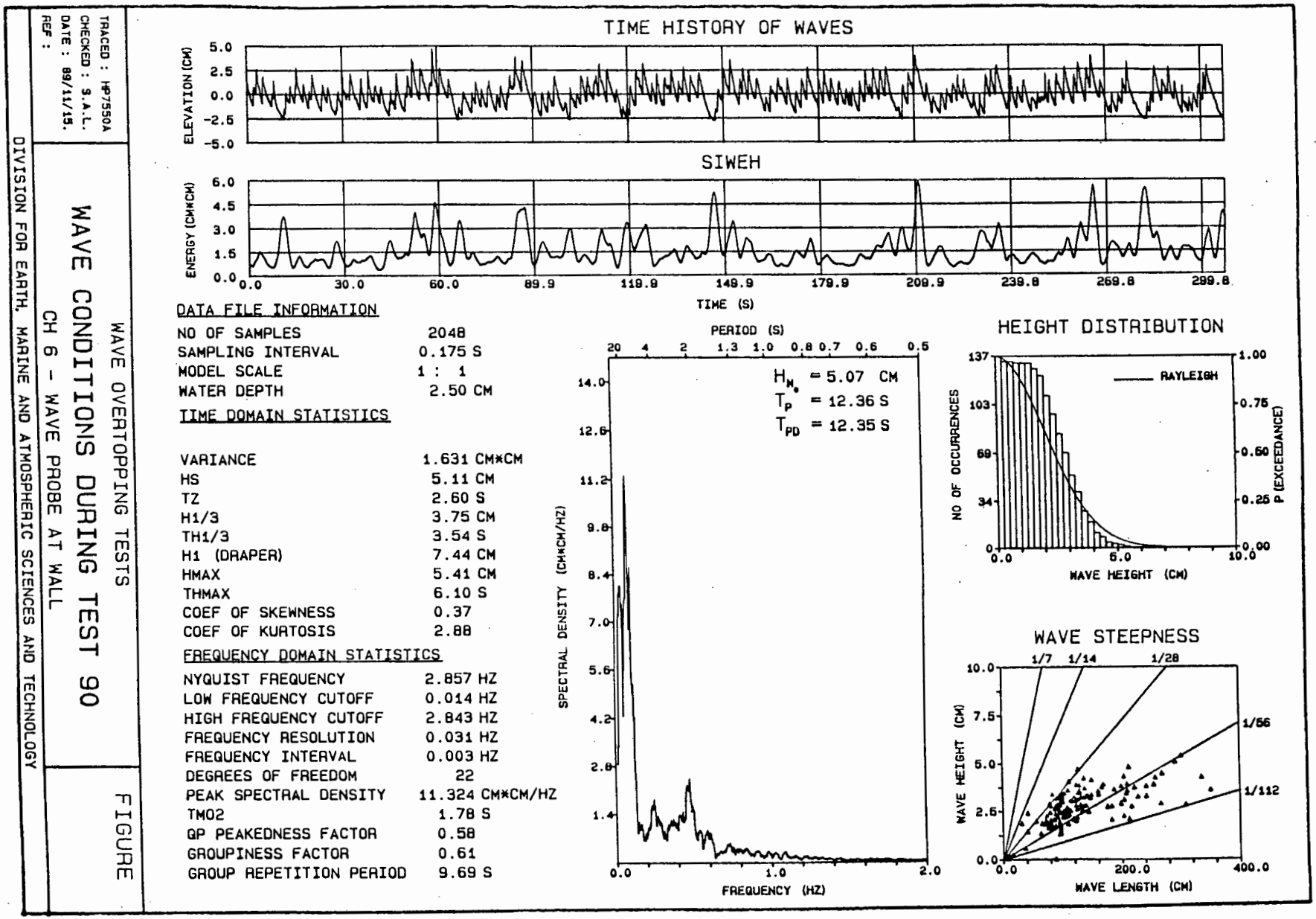
TRACED : HP7550A
CHECKED : S.A.L.
DATE : 89/11/15.
REF :
DIVISION FOR EARTH, MARINE AND ATMOSPHERIC SCIENCES AND TECHNOLOGY
WAVE OVERTOPPING TESTS
WAVE CONDITIONS DURING TEST 90
CH 6 - WAVE PROBE AT WALL
FIGURE
TIME HISTORY OF WAVES
ELEVATION (CM)
5.0
2.5
0.0
-2.5
-5.0
SIWEH
ENERGY (CM*CM)
6.0
4.5
3.0
1.5
0.0
0.0
30.0
60.0
89.9
119.9
149.9
179.9
209.9
239.8
269.8
299.8
TIME (S)
DATA FILE INFORMATION
NO OF SAMPLES 2048
SAMPLING INTERVAL 0.175 S
MODEL SCALE 1 : 1
WATER DEPTH 2.50 CM
TIME DOMAIN STATISTICS
VARIANCE 1.631 CM*CM
HS 5.11 CM
TZ 2.60 S
H1/3 3.75 CM
TH1/3 3.54 S
H1 (DRAPER) 7.44 CM
HMAX 5.41 CM
THMAX 6.10 S
COEF OF SKEWNESS 0.37
COEF OF KURTOSIS 2.88
FREQUENCY DOMAIN STATISTICS
NYQUIST FREQUENCY 2.857 HZ
LOW FREQUENCY CUTOFF 0.014 HZ
HIGH FREQUENCY CUTOFF 2.843 HZ
FREQUENCY RESOLUTION 0.031 HZ
FREQUENCY INTERVAL 0.003 HZ
DEGREES OF FREEDOM 22
PEAK SPECTRAL DENSITY 11.324 CM*CM/HZ
TM02 1.78 S
QP PEAKEDNESS FACTOR 0.58
GROUPINESS FACTOR 0.61
GROUP REPETITION PERIOD 9.69 S
PERIOD (S)
20 4 2 1.3 1.0 0.8 0.7 0.6 0.5
H_{M_0} = 5.07 CM
T_P = 12.36 S
T_{PD} = 12.35 S
SPECTRAL DENSITY (CM*CM/HZ)
14.0
12.6
11.2
9.8
8.4
7.0
5.6
4.2
2.8
1.4
0.0
1.0
2.0
FREQUENCY (HZ)
HEIGHT DISTRIBUTION
RAYLEIGH
NO OF OCCURRENCES
137
103
69
34
0
P (EXCEEDANCE)
1.00
0.75
0.50
0.25
0.00
0.0
6.0
10.0
WAVE HEIGHT (CM)
WAVE STEEPNESS
1/7
1/14
1/28
1/56
1/112
WAVE HEIGHT (CM)
10.0
7.5
5.0
2.5
0.0
0.0
200.0
400.0
WAVE LENGTH (CM)

Figure 6.10

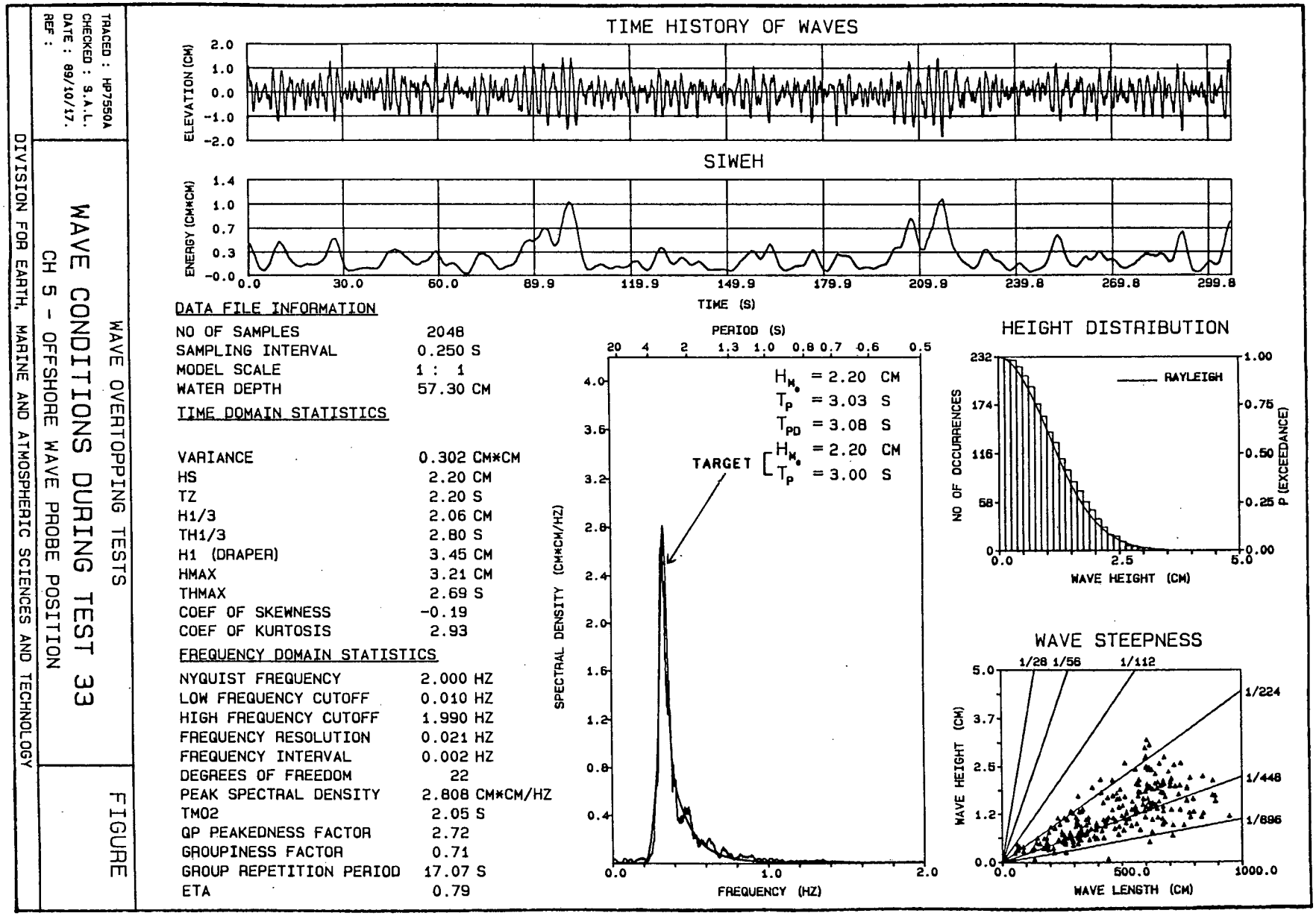
TRACED : HP7550A
CHECKED : S.A.L.
DATE : 89/10/17.
REF :
WAVE OVERTOPPING TESTS
WAVE CONDITIONS DURING TEST 33
CH 5 - OFFSHORE WAVE PROBE POSITION
FIGURE
DIVISION FOR EARTH, MARINE AND ATMOSPHERIC SCIENCES AND TECHNOLOGY
TIME HISTORY OF WAVES
ELEVATION (CM)
SIWEH
ENERGY (CM*CM)
TIME (S)
DATA FILE INFORMATION
NO OF SAMPLES 2048
SAMPLING INTERVAL 0.250 S
MODEL SCALE 1 : 1
WATER DEPTH 57.30 CM
TIME DOMAIN STATISTICS
VARIANCE 0.302 CM*CM
HS 2.20 CM
TZ 2.20 S
H1/3 2.06 CM
TH1/3 2.80 S
H1 (DRAPER) 3.45 CM
HMAX 3.21 CM
THMAX 2.69 S
COEF OF SKEWNESS -0.19
COEF OF KURTOSIS 2.93
FREQUENCY DOMAIN STATISTICS
NYQUIST FREQUENCY 2.000 HZ
LOW FREQUENCY CUTOFF 0.010 HZ
HIGH FREQUENCY CUTOFF 1.990 HZ
FREQUENCY RESOLUTION 0.021 HZ
FREQUENCY INTERVAL 0.002 HZ
DEGREES OF FREEDOM 22
PEAK SPECTRAL DENSITY 2.808 CM*CM/HZ
TM02 2.05 S
QP PEAKEDNESS FACTOR 2.72
GROUPINESS FACTOR 0.71
GROUP REPETITION PERIOD 17.07 S
ETA 0.79
PERIOD (S)
SPECTRAL DENSITY (CM*CM/HZ)
FREQUENCY (HZ)
TARGET
HEIGHT DISTRIBUTION
RAYLEIGH
NO OF OCCURRENCES
P (EXCEEDANCE)
WAVE HEIGHT (CM)
WAVE STEEPNESS
1/28 1/56 1/112 1/224 1/448 1/896
WAVE HEIGHT (CM)
WAVE LENGTH (CM)

Figure 6.11

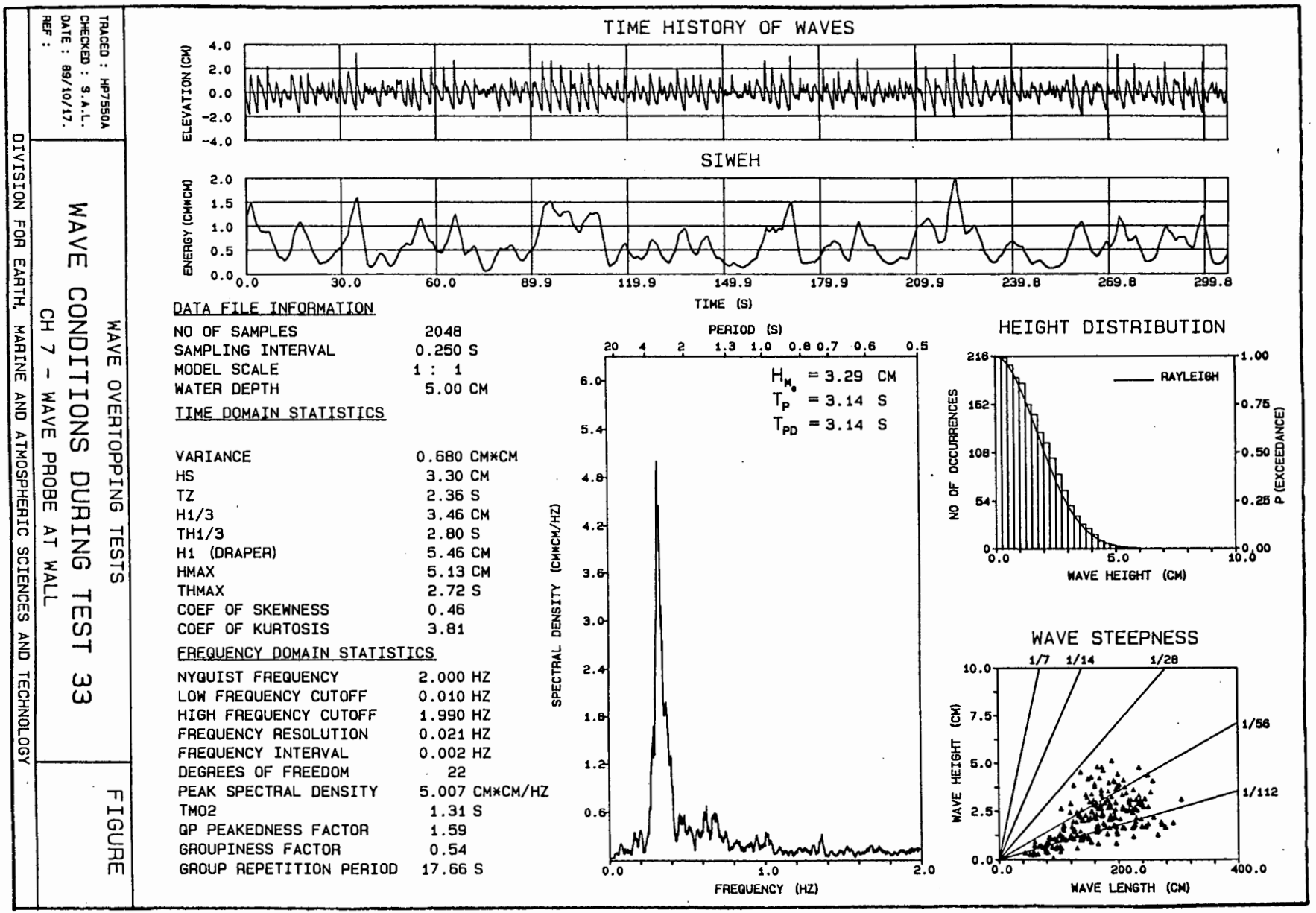
TRACED : HP7550A
CHECKED : S.A.L.
DATE : 89/10/17.
REF :
DIVISION FOR EARTH, MARINE AND ATMOSPHERIC SCIENCES AND TECHNOLOGY
WAVE OVERTOPPING TESTS
WAVE CONDITIONS DURING TEST 33
CH 7 - WAVE PROBE AT WALL
FIGURE
TIME HISTORY OF WAVES
ELEVATION (CM)
SIWEH
ENERGY (CM*CM)
TIME (S)
DATA FILE INFORMATION
NO OF SAMPLES 2048
SAMPLING INTERVAL 0.250 S
MODEL SCALE 1 : 1
WATER DEPTH 5.00 CM
TIME DOMAIN STATISTICS
VARIANCE 0.680 CM*CM
HS 3.30 CM
TZ 2.36 S
H1/3 3.46 CM
TH1/3 2.80 S
H1 (DRAPER) 5.46 CM
HMAX 5.13 CM
THMAX 2.72 S
COEF OF SKEWNESS 0.46
COEF OF KURTOSIS 3.81
FREQUENCY DOMAIN STATISTICS
NYQUIST FREQUENCY 2.000 HZ
LOW FREQUENCY CUTOFF 0.010 HZ
HIGH FREQUENCY CUTOFF 1.990 HZ
FREQUENCY RESOLUTION 0.021 HZ
FREQUENCY INTERVAL 0.002 HZ
DEGREES OF FREEDOM 22
PEAK SPECTRAL DENSITY 5.007 CM*CM/HZ
TM02 1.31 S
QP PEAKEDNESS FACTOR 1.59
GROUPINESS FACTOR 0.54
GROUP REPETITION PERIOD 17.66 S
PERIOD (S)
SPECTRAL DENSITY (CM*CM/HZ)
FREQUENCY (HZ)
HEIGHT DISTRIBUTION
RAYLEIGH
NO OF OCCURRENCES
P (EXCEEDANCE)
WAVE HEIGHT (CM)
WAVE STEEPNESS
1/7
1/14
1/28
1/56
1/112
WAVE HEIGHT (CM)
WAVE LENGTH (CM)

Figure 6.12

6.4 Types of overtopping observed

6.4.1 Waves breaking offshore

Waves which broke offshore of the structure resulted in a turbulent mass of water which surged up over the wall. The forward velocity of the water particles in the mass of water assisted in the overtopping process. An example of this type of overtopping is shown in Plate 6.3 which was photographed during Test 90 (h_c = 100 mm, d_s = 25 mm, T_p = 2,1 s, H_{so} = 104,0 mm, H_{si} = 51,3 mm, Q = 0,4557 $dm^3/s/m$).

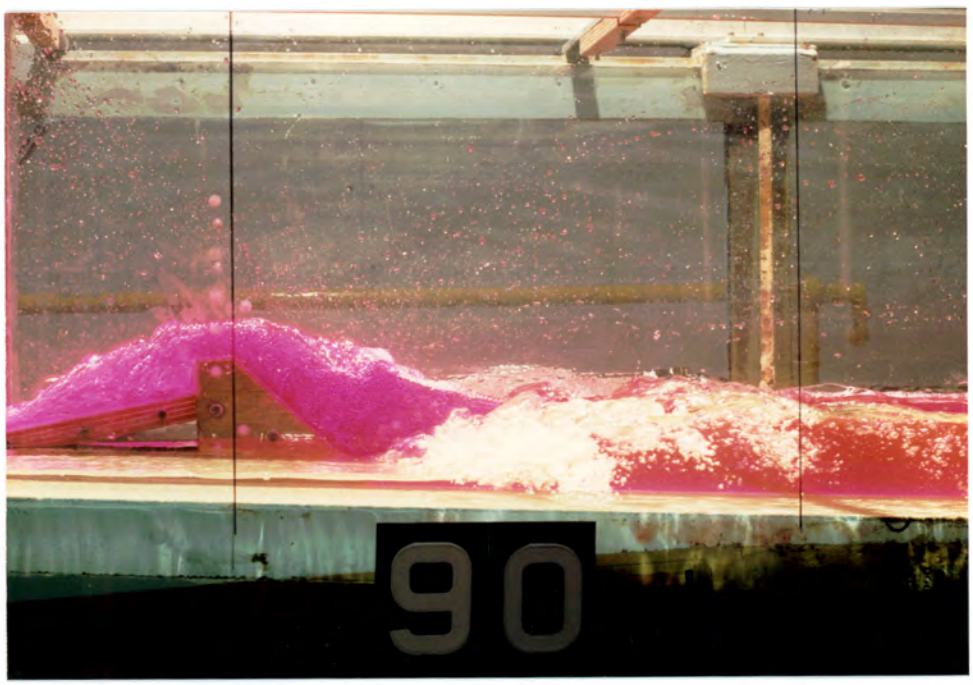

Plate 6.3 : Overtopping due to broken waves

6.4.2 Waves breaking at structure

Waves which broke against the structure caused spray to shoot up as high as 1,5 m into the air and then to fall on the landward side of the wall. This was caused by the considerable forward velocity of the water particles in the crest of the wave at breaking. Due to the irregular nature of the waves the majority of the waves broke either in front of or past the structure and only a few waves actually broke at the structure. An example of a wave breaking at the structure is shown in Plate 6.4 which was photographed during Test 63 (h_c = 200 mm, d_s = 120 mm, T_p = 1,2 s, H_{so} = 118,6 mm, H_{si} = 84,2 mm, Q = 0,8885 $dm^3/s/m$).

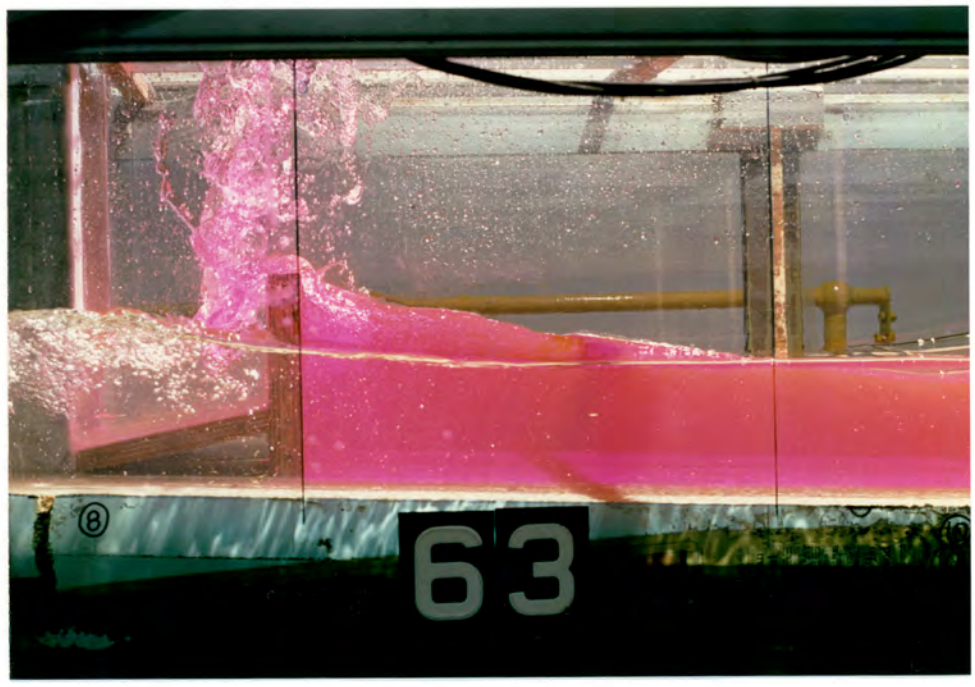

Plate 6.4 : Overtopping due to waves breaking at structure

6.4.3 Unbroken waves

Unbroken waves caused a flow of water over the structure crest for a relatively long period of time. This type of overtopping depended less on the forward velocity of the water particles and more on the elevation of the water surface above the crest of the structure. This process is illustrated in Plate 6.5 which was taken during Test 72 (h_c = 200 mm, d_s = 160 mm, T_p = 2,1 s, H_{so} = 51,5 mm, H_{si} = 54,6 mm, Q = 0,5747 $dm^3/s/m$). Note the similarity between this type of overtopping and the flow over a weir, which was the basis for the analytical overtopping equation developed by Kikkawa (See Section 3.5).

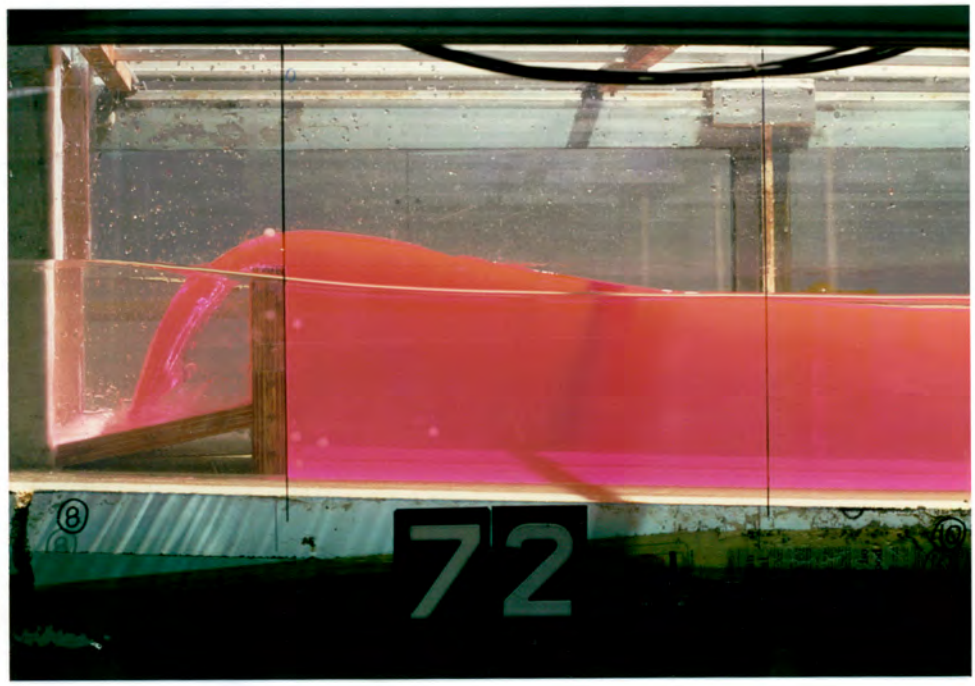

Plate 6.5 : Overtopping due to unbroken waves

6.5 Repeatability of tests

In order to test as many different situations as possible each test was performed once only. Test numbers 6 and 7 were, however, each repeated five times in order to determine the repeatability of the results. Test 6 is typical of a test which involved a low overtopping rate and Test 7 involved a large rate of overtopping. The results obtained are included in Appendix B and are summarized in Table 6.4 below.

		d_s (mm)	H_{st} (mm)	H_{si} (mm)	T_p (s)	d_b (mm)	Q ($dm^3/s/m$)
Test 6	Mean	50,0	23,9	31,9	2,14	32,0	0,0572
	Std deviation	0,0	0,5	0,6	0,06	1,0	0,0029
	Std error (%)	0,0	2,2	1,7	2,8	3,1	5,0
Test 7	Mean	50,0	106,2	62,3	2,08	105,0	1,025
	Std deviation	0,1	2,0	0,3	0,03	4,0	0,026
	Std error (%)	0,2	1,9	0,4	1,2	3,7	2,5

Table 6.4 : Repeatability of tests based on 5 repetitions of each test

The standard error is calculated as the standard deviation divided by the mean value. The standard error in the overtopping rate measured for Test 6 was greater than for Test 7 which was expected since for low overtopping rates the volume of water overtopping the wall depended on a small number of overtopping events and was therefore sensitive to small variations in the wave conditions and water levels.

CHAPTER 7

ANALYSIS OF EXPERIMENTAL RESULTS

7.1 Introduction

The aim of the analysis was to identify the parameters which influence the overtopping process and to determine the relation between these parameters. It was preferable that these parameters be non-dimensional to enable the model results to be easily applied to prototype structures.

7.2 Dimensional analysis

The variables describing the overtopping of a given structure are assumed to be :

Q	=	overtopping rate	$[L^3\ T^{-1}\ L^{-1}]$
H_k	=	characteristic wave height	$[L]$
T_k	=	characteristic wave period	$[T]$
d_s	=	water depth at structure toe	$[L]$
F	=	freeboard	$[L]$
g	=	gravitational acceleration	$[L\ T^{-2}]$
ν	=	kinematic viscosity	$[L^2\ T^{-1}]$

Note that these variables are for a given structure geometry. Since only the Jonswap spectrum was used for the tests the waves are described by a characteristic height and period only and the influence of spectral shape or other parameters relating to the irregularity of the waves were not considered.

A dimensional analysis of these 7 variables having 2 primary dimensions of length and time gives 5 dimensionless terms. One possible combination is

$\frac{Q}{\sqrt{g\ H_k^3}}$ = relative overtopping parameter

$\frac{F}{H_k}$ = relative freeboard

$\frac{d_s}{H_k}$ = relative water depth at structure toe

$\frac{H_k}{g\ T_k^2}$ = wave steepness parameter

$\frac{H_k^2}{\nu\ T_k}$ = a type of Reynolds' number

For waves propagating onto a beach the peak discharge at the point of breaking is given approximately by $1/2\sqrt{\alpha}\ \sqrt{g\ H^3}$, where α is the ratio of the wave height to the water depth at breaking [22]. The physical significance of the relative overtopping parameter is therefore that it is proportional to the ratio of the overtopping discharge to the wave breaking discharge.

With regard to the choice of a characteristic wave height it was thought that the significant wave height measured at the toe of the structure was more relevant than the deepwater significant wave height. This was because the relation between the deepwater wave height and the overtopping rate will be influenced by the processes of wave shoaling and breaking which occur between deep water and the structure toe.

The characteristic wave period selected was the spectral peak wave period measured in intermediate water. The peak wave period measured at the structure toe was not used because when wave breaking occurred offshore of the structure the peak wave period sometimes occurred in the range of long period surf beat (see Figure 6.10). The overtopping is expected to be more dependent on the peak period associated with the individual waves in the wave train than with the period of the surf beat.

Wave overtopping is scaled primarily according to Froude similarity and if it is assumed that viscosity plays a minor part in the overtopping process then Reynolds' number may be neglected. Based on the reasoning given above the overtopping of a given structure can be written in the following dimensionless form

$$\frac{Q}{\sqrt{g\,H_{si}^{\,3}}} = fn\left[\frac{F}{H_{si}}\ ,\ \frac{d_s}{H_{si}}\ ,\ \frac{H_{si}}{g\,T_p^{\,2}}\right] \qquad (7.1)$$

7.3 Relation between dimensionless parameters

When the relative overtopping parameter, $Q/\sqrt{g\,H_{si}^{\,3}}$, was plotted against the relative freeboard parameter, F/H_{si}, the data showed a trend for the relative overtopping parameter to increase sharply as the relative freeboard decreased. This is shown in Figure 7.1 for the combined data from the two vertical walls tested and in Figure 7.2 for the wall with the 45° slope. A copy of the spreadsheet used to calculate these parameters is included in Appendix C.

There remains a large amount of scatter in the data plotted in Figures 7.1 and 7.2. This scatter was thought to be due to the influence of the remaining two dimensionless parameters in Equation 7.1, namely d_s/H_{si} and $H_{si}/gT_p^{\,2}$. Although a number of approaches were used, no clear relation between these parameters and the relative overtopping parameter could be found.

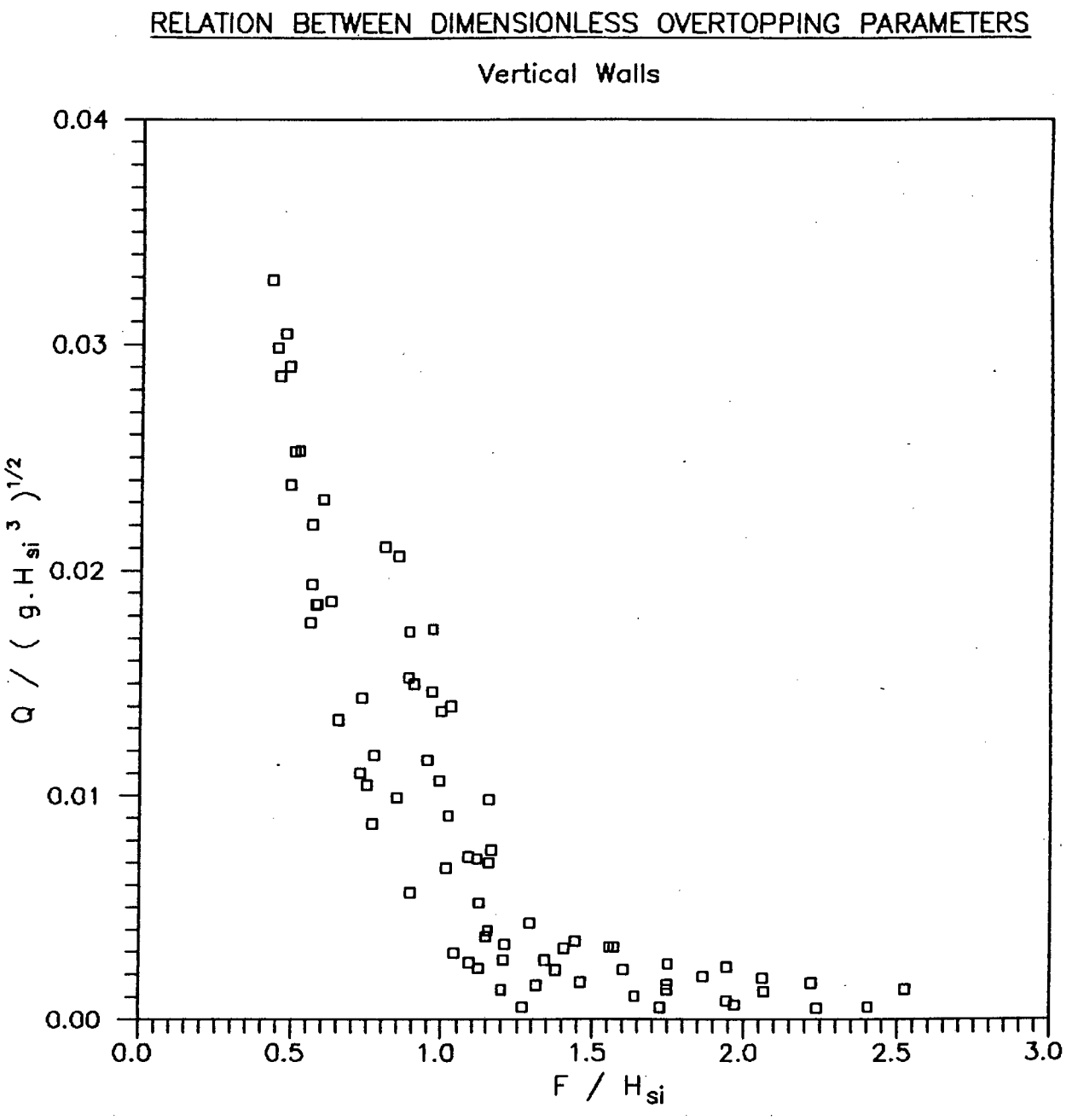
RELATION BETWEEN DIMENSIONLESS OVERTOPPING PARAMETERS
Vertical Walls
0.04
0.03
0.02
0.01
0.00
Q / (g.H si 3)1/2
0.0
0.5
1.0
1.5
2.0
2.5
3.0
F / H si

Figure 7.1

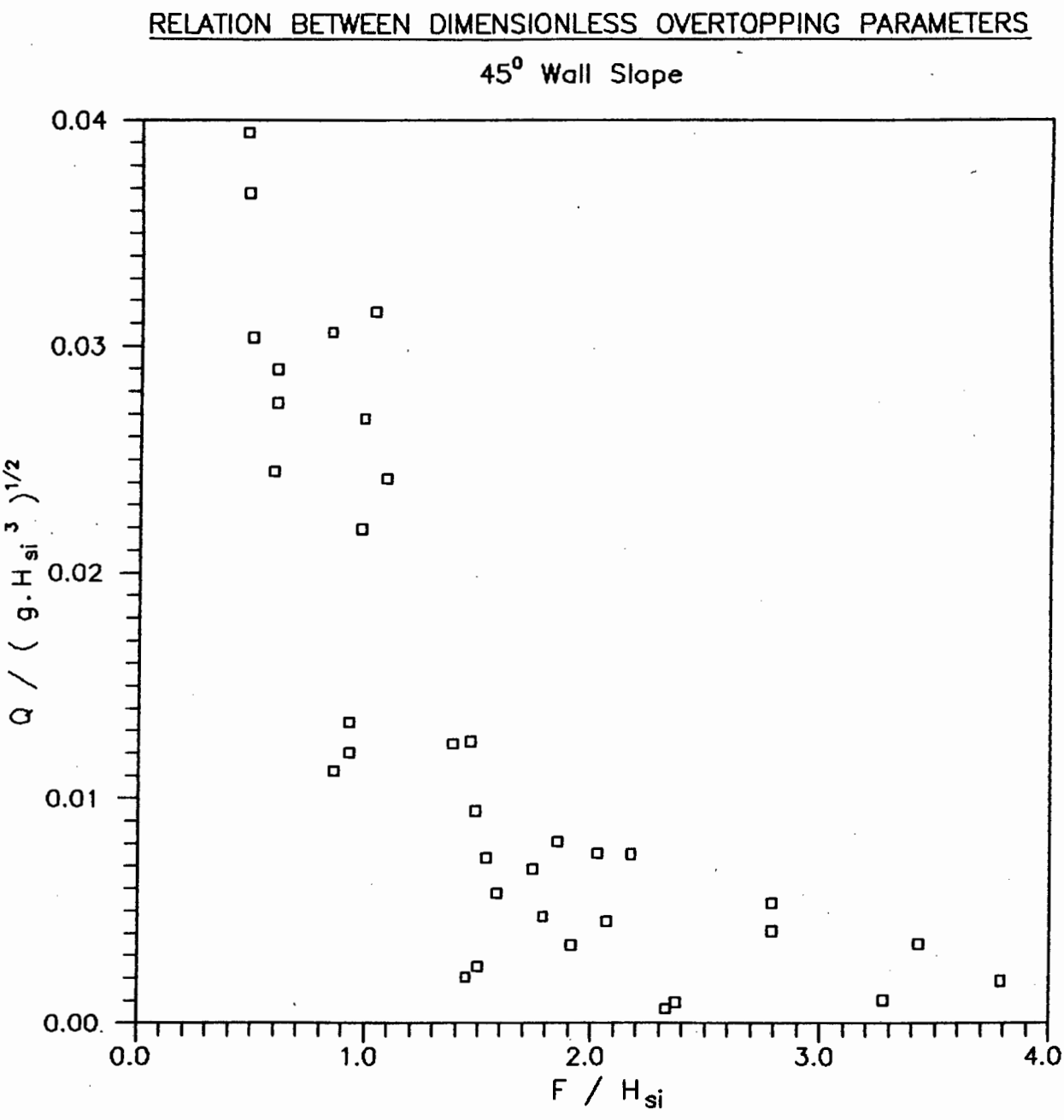
RELATION BETWEEN DIMENSIONLESS OVERTOPPING PARAMETERS
45⁰ Wall Slope
0.04
0.03
0.02
0.01
0.00
Q / (g.H_si^3)^1/2
0.0
1.0
2.0
3.0
4.0
F / H_si

Figure 7.2

Ahrens (Section 3.14) developed an empirical parameter which combines all the variables on the right hand side of Equation 7.1 into a single parameter (the wave period and the depth at the structure are included through the wavelength term). Ahrens' dimensionless freeboard parameter is defined as

$$F' = \frac{F}{(H_{si}^{2} L_{pi})^{1/3}} \qquad (7.2)$$

When plotted against the relative overtopping parameter, $Q/\sqrt{g H_{si}^{3}}$, Ahrens' dimensionless freeboard parameter was found to consolidate all Ahrens' overtopping results for a particular structure into a single trend.

The author's experimental data were plotted using the same parameters used by Ahrens. The data did not form a single trend but showed much more scatter than the data in Figures 7.1 and 7.2. One of the reasons for this scatter was the inclusion of the local wave length, L_{pi}, in Ahrens' freeboard parameter. The relevant graphs showing the author's experimental results (Figures 6.4, 6.5 and 6.6) did not indicate a trend for the overtopping to increase with increasing wave period (or wavelength) which is implied in Ahrens' freeboard parameter. The reason for Ahrens' freeboard parameter giving such a poor result for these data could be due to the more moderate 1:100 foreshore slope used by Ahrens or due to the fact that the range of conditions tested by Ahrens was different.

When the relative overtopping parameter was plotted against the dimensionless freeboard parameter proposed by Owen (Section 3.11), namely $F/\bar{T}\sqrt{g H_{si}}$, the data also showed a large amount of scatter. An analytical approach was then used to develop a model to consolidate the experimental data into a single, well defined trend.

7.4 Analytical approach

7.4.1 Development of analytical approach

The overtopping caused by broken and unbroken waves takes place in different ways and these differences were described in Section 6.4. The reason for the differences is due the different kinematics of the water particles involved, and in order to model these processes the concept of a velocity head, due to the velocity of the particles in the waves, was introduced. This idea was based on the energy equation of Bernoulli where the total energy level is given by

$$EL = \frac{p}{w} + \frac{v^2}{2g} + z \qquad (7.3)$$

where

EL = total energy level (m)
p = pressure (Pa)
w = specific weight (N/m^3)
v = velocity (m/s)
z = elevation above a horizontal datum (m)

All three terms in eqn 7.3 are in units of length or head. The p/w term represents the height of the free water surface and is considered to be related in some way to the significant wave height. The velocity head term is assumed to be applicable to the velocity of the water particles in the wave. If it is assumed that the energy level is measured with the still water level as datum then z = 0.

The total energy level or total head at the structure, above the still water level, is therefore considered to be

$$H_{tot} = H_{si} + H_{vel} \qquad (7.4)$$

$$\text{where } H_{vel} = \frac{v^2}{2g} \qquad (7.5)$$

The appropriate particle velocities to apply in eqn. (7.5) are established below:

(a) Particle velocity in unbroken waves

For waves which are unbroken at the structure toe the linear wave theory equation for the horizontal water particle velocity in intermediate depth water was used

$$v = \frac{H}{2} \frac{gT}{L} \frac{\cosh[2\pi(y + d)/L]}{\cosh(2\pi d/L)} \cos \phi \qquad (7.6)$$

where y = vertical distance above SWL and ϕ = phase angle.

The appropriate velocity to apply in eqn. (7.5) is assumed to be proportional to the maximum forward velocity ($\cos\phi = 1$) at the SWL (y = 0) and is therefore given by

$$v_{unbroken} = c_1 \frac{H_{si}}{2} \frac{g T_p}{L_{pi}} \qquad (7.7)$$

where c_1 is an empirical coefficient and the regular wave parameters (H, T and L) have been replaced by the corresponding irregular wave parameters measured at the structure toe.

(b) Particle velocity in broken waves

For waves which break offshore of the structure the velocity is estimated using a similar approach to the one described in the Shore Protection Manual [1] for calculating the forces on vertical walls due to broken waves. It is assumed that upon breaking the water particle motion changes from oscillatory to translatory motion. Therefore, immediately after breaking, the

water mass in a wave moves forward with the velocity of propagation attained at breaking. Using eqn. (2.5) this velocity is given by

$$v = \sqrt{g\, d_b} \qquad (7.8)$$

Thereafter it is assumed that the velocity decreases in proportion to the square root of the water depth up to the limit of wave runup, as shown in Figure 7.3.

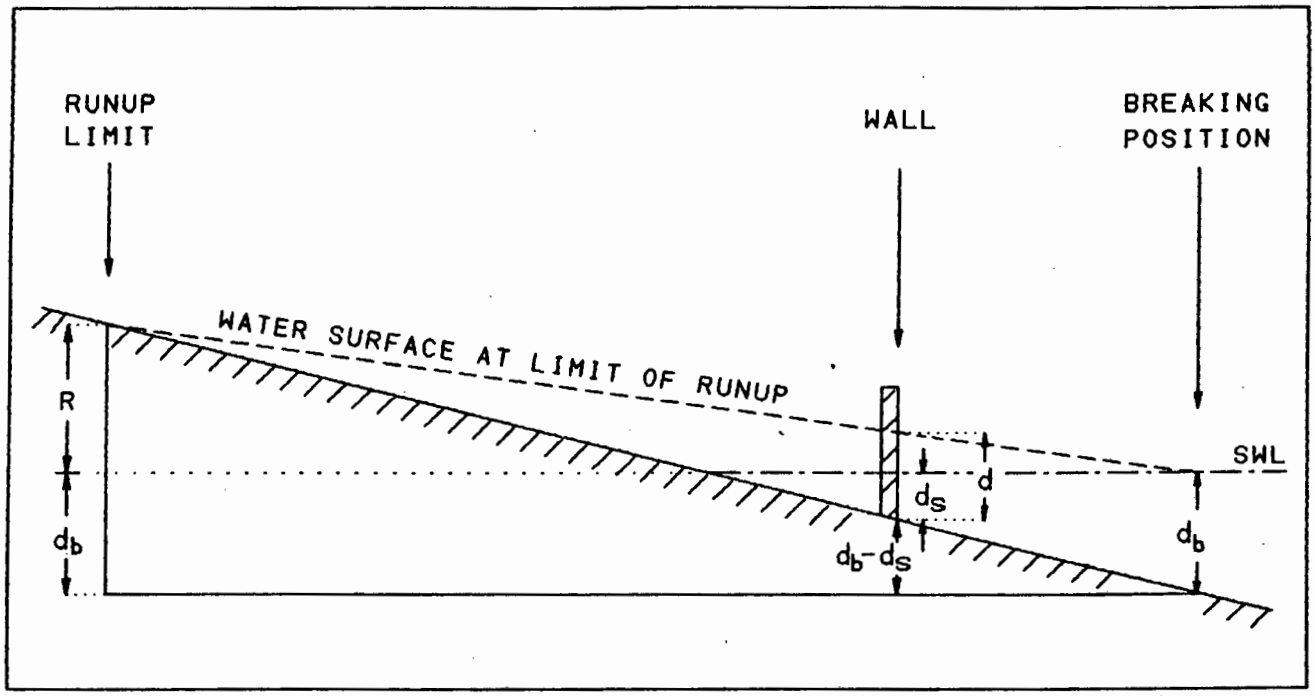

Figure 7.3 : Calculation of particle velocity at structure for broken waves

Using similar triangles it can be shown that

$$\frac{d}{d_b} = 1 - \frac{d_b - d_s}{d_b + R} \qquad (7.9)$$

The particle velocity at the structure toe is therefore assumed to be

$$v_{broken} = c_2 \cdot \sqrt{g\, d_b} \cdot \sqrt{1 - \frac{d_b - d_s}{d_b + R}} \qquad (7.10)$$

where c_2 is an empirical coefficient and R is the vertical distance between the SWL and the runup limit.

In order to simplify eqn. (7.10) it was assumed that the runup height, R, is equal to twice the breaker height, H_b, and that the ratio of the wave height to water depth at breaking is 0,78. This gives the runup as

$$R = 1{,}56\, d_b \qquad (7.11)$$

The assumption that $H_b/d_b = 0{,}78$ is derived from solitary wave theory and is an oversimplification since this ratio has been found to depend on the beach slope and the wave steepness. During the 6 tests where breaking occurred near the model structure the average value of H_{si}/d_b was found to be 0,83 compared to the value of 0,78 which was assumed above. The assumption that $R = 2\, H_b$ is the same assumption which was used in the Shore Protection Manual [1] for estimating broken wave forces.

Substitution of eqn. (7.11) into (7.10) gives the particle velocity of broken waves at the structure toe as

$$v_{broken} = c_2 \cdot \sqrt{g\, d_b} \cdot \sqrt{\frac{1{,}56\, d_b + d_s}{2{,}56\, d_b}} \qquad (7.12)$$

If breaking occurs at the toe of the structure the velocity calculated using eqns.(7.7) and (7.12) should be equal, ie.

$$c_1 \frac{H_{si}}{2} \frac{g\, T_p}{L_{pi}} = c_2 \cdot \sqrt{g\, d_b} \cdot \sqrt{\frac{1{,}56\, d_b + d_s}{2{,}56\, d_b}} \qquad (7.13)$$

If the following substitutions are made

$$d_b = d_s$$

$$L_{pi} = T_p \sqrt{g\, d_s} \qquad \text{(linear wave theory in shallow water)}$$

$$H_{si} = 0{,}78\, d_b$$

then eqn. (7.13) simplifies to

$$c_1 . 0{,}39 . \sqrt{g\, d_b} = c_2 . \sqrt{g\, d_b} \qquad (7.14)$$

This gives the relation between the two coefficients as

$$c_1 = 2{,}56\, c_2 \qquad (7.15)$$

The velocity heads at the structure toe due to unbroken and broken waves are obtained by substituting eqns. (7.7) and (7.12) respectively into eqn. (7.5).

Unbroken waves :

$$H_{vel} = c . 0{,}82 . g . \left[\frac{H_{si}\, T_p}{L_{pi}} \right]^2 \qquad (7.16)$$

Broken waves :

$$H_{vel} = c . \frac{d_b}{2} . \left[\frac{1.56\, d_b + d_s}{2{,}56\, d_b} \right] \qquad (7.17)$$

where $c = c_2^2$. Note: c is an empirical coefficient which can be considered to account for the difference between the actual particle velocities and the velocities used to derive eqns. (7.16) and (7.17).

7.4.2 Comparison with experimental data

The dimensionless overtopping parameter, $Q/\sqrt{g\ H_{tot}^3}$, was plotted against the ratio of the freeboard to the total energy level, F/H_{tot}. The value of the empirical coefficient, c, was chosen to minimize the scatter in the data and a value of c = 0,75 was found to give the least scatter. The results are shown in Figure 7.4 for the combined data from the two vertical walls tested and in Figure 7.5 for the wall with the 45° slope. A copy of the spreadsheet used to calculate these parameters is included in Appendix C.

These parameters appear to consolidate a wide range of overtopping data into a single, well defined trend. The data shows significantly less scatter than in Figures 7.1 and 7.2. It therefore appears that the velocity head is an important factor in the overtopping process and that the overtopping process is dependent on the total energy level at the structure. The physical interpretation of the freeboard parameter, F/H_{tot}, is the ratio of the height of the structure crest above the SWL to the height of the energy level above the SWL.

RELATION BETWEEN DIMENSIONLESS OVERTOPPING PARAMETERS INCORPORATING THE TOTAL HEAD TERM

Vertical Walls

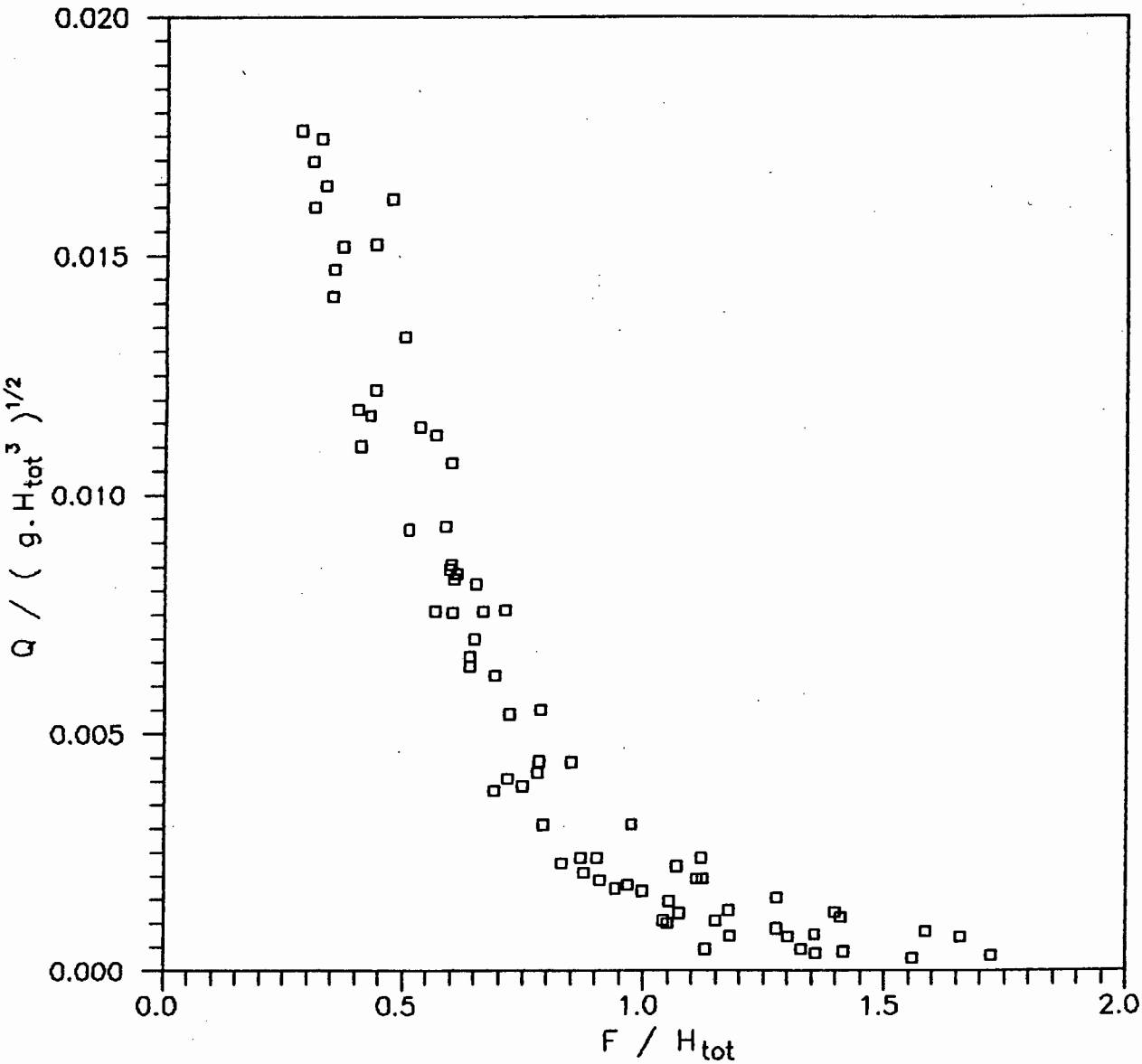

Figure 7.4

RELATION BETWEEN DIMENSIONLESS OVERTOPPING PARAMETERS INCORPORATING THE TOTAL HEAD TERM

45° Wall Slope

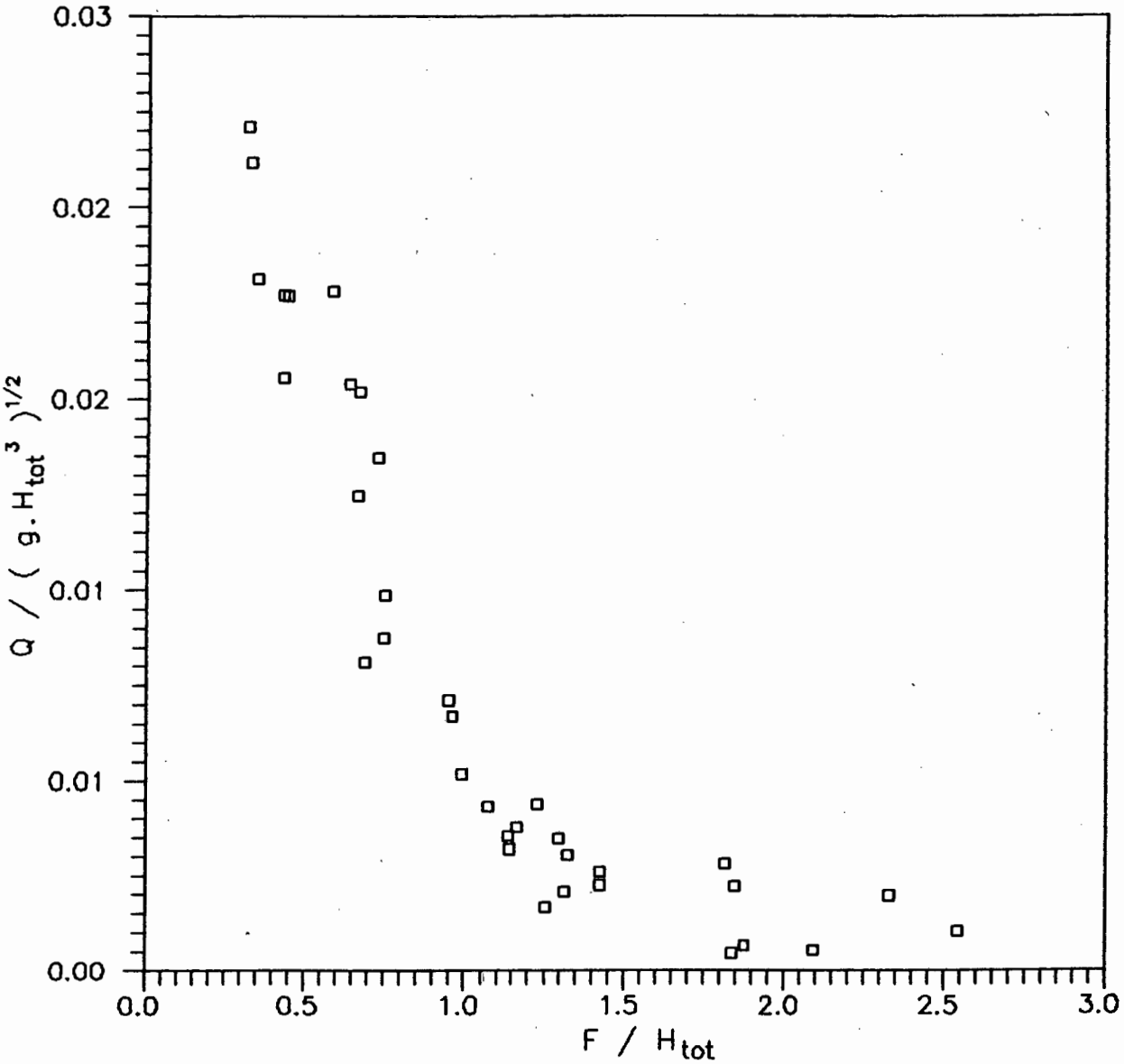

Figure 7.5

The ratio of the velocity head to the total head is plotted against the position of wave breaking in Figures 7.6, 7.7 and 7.8. For waves which break offshore of the structure ($d_b/d_s > 1$) the velocity head makes up between 25 % and 45 % of the total head. The velocity head makes up approximately 35 % of the total head for waves which break at the structure and becomes less significant for waves which break beyond the structure. The trend of these graphs therefore coincides with the observations made in Section 6.4 with regard to the different types of overtopping observed.

Figure 7.6 also shows that for d_s = 25 mm the 1,2 s waves have larger velocity head-to-total head ratios than the 3,0 s waves which in turn have larger ratios than the 2,1 s waves. It would be expected that the trend would either be 1,2 s - 2,1 s - 3,0 s or 3,0 s - 2,1 s - 1,2 s. However, the same trend can be seen in the experimental results shown in Figure 6.4 and this demonstrates how the total head is capable of consolidating all the data into a single trend.

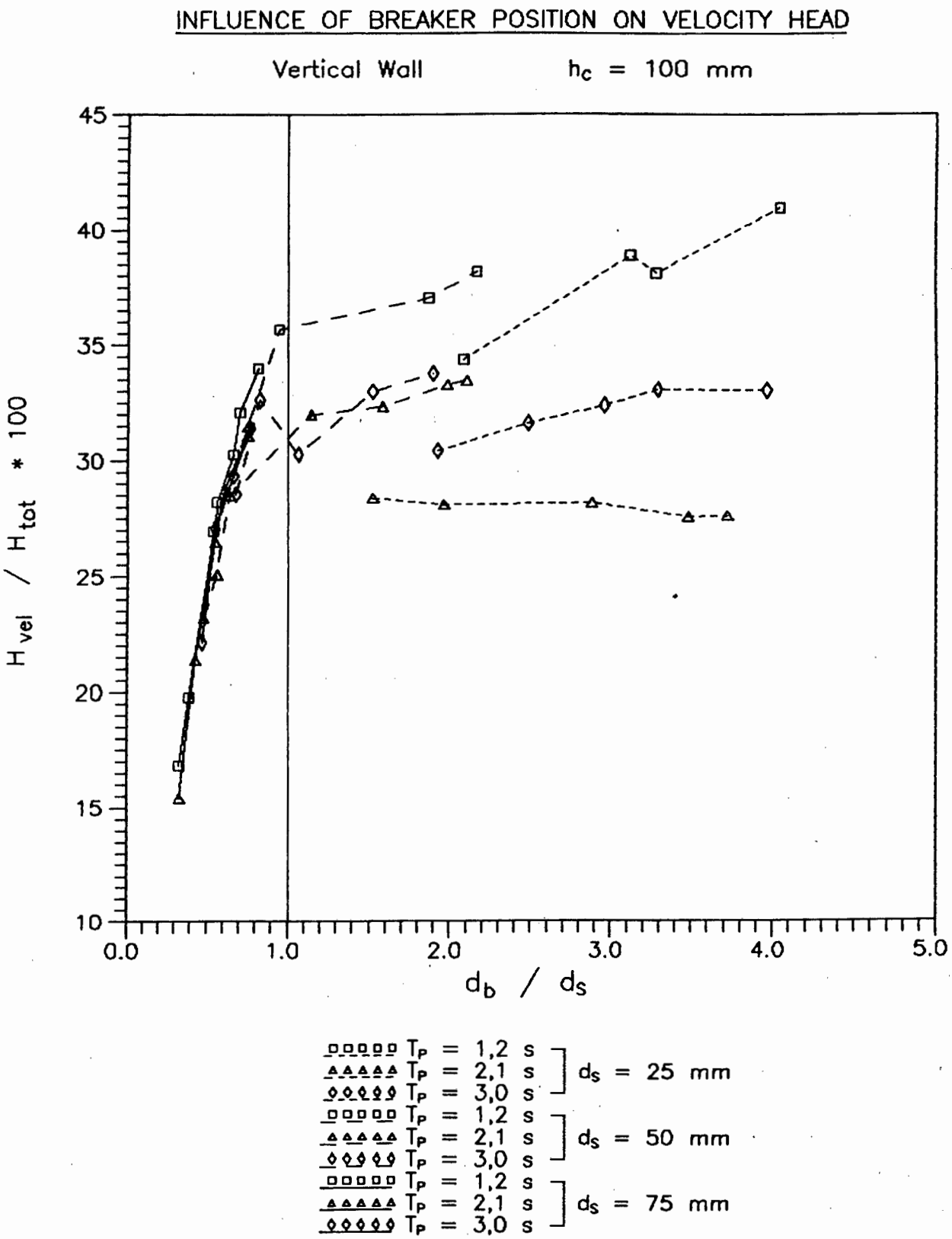
INFLUENCE OF BREAKER POSITION ON VELOCITY HEAD
Vertical Wall
h_c = 100 mm
H_{vel} / H_{tot} * 100
45
40
35
30
25
20
15
10
0.0
1.0
2.0
3.0
4.0
5.0
d_b / d_s
T_P = 1,2 s
T_P = 2,1 s
T_P = 3,0 s
d_s = 25 mm
T_P = 1,2 s
T_P = 2,1 s
T_P = 3,0 s
d_s = 50 mm
T_P = 1,2 s
T_P = 2,1 s
T_P = 3,0 s
d_s = 75 mm

Figure 7.6

INFLUENCE OF BREAKER POSITION ON VELOCITY HEAD

Vertical Wall h_c = 200 mm

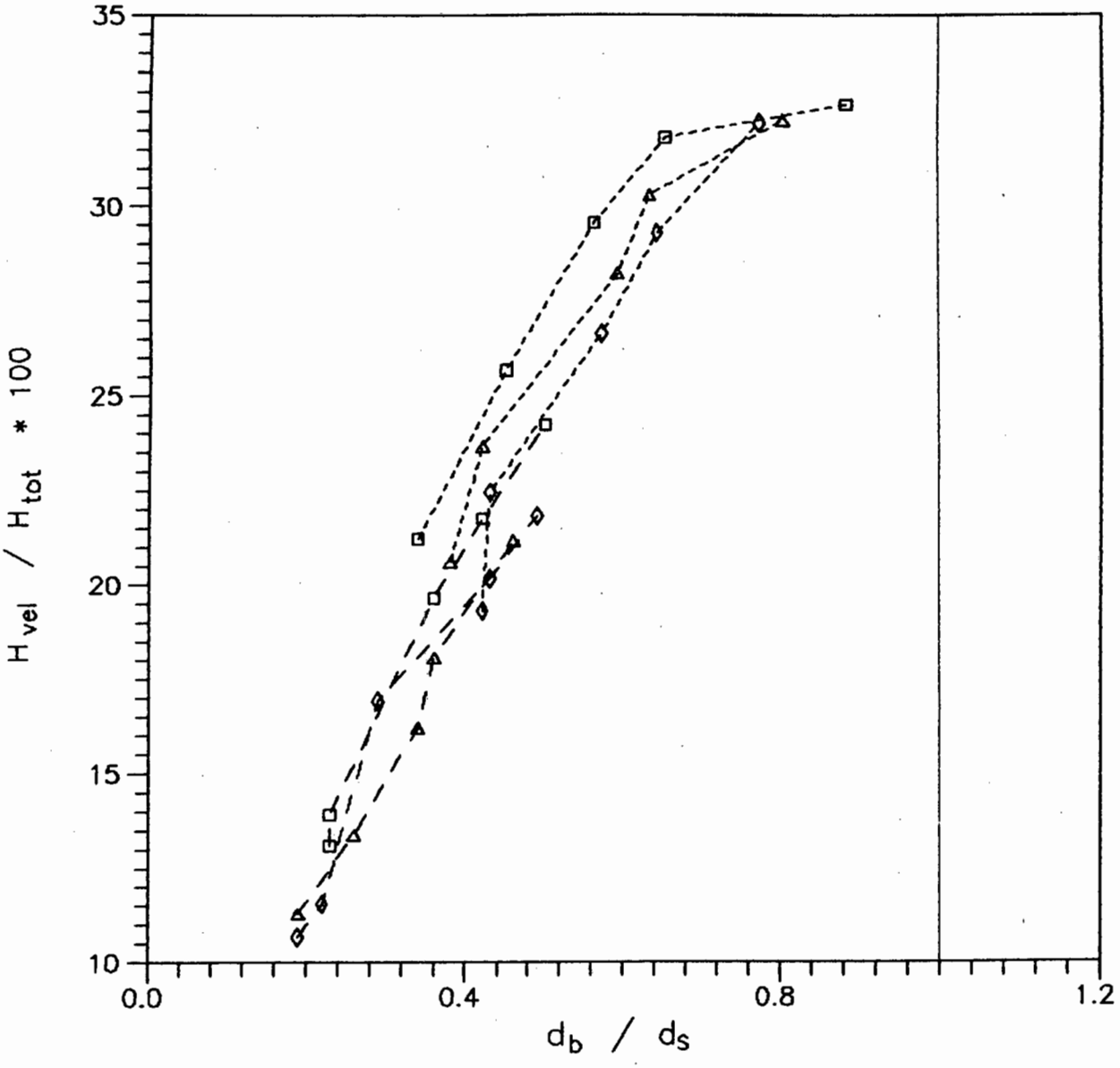

□□□□□ T_P = 1,2 s
△△△△△ T_P = 2,1 s
◇◇◇◇◇ T_P = 3,0 s
] d_s = 120 mm

□□□□□ T_P = 1,2 s
△△△△△ T_P = 2,1 s
◇◇◇◇◇ T_P = 3,0 s
] d_s = 160 mm

Figure 7.7

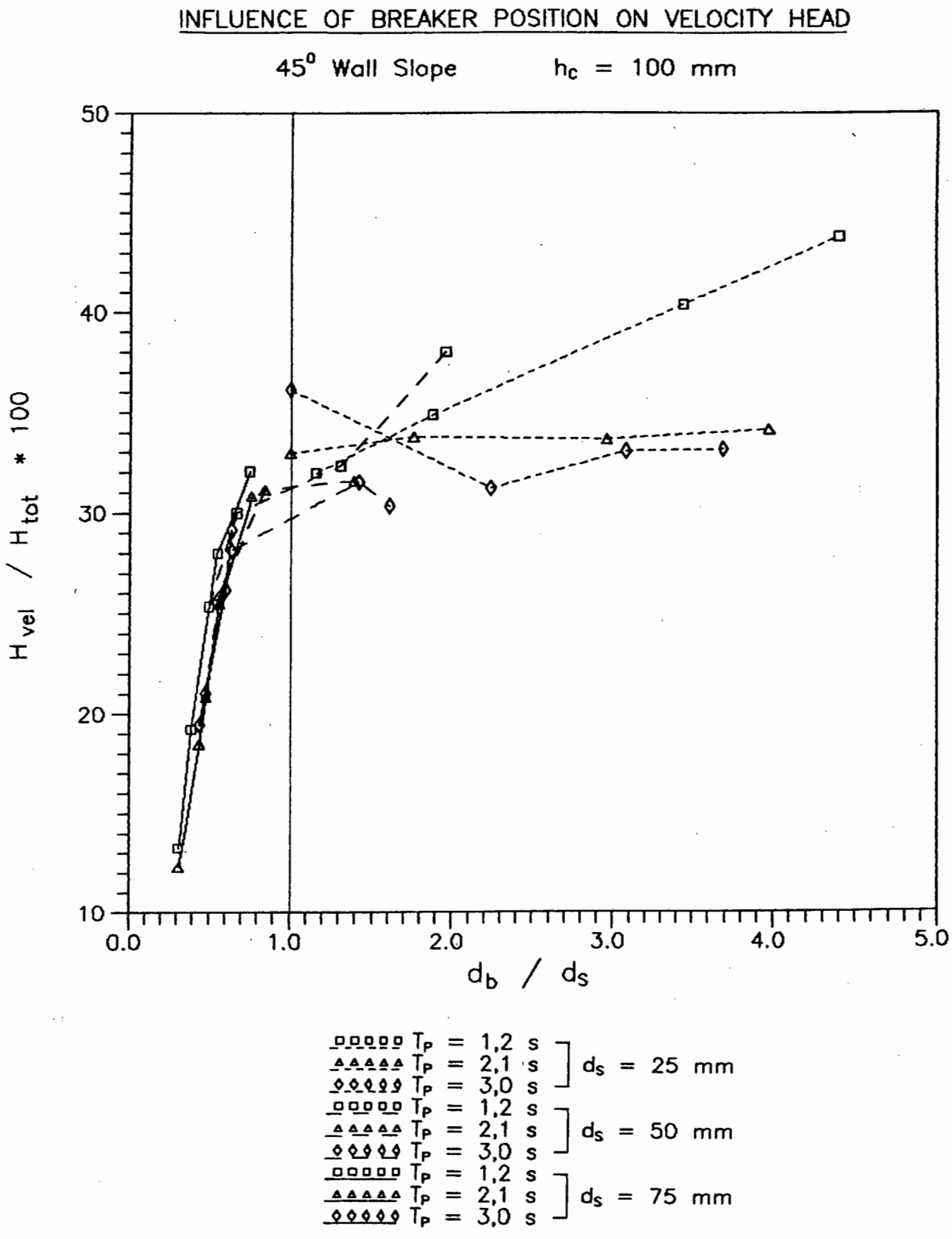
INFLUENCE OF BREAKER POSITION ON VELOCITY HEAD
45° Wall Slope
h_c = 100 mm
H_{vel} / H_{tot} * 100
50
40
30
20
10
0.0
1.0
2.0
3.0
4.0
5.0
d_b / d_s
T_P = 1,2 s
T_P = 2,1 s
T_P = 3,0 s
d_s = 25 mm
T_P = 1,2 s
T_P = 2,1 s
T_P = 3,0 s
d_s = 50 mm
T_P = 1,2 s
T_P = 2,1 s
T_P = 3,0 s
d_s = 75 mm

Figure 7.8

7.5 Design procedure

The trend of the data in Figures 7.4 and 7.5 was found to approximate an exponential equation of the form

$$\frac{Q}{\sqrt{g\ H_{tot}^{\ 3}}} = a\ .\ \exp\left[\ b.\frac{F}{H_{tot}}\ \right] \qquad (7.18)$$

The coefficients a, b and the correlation coefficient obtained from a regression analysis are given in Table 7.1. Figure 7.9 shows the data for both structure geometries tested as well as the fitted exponential curves. As would be expected, the wall with the 45° slope gives more overtopping than the vertical wall.

Structure geometry	a	b	R squared
Vertical wall	0,04497	-3,0446	0,908
45° wall slope	0,03227	-1,6947	0,829

Table 7.1 : Regression coefficients for exponential model

EXPONENTIAL EQUATIONS FITTED TO DIMENSIONLESS DATA

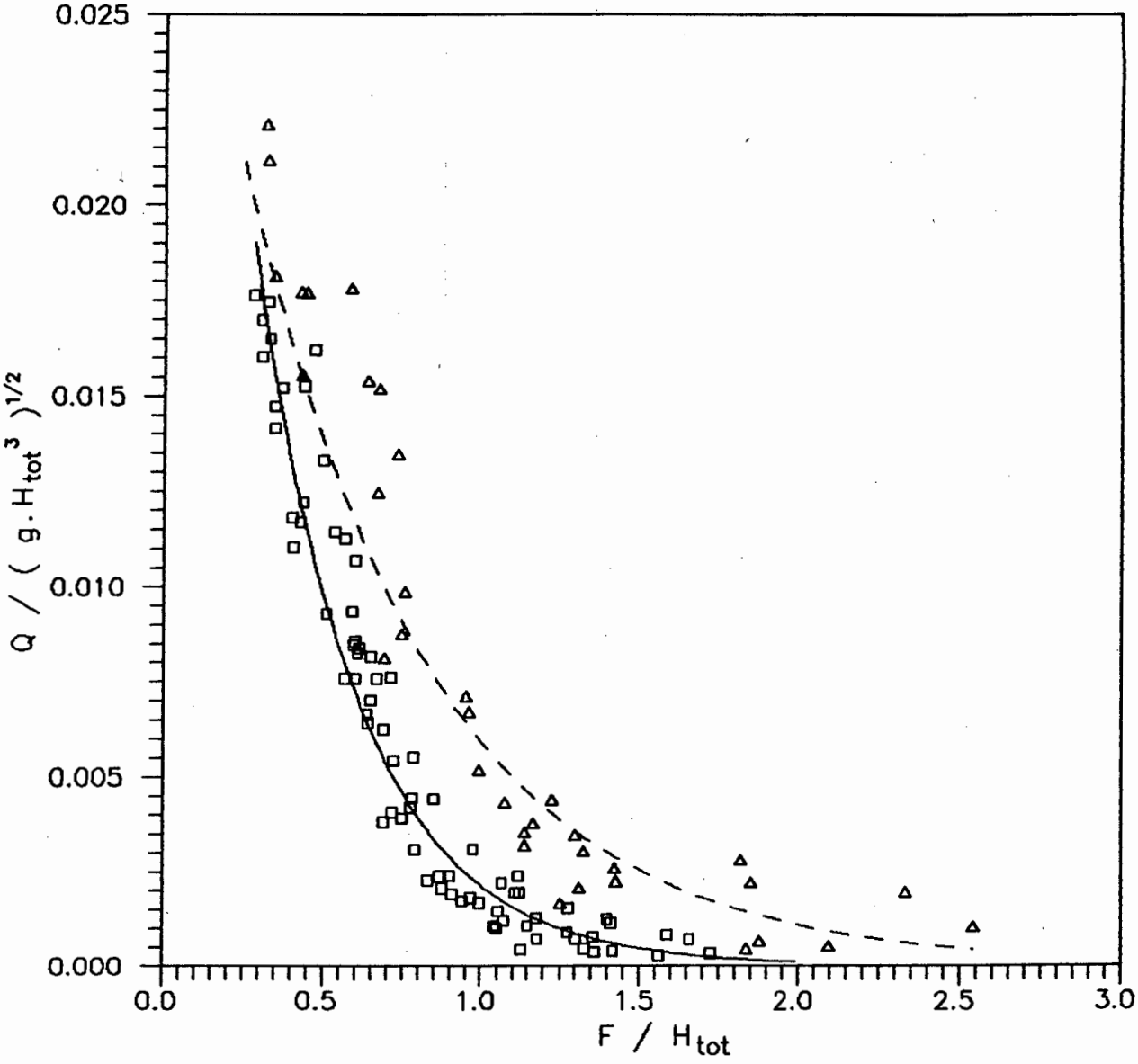

Figure 7.9

Eqn. (7.18) or alternatively Fig. 7.9 may be used for a preliminary design calculation to estimate the overtopping rate expected for either of the structure geometries tested.

If the waves are unbroken at the structure the information required is the freeboard, the depth at the structure toe, the significant wave height at the structure toe and the peak wave period. The wavelength at the structure toe is calculated using eqn. (2.3).

For broken waves the information required is the freeboard, the depth at the structure toe, the significant wave height and the breaker depth. If the foreshore slope is approximately 1:20 then the depth of breaking can be estimated using Figure 6.8, provided that the deepwater wave steepness is known.

The breaker depth can also be estimated using design charts such as those given by Shore Protection Manual (SPM) or Goda (see Appendix D). A comparison between the breaker depths measured experimentally and those obtained from the SPM and Goda for a 1:20 foreshore slope is shown in Figure 7.10.

Although the experimentally measured breaker depths are smaller than those obtained from the design charts, there is a linear relation between the breaker depths which is given by

$$d_b(\text{experimental}) = 0{,}45\ d_b(\text{Goda}) \qquad (7.19)$$

$$d_b(\text{experimental}) = 0{,}66\ d_b(\text{SPM}) \qquad (7.20)$$

The reasons for this discrepancy in the breaker depths include the fact that the depths obtained from the SPM are based on tests using regular waves, while Goda's values are based on a mathematical model and not directly on experimental measurements.

If it is assumed that eqns. (7.19) and (7.20) which pertain to a 1:20 slope are valid for other foreshore slopes, then the design charts can be used to estimate the breaker depth for other foreshore slopes and eqns. (7.19) or (7.20) can be used to determine the breaker depths which should be applied in eqn. (7.17) to calculate the velocity head. This approach provides a tentative method for extending these experimental results to foreshore slopes other than the 1:20 slope used in the tests.

COMPARISON BETWEEN BREAKER DEPTHS MEASURED EXPERIMENTALLY AND BREAKER DEPTHS OBTAINED FROM GODA AND SHORE PROTECTION MANUAL

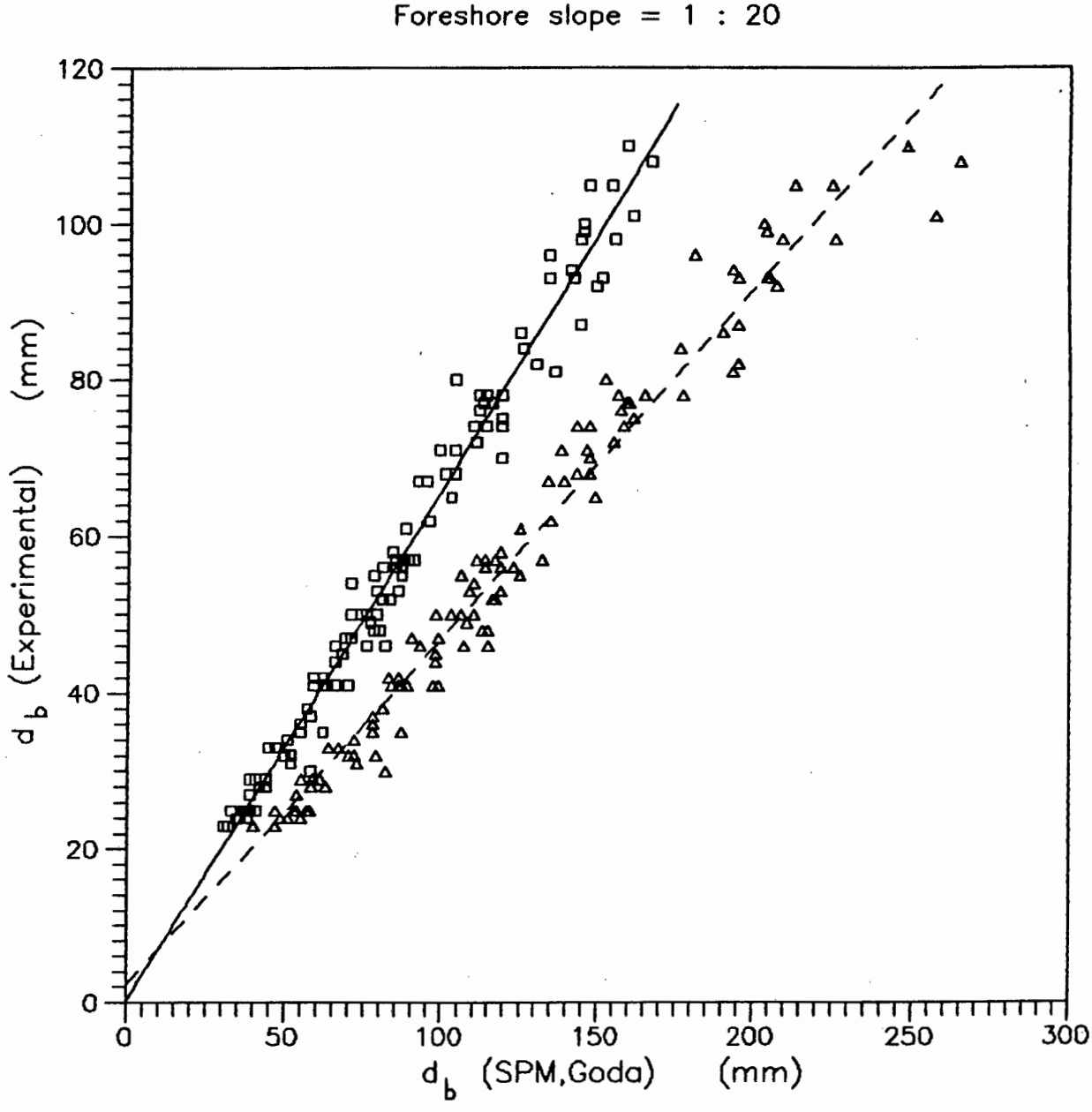

Figure 7.10

CHAPTER 8

CONCLUSIONS

Based on the tests performed and the analysis of the experimental data the following conclusions can be drawn :

1. The mechanism of overtopping is different for unbroken, breaking and broken waves. This can be ascribed to the different kinematics of the water particles involved, with broken and breaking waves relying largely on the forward velocity of the water particles to overtop the structure crest. Unbroken waves were found to rely more on the difference in height between the wave crest and the structure crest.

2. The energy level or total head of the incoming waves was found to be an important parameter for predicting the overtopping rate. The total head is defined as

$$H_{tot} = H_{si} + H_{vel}$$

where $H_{vel} = \frac{v^2}{2g}$ is a velocity head due to the velocity of the water particles in the waves. Expressions were developed for calculating the velocity head for both unbroken and broken waves. The velocity heads are given by

$$H_{vel} = c \cdot 0{,}82 \cdot g \cdot \left[\frac{H_{si}\ T_p}{L_{pi}}\right]^2 \qquad \text{(unbroken waves)}$$

$$H_{vel} = c \cdot \frac{d_b}{2} \cdot \left[\frac{1{,}56\ d_b + d_s}{2{,}56\ d_b} \right] \qquad \text{(broken waves)}$$

where c is an empirical coefficient which was found to be approximately 0,75.

3. Two dimensionless parameters $Q/\sqrt{g\ H_{tot}^{\ 3}}$ and F/H_{tot} were found to consolidate all the overtopping data for a particular structure geometry into a single, well defined trend. The relationship between these two parameters was approximated by an exponential equation of the form

$$\frac{Q}{\sqrt{g\ H_{tot}^{\ 3}}} = a \cdot \exp\left[b \cdot \frac{F}{H_{tot}} \right]$$

where a and b are regression coefficients.

LIST OF REFERENCES

1. 'Shore Protection Manual', US Army Engineer Waterways Experiment Station, Coastal Engineering Research Centre, Vols. 1 and 2, US Government Printing Office, Washington DC, 1984.

2. GODA, Y. 'Random seas and the design of maritime structures', University of Tokyo Press, Tokyo, 1985.

3. THOMPSON, E. F. and VINCENT, C. L. 'Significant wave height for shallow water design', Journal of Waterway Port Coastal and Ocean Engineering, Vol. 3, No. 5, September, 1985, 828-842.

4. RYE, H. 'The stability of some currently used wave parameters', Coastal Engineering, 1, 1977, 17-30.

5. SAVILLE, T. and CALDWELL, J. 'Experimental study of wave overtopping on shore structures', Proc. Minnesota International Hydraulics Convention, Sept, 1953, 261-269.

6. SAVILLE, T. 'Laboratory data on wave run-up and overtopping on shore structures', Techncal Memorandum No. 64, Beach Erosion Board, Corps of Engineers, October, 1955.

7. ISHIHARA, T., INAGAKI, Y. and MITSU, H. 'Wave overtopping of seawalls', Coastal Eng. in Japan, Vol. 3, 1960, 53-62.

8. PAAPE, A. 'Experimental data on the overtopping of seawalls by waves', Proc. 7th Conf. Coastal Eng., The Hague, Vol. 2, 1960, 674-681.

9. KIKKAWA, H., SHI-IGAI, H. and KONO, T. 'Fundamental study of wave overtopping on levees', Coastal Eng. in Japan, Vol. 11, 1968, 107-115.

10. SHI-IGAI, H. and KONO, T. 'Analytical approach on wave overtopping of levees', Proc. 12th Conf. Coastal Eng., Vol. 1, Washington DC, 1970, 563-573.

11. TAKADA, A. 'Estimation of wave overtopping quantity over seawalls', Proc. 14th Conf. Coastal Eng., 1974, 1996-2014.

12. TSURUTA, S. and GODA, Y. 'Expected discharge of irregular wave overtopping', Proc. 11th Conf. Coastal Eng., Vol. 2, London, 1968, 833-852.

13. GODA, Y. 'Expected rate of irregular wave overtopping of seawalls', Coastal Eng. in Japan, Vol. 14, 1971, 43-51.

14. BATTJES, J. 'Computation of set-up, longshore currents, run-up and overtopping due to wind-generated waves', Report No. 74-2, Delft University of Technology, Department of Civil Engineering, Delft, Holland, 1974.

15. DOUGLASS, L. 'Review and comparison of methods for estimating irregular wave overtopping rates', Technical Report No. CERC-86-12, US Army Engineer Waterways Experiment Station, Coastal Engineering Research Centre, 1986.

16. WEGGEL, J. 'Wave overtopping equation', Proc. 15th Coastal Eng. Conf., Honolulu, 1976, 2737-2755.

17. AHRENS, J. 'Prediction of irregular wave overtopping', CETA 77-7, US Army Engineer Waterways Experiment Station, Coastal Engineering Research Centre, 1977.

18. AHRENS, J. 'Prediction of irregular wave runup', CETA 77-2, US Army Engineer Waterways Experiment Station, Coastal Engineering Research Centre, 1977.

19. AHRENS, J. 'Wave runup on idealized structures', Coastal Structures '83 Speciality Conference, Arlington, Va., 1983, 925-938.

20. JENSEN, O. and SORENSEN, T. 'Overspilling/overtopping of rubble-mound breakwaters. Results of studies useful in design procedures', Coastal Engineering, Vol. 3, 1979, 51-65.

21. JENSEN, O. and SORENSEN, T. 'Wave overtopping on breakwaters and sea dikes', 2nd Int. Conf. on Coastal and Port Eng. in Developing Countries, 1987, 716-730.

22. OWEN, M. 'Overtopping of sea defences', Int. Conf. on Hydraulic Modelling of Civil Engineering Structures, England, 1982, 469-480.

23. OWEN, M. 'Design of seawalls allowing for wave overtopping', Report No. EX 924, Hydraulics Research Station, Wallingford, England, 1980.

24. KOBAYASHI, N. and REECE, A. 'Irregular wave overtopping on gravel islands', Journal of Waterway Port Coastal and Ocean Engineering, ASCE, WW4, Vol. 109, 1983, 429-444.

25. KOBAYASHI, N. and WURJANTO, A. 'Wave overtopping on coastal structures', Journal of Waterway Port Coastal and Ocean Engineering, Vol. 115, No. 2, 1989, 235-251.

26. AHRENS, J. and HEIMBAUGH, M. 'Seawall overtopping model', 21st Coastal Eng. Conf., Spain, 1988, 795-806.

27. 'Table Bay Harbour : Repairs to western breakwater - model tests', CSIR Report C/SEA 8528, Stellenbosch, 1985.

28. MANSARD, E. and FUNKE, E. 'The measurement of incident and reflected spectra using a least squares method', Proc. 17th Coastal Eng. Conf., Sydney, 1980, 154-172.

BIBLIOGRAPHY

AHRENS, J. 'Prediction of irregular wave overtopping', CETA 77-7, US Army Engineer Waterways Experiment Station, Coastal Engineering Research Centre, 1977.

AHRENS, J. 'Prediction of irregular wave runup', CETA 77-2, US Army Engineer Waterways Experiment Station, Coastal Engineering Research Centre, 1977.

AHRENS, J. 'Wave runup on idealized structures', Coastal Structures '83 Speciality Conference, Arlington, Va., 1983, 925-938.

AHRENS, J. and HEIMBAUGH, M. 'Seawall overtopping model', 21st Coastal Eng. Conf., Spain, 1988, 795-806.

AHRENS, J., HEIMBAUGH, M. and DAVIDSON, D. 'Irregular wave overtopping of seawall/revetment configurations Roughans Point Massachusetts, Technical Report CERC-86-7, US Army Engineer Waterways Experiment Station, Coastal Engineering Research Centre, 1986.

BATTJES, J. 'Computation of set-up, longshore currents, run-up and overtopping due to wind-generated waves', Report No. 74-2, Delft University of Technology, Department of Civil Engineering, Delft, Holland, 1974.

CROSS, R. and SOLLITT, C. 'Wave transmission by overtopping', Journal of the Waterways Harbours and Coastal Eng. Div., Proc. ASCE, August, 1972, 295-309.

DOUGLASS, L. 'Review and comparison of methods for estimating irregular wave overtopping rates', Technical Report No. CERC-86-12, US Army Engineer Waterways Experiment Station, Coastal Engineering Research Centre, 1986.

GADD, P. E. 'Wave runup and overtopping : A review and recommendations', 16th Offshore Technology Conference, Houston, 1984, 239-249.

GODA, Y. 'Random seas and the design of maritime structures', University of Tokyo Press, Tokyo, 1985.

GODA, Y. 'Expected rate of irregular wave overtopping of seawalls', Coastal Eng. in Japan, Vol. 14, 1971, 43-51.

HUNT, I. A. 'Design of seawalls and breakwaters', Journal of the Waterways and Harbour Division, Proc. ASCE, September, 1959, 123-152.

'Hydraulic Engineering', CIV 302 course notes, University of Cape Town, 1987.

'Hydraulic Engineering', CIV 403 course notes, University of Cape Town, 1988.

ISHIHARA, T., INAGAKI, Y. and MITSU, H. 'Wave overtopping of seawalls', Coastal Eng. in Japan, Vol. 3, 1960, 53-62.

IWAGAKI, Y., SHIMA, A. and INOUE, M. 'Effects of wave height and sea level on wave overtopping and wave run-up', Coastal Eng. in Japan, Vol. 8, 1965, 141-151.

JENSEN, O. and SORENSEN, T. 'Overspilling/overtopping of rubble-mound breakwaters. Results of studies useful in design procedures', Coastal Engineering, Vol. 3, 1979, 51-65.

JENSEN, O. and SORENSEN, T. 'Wave overtopping on breakwaters and sea dikes', 2nd Int. Conf. on Coastal and Port Eng. in Developing Countries, 1987, 716-730.

KIKKAWA, H., SHI-IGAI, H. and KONO, T. 'Fundamental study of wave overtopping on levees', Coastal Eng. in Japan, Vol. 11, 1968, 107-115.

KOBAYASHI, N. and REECE, A. 'Irregular wave overtopping on gravel islands', Journal of Waterway Port Coastal and Ocean Engineering, ASCE, WW4, Vol. 109, 1983, 429-444.

KOBAYASHI, N. and WURJANTO, A. 'Wave overtopping on coastal structures', Journal of Waterway Port Coastal and Ocean Engineering, Vol. 115, No. 2, 1989, 235-251.

MANSARD, E. and FUNKE, E. 'The measurement of incident and reflected spectra using a least squares method', Proc. 17th Coastal Eng. Conf., Sydney, 1980, 154-172.

OWEN, M. 'Overtopping of sea defences', Int. Conf. on Hydraulic Modelling of Civil Engineering Structures, England, 1982, 469-480.

OWEN, M. 'Design of seawalls allowing for wave overtopping', Report No. EX 924, Hydraulics Research Station, Wallingford, England, 1980.

PAAPE, A. 'Experimental data on the overtopping of seawalls by waves', Proc. 7th Conf. Coastal Eng., The Hague, Vol. 2, 1960, 674-681.

RYE, H. 'The stability of some currently used wave parameters', Coastal Engineering, 1, 1977, 17-30.

SAVILLE, T. and CALDWELL, J. 'Experimental study of wave overtopping on shore structures', Proc. Minnesota International Hydraulics Convention, Sept, 1953, 261-269.

SAVILLE, T. 'Laboratory data on wave run-up and overtopping on shore structures', Technical Memorandum No. 64, Beach Erosion Board, Corps of Engineers, October, 1955.

SHI-IGAI, H. and KONO, T. 'Analytical approach on wave overtopping of levees', Proc. 12th Conf. Coastal Eng., Vol. 1, Washington DC, 1970, 563-573.

'Shore Protection Manual', US Army Engineer Waterways Experiment Station, Coastal Engineering Research Centre, Vols. 1 and 2, US Government Printing Office, Washington DC, 1984.

'Table Bay Harbour : Repairs to western breakwater - model tests', CSIR Report C/SEA 8528, Stellenbosch, 1985.

TAKADA, A. 'Estimation of wave overtopping quantity over seawalls', Proc. 14th Conf. Coastal Eng., 1974, 1996-2014.

THOMPSON, E. F. and VINCENT, C. L. 'Significant wave height for shallow water design', Journal of Waterway Port Coastal and Ocean Engineering, Vol. 3, No. 5, September, 1985, 828-842.

TSURUTA, S. and GODA, Y. 'Expected discharge of irregular wave overtopping', Proc. 11th Conf. Coastal Eng., Vol. 2, London, 1968, 833-852.

UNDERHILL, L. 'Introstat', 4th Edition, Juta and Co., Cape Town, 1985.

'Wave run-up and overtopping', Technical Advisory Committee on Protection against Inundation, Government publishing office, The Hague, 1974.

WEGGEL, J. 'Wave overtopping equation', Proc. 15th Coastal Eng. Conf., Honolulu, 1976, 2737-2755.

APPENDIX A

LIST OF PARAMETERS CALCULATED BY THE SPECTRAL ANALYSIS WAVE PROGRAM

COEF OF SKEWNESS — Skewness of surface elevations of the time series. Should be 0 for Gaussian distribution.

COEF OF KURTOSIS — Kurtosis of surface elevations of the time series. Should be 3 for Gaussian distribution.

DEGREES OF FREEDOM — The chi-squared number of degrees of freedom of the estimated spectrum.

ETA — Goodness-of-fit parameter between target and measured spectra determined as

$$1 - \left[\frac{\int_{f_1}^{f_2} (s(f) - s^*(f))^2 \, df}{\int_{f_1}^{f_2} s^*(f)^2 \, df} \right]^{\frac{1}{2}}$$

where

$S(f)$ = measured spectral density

$S^*(F)$ = target spectral density

FREQUENCY RESOLUTION — The resolution bandwidth of S(f) in the frequency domain.

FREQUENCY INTERVAL — The frequency interval at which estimates of S(f) are made.

GROUPINESS FACTOR	The groupiness factor calculated from the smoothed instantaneous wave energy history (SIWEH).
GROUP REPETITION PERIOD	The average time between wave groups.
HS	The significant wave height determined in the time domain as 4σ, σ being the standard deviation of the time series.
H1/3	The zero-downcrossing significant wave height calculated in the time domain as the average of the highest one-third zero-downcrossing wave heights.
H_{m_0}	The significant wave height determined in the frequency domain as $4\sqrt{m_0}$ where m_0 is the area under the spectral curve S(f) between an upper and lower cut-off frequency.
H1 (DRAPER)	The difference between the maximum and minimum water surface elevation in a record as used in Draper type analysis.
HMAX	The maximum zero-downcrossing wave height.
HIGH FREQUENCY CUT-OFF	The high frequency cut-off limit of S(f).
LOW FREQUENCY CUT-OFF	The low frequency cut-off limit of S(f).
MODEL SCALE	The Froude model scale of the tests.
m_n	The n th moment of spectral density.
NO OF SAMPLES	The number of samples in a record.

NYQUIST FREQUENCY	The highest frequecy to which the spectrum S(f) can be estimated.
PEAK SPECTRAL DENSITY	The spectral density at which S(f) has its maximum value.
QP PEAKEDNESS FACTOR	The spectral width parameter defined as $\frac{2}{m_o^2} \int_0^\infty f\,[s(f)]^2\,df$ This parameter takes values of 1 for white noise, around 2 for wind waves, and higher values for swell
SAMPLING INTERVAL	The time interval at which the data were sampled.
S(f)	The spectral density function.
TH1/3	The significant wave period calculated in the time domain as the average period of the highest one-third of zero-downcrossing wave heights.
THMAX	The period of the maximum height zero-downcrossing wave.
TP	The spectral peak period being equal to $1/f_p$, where f_p is the frequency at which S(f) is a maximum.

TPD	The spectral peak period being equal to $1/f_{pd}$, where f_{pd} is computed by the centroid of the spectral band between the upper and lower intercepts of the the spectral density and the threshold, which is 80% of $S(f_p)$.
TM02	The average wave period determined in the frequency domain by $\sqrt{m_0/m_2}$.
TZ	The average wave period by zero-downcrossing.
VARIANCE	The variance of the time series in the time domain.
WATER DEPTH	The water depth where the measurement was made.

APPENDIX B

REPEATABILITY OF THE TEST RESULTS

	Test No.	d_s (mm)	H_{st} (mm)	H_{si} (mm)	T_p (s)	d_b (mm)	Q ($dm^3/s/m$)
	6A	50.0	23.0	31.6	2.06	31	0.0538
	6B	50.0	24.2	32.4	2.17	33	0.0608
	6C	50.0	24.3	32.2	2.20	31	0.0561
	6D	50.0	23.8	32.3	2.18	33	0.0595
	6E	50.0	24.1	31.1	2.10	32	0.0558
Mean		50.0	23.9	31.9	2.14	32	0.0572
Std deviation		0.0	0.5	0.6	0.06	1.0	0.0029
Std error (%)		0.0	2.2	1.7	2.8	3.1	5.0
	7A	50.0	108.1	62.6	2.1	110	1.0338
	7B	50.0	108.4	62.3	2.1	107	1.0308
	7C	50.2	105.8	62.2	2.1	103	1.0499
	7D	50.0	103.8	61.9	2.1	104	0.9818
	7E	50.0	104.7	62.3	2.1	100	1.0271
Mean		50.0	106.2	62.3	2.1	105	1.0250
Std deviation		0.1	2.0	0.3	0.03	4.0	0.0260
Std error (%)		0.2	1.9	0.4	1.2	3.7	2.5

APPENDIX C

CALCULATION OF DIMENSIONLESS OVERTOPPING PARAMETERS

Ref. no.	$\frac{F}{H_{s1}}$ ( )	$\frac{d_s}{H_{s1}}$ ( )	$\frac{H_{s1}}{g\,T_p^2}$ ( )	$\frac{Q}{\sqrt{g\,H_{s1}^3}}$ ( )	H_{vel} (mm)	H_{tot} (mm)	$\frac{F}{H_{tot}}$ ( )	$\frac{Q}{\sqrt{g\,H_{tot}^3}}$ ( )
1	2.525	0.842	0.0022116	0.0013411	15.54	45.24	1.6576	0.0007133
2	2.219	0.740	0.0025170	0.0016082	21.49	55.29	1.3566	0.0007687
3	2.060	0.687	0.0027106	0.0018252	22.40	58.80	1.2755	0.0008890
4	1.943	0.648	0.0028744	0.0023239	26.74	65.34	1.1478	0.0010551
5	2.404	0.801	0.0007281	0.0005446	12.35	43.55	1.7223	0.0003303
6	1.969	0.656	0.0008977	0.0006569	14.86	52.96	1.4162	0.0004008
7	1.459	0.486	0.0011769	0.0016411	20.12	71.52	1.0487	0.0010000
8	1.210	0.403	0.0014608	0.0033400	23.54	85.54	0.8768	0.0020609
9	1.145	0.382	0.0015433	0.0036778	24.91	90.41	0.8295	0.0022677
10	2.239	0.746	0.0003871	0.0004738	14.63	48.13	1.5583	0.0002752
11	1.943	0.648	0.0003991	0.0008125	17.83	56.43	1.3291	0.0004597
12	1.744	0.581	0.0004743	0.0013105	20.57	63.57	1.1798	0.0007290
13	1.602	0.548	0.0005338	0.0022098	22.93	69.43	1.0730	0.0012112
14	1.404	0.468	0.0006171	0.0031643	26.29	79.69	0.9412	0.0017359
15	1.748	1.748	0.0020587	0.0024556	10.55	39.15	1.2772	0.0015334
16	1.163	1.163	0.0030953	0.0075695	23.84	66.84	0.7480	0.0039058
17	1.029	1.029	0.0034404	0.0140058	28.58	77.18	0.6479	0.0069990
18	0.965	0.965	0.0037922	0.0174025	32.00	83.80	0.5966	0.0084569
19	2.066	2.066	0.0005594	0.0012297	7.31	31.51	1.5868	0.0008277
20	1.866	1.866	0.0006195	0.0019066	8.96	35.76	1.3980	0.0012367
21	1.567	1.567	0.0007101	0.0032054	12.70	44.60	1.1211	0.0019390
22	1.155	1.155	0.0010009	0.0098297	20.35	63.65	0.7856	0.0055154
23	0.962	0.943	0.0012370	0.0146350	25.08	77.58	0.6510	0.0081479
24	0.849	0.832	0.0013753	0.0206432	29.65	89.15	0.5665	0.0112565
25	0.803	0.803	0.0014679	0.0210454	31.32	93.62	0.5341	0.0114248
26	1.553	1.553	0.0003460	0.0032214	12.85	45.05	1.1099	0.0019467
27	1.290	1.280	0.0004153	0.0042987	18.82	57.72	0.8697	0.0023782
28	1.116	1.116	0.0004942	0.0071886	19.44	64.24	0.7784	0.0041870
29	0.996	0.996	0.0005537	0.0137986	24.69	74.89	0.6676	0.0075726
30	0.888	0.881	0.0006315	0.0173023	28.78	85.28	0.5887	0.0093313
31	1.092	3.275	0.0017053	0.0025244	4.63	27.53	0.9080	0.0019150
32	0.896	2.688	0.0020776	0.0056521	6.87	34.77	0.7189	0.0040618
33	0.562	1.685	0.0032033	0.0193899	17.47	61.97	0.4034	0.0117981
34	0.503	1.525	0.0034899	0.0252384	21.37	70.67	0.3509	0.0147051
35	0.455	1.401	0.0038156	0.0285938	25.44	79.34	0.3088	0.0160101
36	0.428	1.284	0.0041341	0.0328347	30.05	88.45	0.2826	0.0176162
37	1.152	3.456	0.0005016	0.0039652	3.95	25.65	0.9747	0.0030855
38	0.772	2.315	0.0007489	0.0118141	8.81	41.21	0.6067	0.0082373
39	0.583	1.748	0.0009823	0.0184977	15.45	58.35	0.4285	0.0116625
40	0.520	1.559	0.0011013	0.0252626	19.42	67.52	0.3703	0.0151907
41	0.471	1.398	0.0012485	0.0304554	24.08	77.58	0.3248	0.0174420
42	0.486	1.369	0.0012459	0.0290275	24.76	78.66	0.3331	0.0164662
43	0.729	2.187	0.0003834	0.0110221	9.76	44.06	0.5675	0.0075719
44	0.559	1.678	0.0005131	0.0176992	16.57	61.27	0.4081	0.0110300
45	0.492	1.500	0.0005841	0.0237849	20.83	71.03	0.3478	0.0141325
46	0.446	1.359	0.0006359	0.0298620	25.35	80.75	0.3059	0.0169702

Ref. no.	$\frac{F}{H_{si}}$ ( )	$\frac{d_s}{H_{si}}$ ( )	$\frac{H_{si}}{g\,T_p^2}$ ( )	$\frac{Q}{\sqrt{g\,H_{si}^3}}$ ( )	H_{vel} (mm)	H_{tot} (mm)	$\frac{F}{H_{tot}}$ ( )	$\frac{Q}{\sqrt{g\,H_{tot}^3}}$ ( )
47	1.724	2.586	0.0035151	0.0005303	12.49	58.89	1.3585	0.0003709
48	1.341	2.003	0.0043047	0.0026243	20.63	80.43	0.9972	0.0016825
49	1.122	1.683	0.0058989	0.0052037	29.86	101.16	0.7908	0.0030793
50	1.014	1.521	0.0067695	0.0067637	36.74	115.64	0.6918	0.0038117
51	0.950	1.425	0.0059605	0.0116106	40.78	124.98	0.6401	0.0064205
52	1.639	2.459	0.0011280	0.0010159	12.66	61.46	1.3016	0.0007187
53	1.379	2.069	0.0014930	0.0021897	17.97	75.97	1.0531	0.0014608
54	1.088	1.633	0.0018920	0.0072727	28.85	102.35	0.7816	0.0044256
55	0.991	1.472	0.0018769	0.0106993	35.21	116.41	0.6915	0.0062329
56	0.904	1.343	0.0020572	0.0149806	42.30	131.30	0.6131	0.0083599
57	1.747	2.620	0.0005187	0.0015635	10.94	56.74	1.4098	0.0011338
58	1.441	2.162	0.0006286	0.0034895	16.07	71.57	1.1178	0.0023828
59	1.156	1.726	0.0007860	0.0070150	25.18	94.58	0.8480	0.0044096
60	1.020	1.515	0.0008936	0.0091134	32.62	111.52	0.7218	0.0054232
61	0.885	1.322	0.0010262	0.0152809	42.91	133.51	0.6007	0.0085426
62	1.198	4.790	0.0024452	0.0013076	5.04	38.44	1.0407	0.0010592
63	1.124	4.494	0.0026969	0.0022673	5.76	41.36	0.9672	0.0018108
64	0.749	2.976	0.0040681	0.0104911	13.12	66.82	0.6017	0.0075590
65	0.653	2.610	0.0045648	0.0134024	17.03	78.33	0.5107	0.0092789
66	0.578	2.312	0.0057252	0.0184879	22.10	91.30	0.4381	0.0121986
67	1.270	5.079	0.0007281	0.0005425	4.01	35.51	1.1266	0.0004533
68	1.042	4.167	0.0008162	0.0029573	5.93	44.33	0.9023	0.0023841
69	0.849	3.344	0.0011026	0.0099082	9.22	56.92	0.7116	0.0076019
70	0.733	2.930	0.0012621	0.0143819	12.04	66.64	0.6003	0.0106668
71	0.600	2.399	0.0014439	0.0231160	17.90	84.60	0.4728	0.0161816
72	1.316	5.263	0.0003246	0.0015119	3.63	34.03	1.1753	0.0012764
73	1.205	4.819	0.0003544	0.0026495	4.33	37.53	1.0657	0.0022042
74	0.768	3.093	0.0005867	0.0087527	10.55	62.35	0.6383	0.0066278
75	0.627	2.493	0.0006933	0.0186326	16.18	80.28	0.5007	0.0132939
76	0.563	2.254	0.0007580	0.0220489	19.82	90.82	0.4404	0.0152414

Ref. no.	$\frac{F}{H_{si}}$ ( )	$\frac{d_s}{H_{si}}$ ( )	$\frac{H_{si}}{g\,T_p^2}$ ( )	$\frac{Q}{\sqrt{g\,H_{si}^3}}$ ( )	H_{vel} (mm)	H_{tot} (mm)	$\frac{F}{H_{tot}}$ ( )	$\frac{Q}{\sqrt{g\,H_{tot}^3}}$ ( )
77	3.425	1.142	0.0016590	0.0035268	10.29	32.19	2.3300	0.0019792
78	2.788	0.929	0.0020378	0.0053479	14.40	41.30	1.8159	0.0028109
79	2.174	0.725	0.0025691	0.0075334	23.31	57.81	1.2973	0.0034727
80	2.027	0.676	0.0027552	0.0075769	28.80	65.80	1.1398	0.0031950
81	3.788	1.263	0.0004665	0.0018794	9.72	29.52	2.5406	0.0010323
82	2.788	0.929	0.0006399	0.0041104	13.72	40.62	1.8465	0.0022154
83	1.847	0.616	0.0009122	0.0081022	20.57	61.17	1.2260	0.0043809
84	1.458	0.491	0.0011858	0.0125218	26.54	77.84	0.9609	0.0066991
85	3.275	1.092	0.0002594	0.0010411	12.95	35.85	2.0922	0.0005316
86	2.066	0.689	0.0004195	0.0045379	16.46	52.76	1.4216	0.0025898
87	1.740	0.580	0.0004882	0.0068866	21.26	64.36	1.1654	0.0037742
88	1.484	0.500	0.0005785	0.0094614	24.94	75.34	0.9928	0.0051764
89	1.908	1.908	0.0020195	0.0034857	8.89	35.09	1.4250	0.0022491
90	1.535	1.505	0.0023683	0.0073780	14.09	46.99	1.0746	0.0043217
91	1.082	1.073	0.0034552	0.0241528	22.15	68.55	0.7323	0.0134508
92	1.031	1.031	0.0034333	0.0315090	29.72	78.22	0.6392	0.0153844
93	2.370	2.370	0.0004877	0.0009375	5.56	26.66	1.8757	0.0006602
94	1.786	1.786	0.0006472	0.0047565	9.79	37.79	1.3233	0.0030341
95	1.381	1.381	0.0008368	0.0124372	16.36	52.56	0.9514	0.0071096
96	0.984	0.992	0.0011696	0.0267882	23.35	73.95	0.6734	0.0151623
97	2.326	2.326	0.0002310	0.0006583	5.73	27.23	1.8363	0.0004619
98	1.582	1.582	0.0003374	0.0058145	12.37	43.97	1.1370	0.0035419
99	0.977	0.977	0.0005685	0.0219534	23.55	74.75	0.6689	0.0124451
100	0.838	0.845	0.0006595	0.0306064	25.86	85.26	0.5841	0.0177971
101	1.445	4.335	0.0012665	0.0020626	2.64	19.94	1.2535	0.0016662
102	0.926	2.778	0.0019113	0.0120469	6.42	33.42	0.7480	0.0087469
103	0.598	1.701	0.0031313	0.0289692	16.90	60.40	0.4304	0.0177049
104	0.467	1.402	0.0037872	0.0394547	25.22	78.72	0.3176	0.0221063
105	1.497	4.491	0.0003860	0.0025150	2.34	19.04	1.3131	0.0020660
106	0.926	2.778	0.0006124	0.0133926	6.11	33.11	0.7550	0.0098602
107	0.598	1.841	0.0009568	0.0274823	14.01	55.01	0.4453	0.0176818
108	0.471	1.412	0.0012274	0.0367754	23.65	76.75	0.3257	0.0211630
109	0.859	2.577	0.0003296	0.0112298	7.02	36.12	0.6921	0.0081201
110	0.585	1.756	0.0004836	0.0244716	15.12	57.82	0.4324	0.0155313
111	0.491	1.513	0.0005540	0.0303785	20.51	70.41	0.3479	0.0181234

APPENDIX D

DIAGRAMS FOR PREDICTING DEPTH AT BREAKING

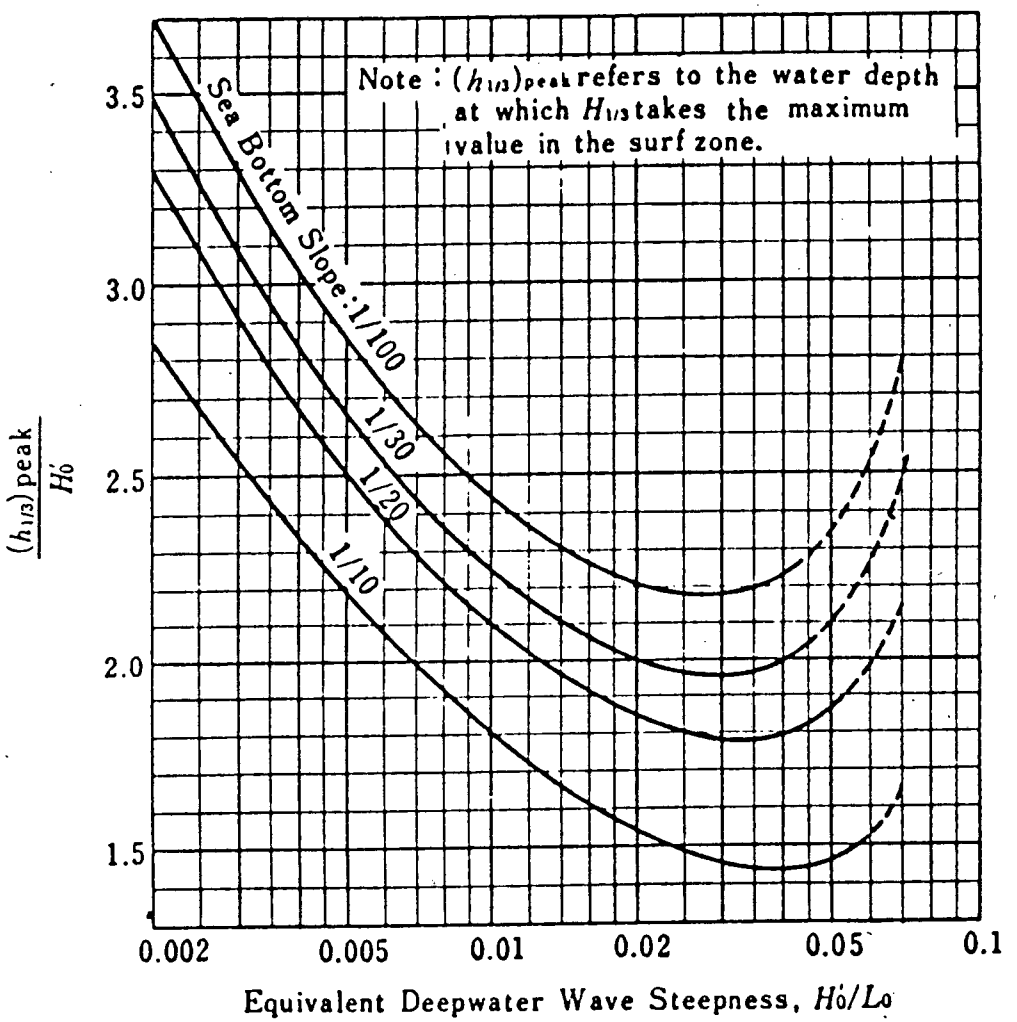

Diagram given by Goda [2].

Note : Goda uses the parameter $(h_{1/3})_{peak}$ to estimate the breaker depth d_b for irregular waves.

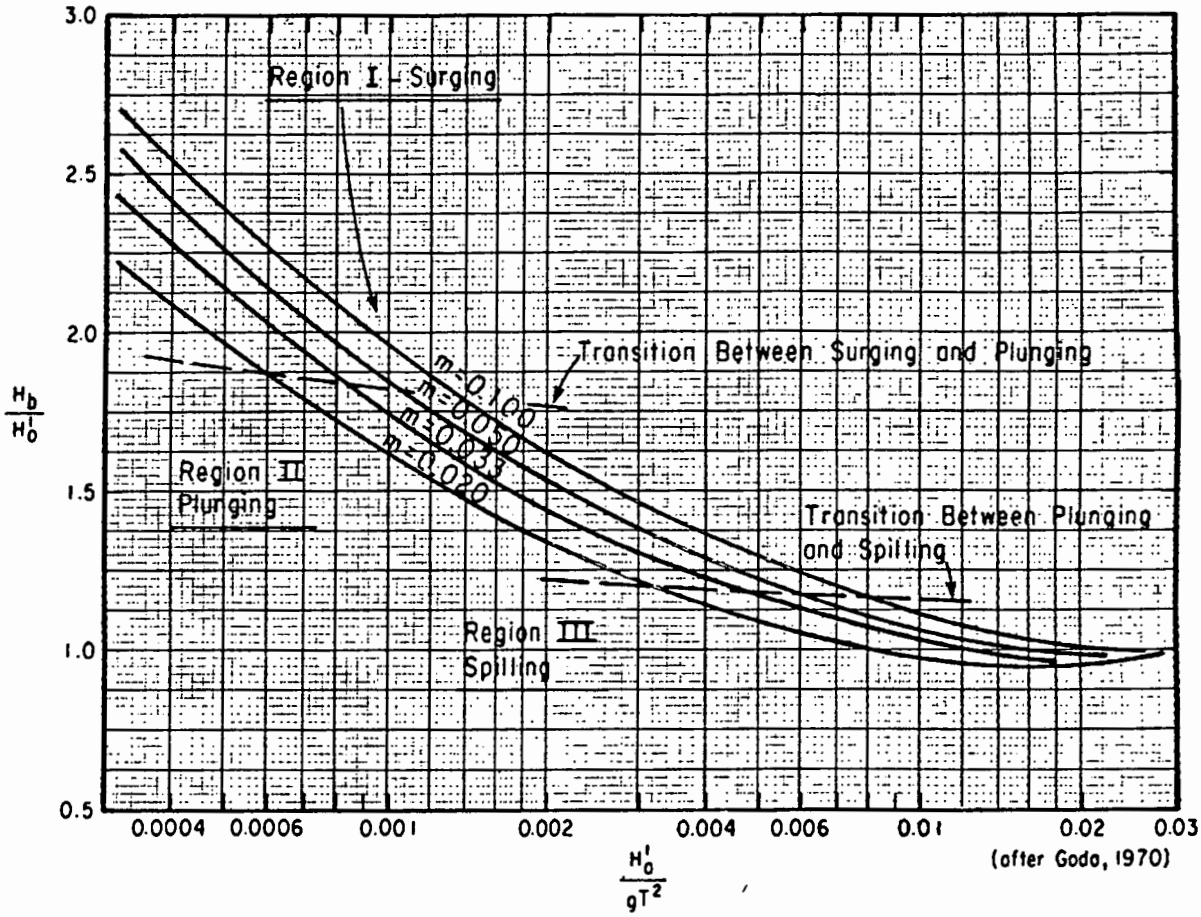

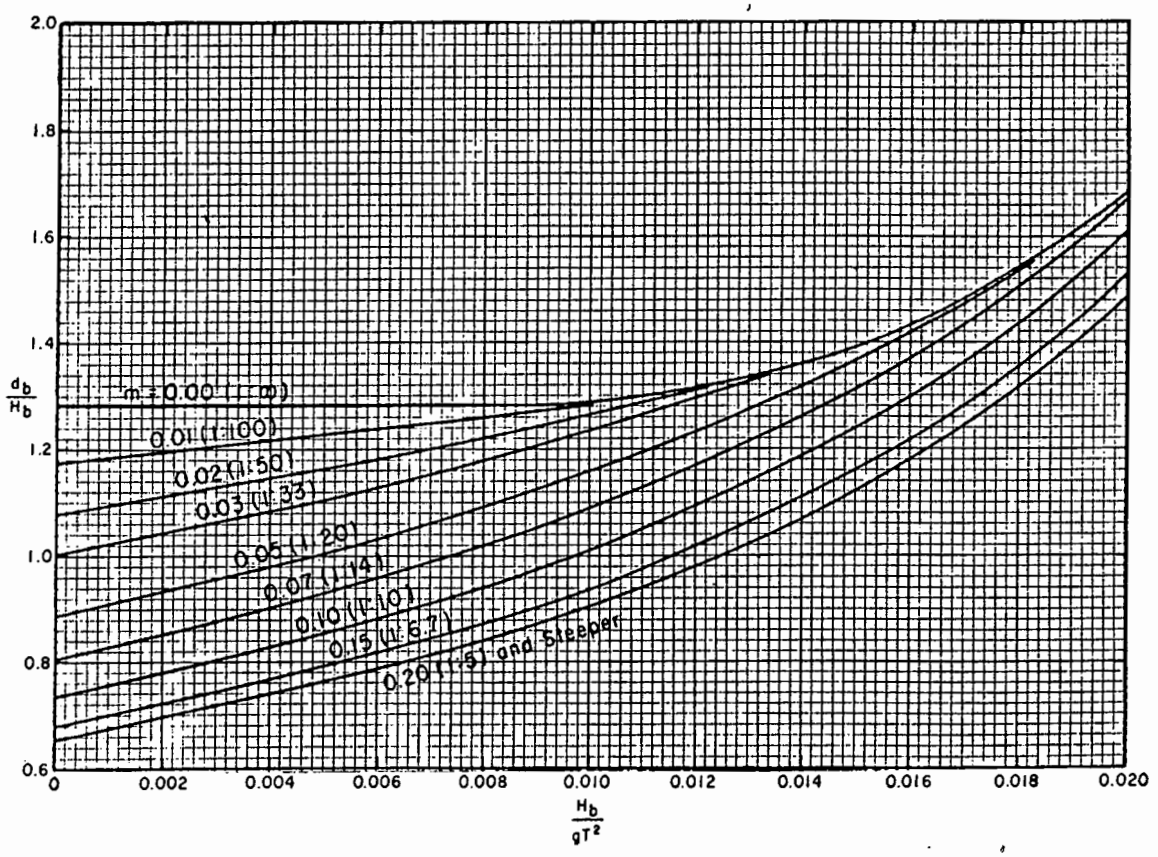

Diagrams given by the Shore Protection Manual [1].

Note : The upper diagram is entered to obtain the breaker height H_b which is then used in the lower diagram to obtain the breaker depth d_b.

APPENDIX E

EXAMINATIONS WRITTEN BY THE AUTHOR TO COMPLETE THE REQUIREMENTS OF THE DEGREE

Examination		Credit Rating
CIV 518S	Pumps	5
CIV 519F	Advanced Hydraulic Structures (The examination for this course takes the form of three projects)	5
CAM 502Z	An Introduction into Finite Elements	3
CAM 503Z	Finite Element Analysis	4
CAM 504Z	Engineering Software Design and Development	3
Thesis :	"Overtopping of Coastal Structures caused by Irregular Waves"	20
	TOTAL	40
Credits required for degree		40

UNIVERISITY OF CAPE TOWN

DEPARTMENT OF CIVIL ENGINEERING

UNIVERSITY EXAMINATION NOVEMBER 1990

CIV 518S : PUMPS

Time allowed : 3½ hours All questions may be attempted

1. A centrifugal pump produced the following performance data when running at 1 500 rev/min on a test run.

Flow (m^3/s)	0,075	0,150	0,200	0,250	0,300
Total head (m)	70	68	64	58	49
Input power (kW)	97	127	147	163	170

The pump is required to deliver water from a sump to a reservoir whose level is 60 m above that of the sump. Suction and delivery pipes of 300 mm diameter will have a combined length of 120 m (f = 0,006), 12 m of which is on the suction side, and the pump inlet is 3 m above the water level in the supply sump. What will be the efficiency and the discharge of the pump at the duty point? What would be the most economical speed to operate the pump and what suction head would occur at the pump inlet under these optimum speed conditions?

2. A centrifugal pump with an impeller of 300 mm diameter delivers 10 m^3/min of fresh water against a head of 20 m. What would be an ideal speed at which to operate the pump for a shape number of S_N = 1,5. The overall efficiency at the BEP is 80%.

   (a) If the head is doubled to 40 m, what rotational speed would be required and what would be the flow and power requirement?

   (b) If the density of fluid is increased by 20%, what would be the percentage head, flow and power increase?

   (c) If a dimensionally similar prototype pump is constructed 20% greater than the original, what percentage head, flow and power increase may be expected?

   (d) If the impeller is skimmed by 20%, what is the head, flow and power decrease expected at the same speed?

3. (a) Explain how filling a pipeline can cause cavitation in a pumping system which does not cavitate when the pipeline is running full.

(b) The graphs on page 3 are for a 150-315 pump with an impeller width of 33 mm operating at 1 450 rev/min. An impeller diameter has to be selected between 270 and 319 mm.

The total static head is 20 m and the pipeline details are given below :

Delivery pipe diameter	=	150 mm
Delivery pipe length	=	28,5 m
Suction pipe diameter	=	300 mm
Suction pipe length	=	60 m
Friction factor (f)	=	0,00ø5

Determine the duty point (flow and head).

(c) Which impeller diameter is used for this duty?

(d) What is the overall efficiency?

(e) What is the maximum static suction lift to avoid cavitation if the water temperature is 30°C? At this temperature the vapour pressure head is 0,43 m and the atmospheric pressure head is 10,2 m.

(f) If the static suction lift is fixed in section (e) and the pump is started up so that the delivery pipe is replaced by a very short pipe discharging directly into the delivery tank (so that the friction in the delivery pipe is assumed to be zero but the total static head remains at 20 m) show that the pump cavitates.

(g) Determine the maximum static lift to avoid cavitation when the delivery pipe is empty. What is the flow and total head in this case?

(h) Determine the shape number for the pump when operating at the duty point in (b) above. Comment on this shape number.

(i) By using curves such as Figures 17 and 18 in Chapter 11 on "Cavitation and NPSH" determine two values for $(NPSH)_R$ and compare them with the value used in Section (e) at the duty point in Section (b).

(j) When operating at the duty point in (b), determine the vane outlet angle if 15% of the outlet area of the impeller is lost due to blade blockage.

4. A solids-handling pump operates at a head of H = 30 m and a flow of Q = 0,7 m^3/s when pumping water.

Determine the effective pressure differential across the pump and power required at 80% efficiency when pumping :

(a) a homogeneous slurry of relative density 2,65 with a volumetric concentration of 14,5%

(b) a heterogeneous slurry consisting of an average of 1 mm diameter sand particles of relative density 2,65 at a weight concentration of 25%

(c) a viscous slurry with a kinematic viscosity of 500 centistokes and a relative density of 1,1.

(d) Comment on the power input in the above three cases.

UNIVERSITY OF CAPE TOWN

FRD/UCT CENTRE FOR RESEARCH IN
COMPUTATIONAL AND APPLIED MECHANICS

UNIVERSITY EXAMINATION : 28 MAY 1990

CAM 502Z : AN INTRODUCTION INTO FINITE ELEMENTS

PAPER 1

ANSWER ALL QUESTIONS

Time : $1\frac{1}{2}$ Hours

TOTAL 40 MARKS

CAM 502Z - AN INTRODUCTION INTO FINITE ELEMENTS : Paper 1

Question 1

A one dimensional infinite element is shown in Figure 1 with node 3 at infinity. Using the auxiliary 'pole' node 0 ($x = x_0$) the geometric mapping of this element is obtained by mapping the standard one dimensional parent element according to

$$x = \hat{N}_0(\xi)x_0 + \hat{N}_2(\xi)x_2$$

where

$$\hat{N}_0(\xi) = -\frac{\xi}{1-\xi}$$
$$\hat{N}_2(\xi) = 1 + \frac{\xi}{1-\xi}$$

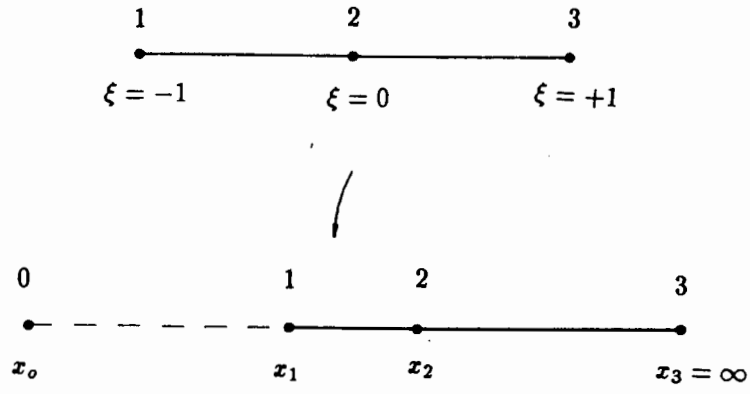

Figure 1 : One dimensional isoparametric infinite element mapping

a) Verify the ξ to x mapping given above.

b) For what position of node 1 relative to nodes 0 and 2 does the mapping hold?

c) Rewrite the mapping in terms of x_1 and x_2, ie. find N_1 and N_2 in

$$x = N_1(\xi)x_1 + N_2(\xi)x_2$$

d) Verify that this new mapping retains the characteristics of the initial mapping.

[15 marks]

CAM 502Z - AN INTRODUCTION INTO FINITE ELEMENTS : Paper 1

Question 2

Briefly discuss the problems with each of the following finite element meshes. Sketch any suggested improvements or corrections.

a) Square plate with central hole subjected to biaxial tension

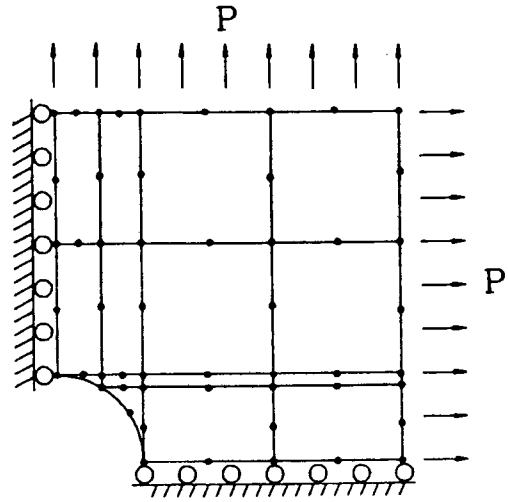

(Displacements and stresses required)

b) Thick cylinder with internal pressure

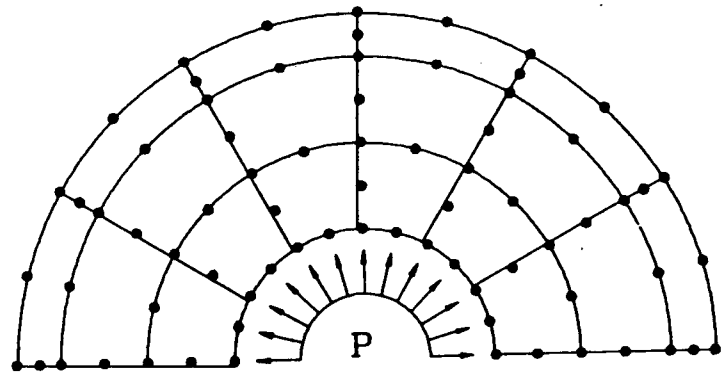

(Displacements and stresses required)

Question 2 cont.

c) Arbitrary component (plane stress)

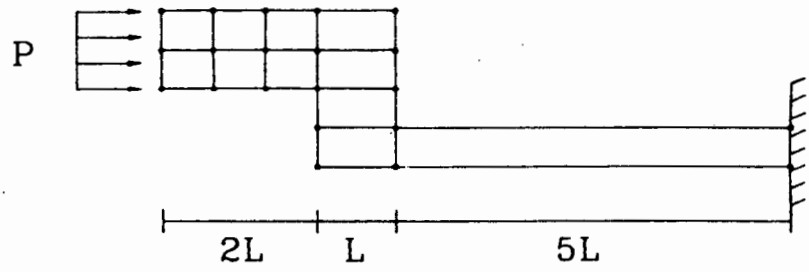

(Displacements required)

d) Transition Section

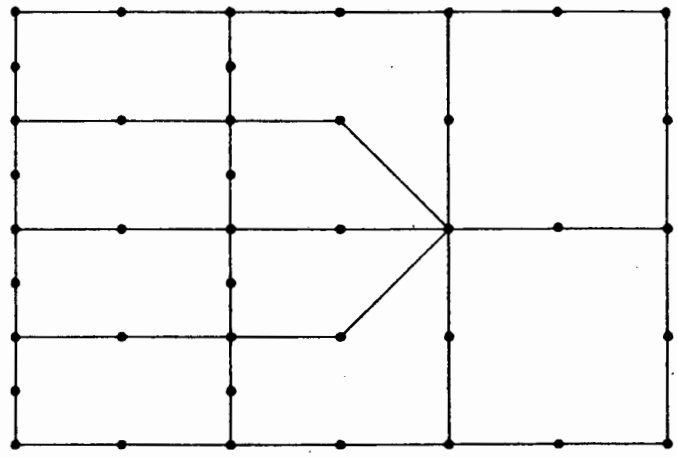

(Use similar elements)

[8 marks]

CAM 502Z - AN INTRODUCTION INTO FINITE ELEMENTS : Paper 1

Question 3

A 3-node axial bar, length L, is subjected to a linearly distributed axial load p of the form

$$p = p_1 + (p_3 - p_1)\frac{x}{L}$$

where p_1 and p_3 are the values of the load at the two ends as shown below.

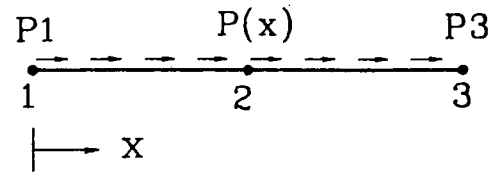

Calculate the load vector for this element.

[10 marks]

CAM 502Z - AN INTRODUCTION INTO FINITE ELEMENTS : Paper 1

Question 4

Show how symmetric (and/or antisymmetric) loading and boundary conditions can be used so that only part of each structure need be modelled. Sketch the proposed idealisation illustrating the boundary conditions clearly.

a) Built in beam

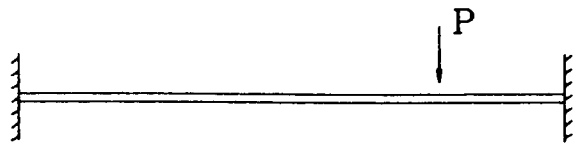

b) Deep cantilever

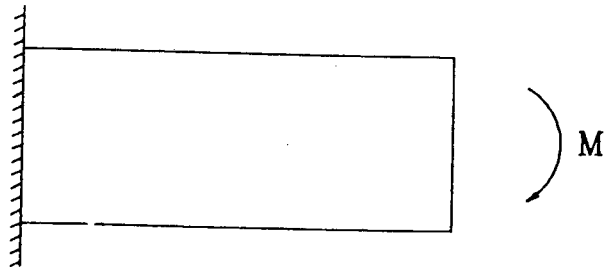

c) Rectangular plate with central line load p

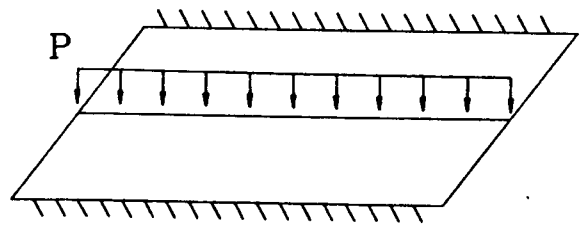

[7 marks]

UNIVERSITY OF CAPE TOWN

FRD/UCT CENTRE FOR RESEARCH IN
COMPUTATIONAL AND APPLIED MECHANICS

UNIVERSITY EXAMINATION : 28 MAY 1990

CAM 502Z : AN INTRODUCTION INTO FINITE ELEMENTS

PAPER 2

ANSWER ALL QUESTIONS

HAND IN : 17h00, 1 JUNE 1990

TOTAL 60 MARKS

CAM 502Z - AN INTRODUCTION INTO FINITE ELEMENTS : Paper 2

Question 1

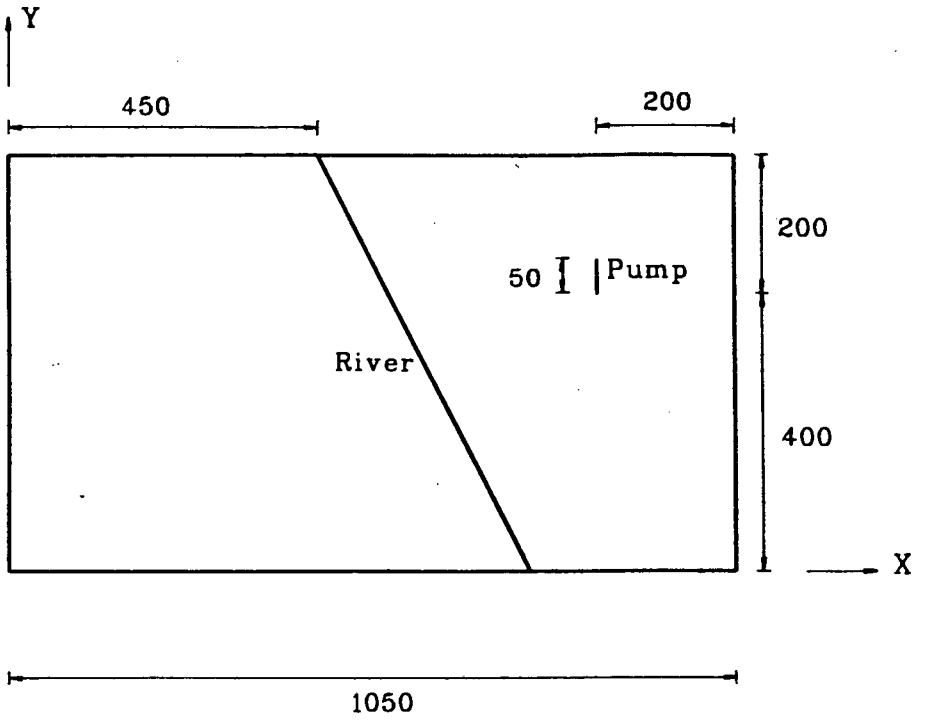

A rectangular aquifer 1050m X 600m is shown above. The top, bottom and left hand side boundaries are impermeable. The right hand side has a constant piezometric head ϕ of 100m. A river passes through the aquifer infiltrating at a rate of 0.5 m^3/day per metre length. A pump, configured as shown, pumps at a rate of 200 m^3/day.

Solve the ground water flow problem, using μField , and determine the piezometric head at the pump. Take permeability $k = 0.864m^3$/day. Include in your results a plot showing the equipotential lines for the aquifer.

Note :

Darcy's Law for flow rate :

$$q = +k\phi'$$

with

q - flow rate (flux)
k - permeability (material modulus)
ϕ - piezometric head (state variable)

Governing equations

$$k\frac{\partial^2\phi}{\partial x^2} + k\frac{\partial^2\phi}{\partial y^2} + Q = 0$$

with Q - flow

CAM 502Z - AN INTRODUCTION INTO FINITE ELEMENTS : Paper 2

Question 2

A two stage project is planned for a hillside with slope 20°. The first part involves the construction of a road and retaining wall. Further development requires a deep excavation close to the road with a sheet pile wall used to protect the excavation. The final configuration is shown below.

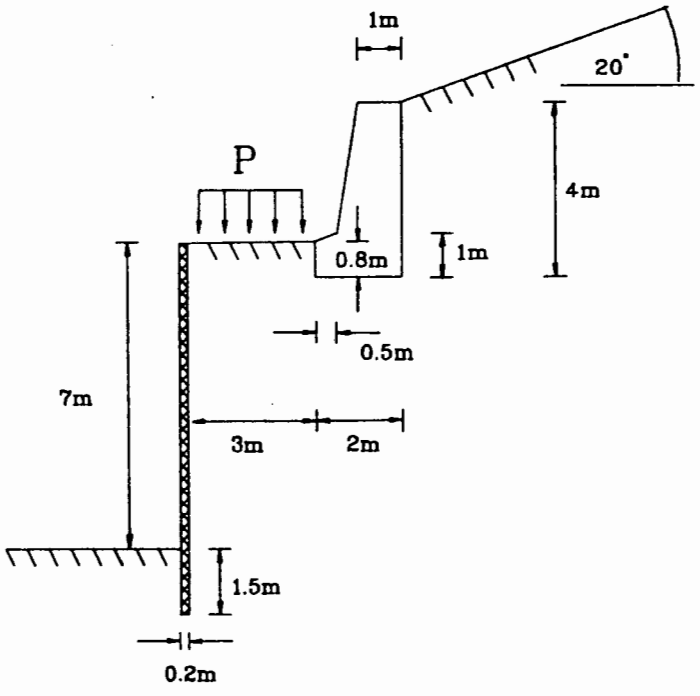

a) Determine the displaced shape which results from excavating for the first stage, i.e. a wedge of material up to road level plus material for the retaining wall.

b) Model the retaining wall and apply the given road pressure p. Produce contour plots of the cartesian stress components and Von Mises equivalent stress.

c) Model the final stage as shown in the diagram. Perform a fe analysis and plot the deformation and stress distribution of the system. Determine the maximum horizontal displacement of the sheet pile wall and estimate the force required (applied at node closest to maximum displacement) to halve the obtained displacement.

Assume only elastic deformations and complete coupling between materials.

CAM 502Z - AN INTRODUCTION INTO FINITE ELEMENTS : Paper 2

Material properties

Soil :	E	$= 0.112$ GPa
	ν	$= 0.36$
	ρ	$= 1936$ kg/m^3
Concrete :	E	$= 20$ GPa
	ν	$= 0.2$
	ρ	$= 2446$ kg/m^3
Sheet Metal :	E	$= 200$ GPa
	ν	$= 0.3$
	ρ	$= 7500$ kg/m^3
Loading :	p	$= 10$ kN.m^{-2}

UNIVERSITY OF CAPE TOWN

FRD/UCT Centre for Research in Computational and Applied Mechanics

UNIVERSITY EXAMINATION

CAM503Z Finite Element Analysis : 1990

Closed Book

Date: 2nd November 1990

Note: Answer all questions.

MAXIMUM: 100 MARKS

Question 1 [10 marks]

Derive the Lagrange interpolation functions for nodes 1 and 3 of the one dimensional cubic element depicted in Figure 1 below. Use the natural coordinate system, ξ.

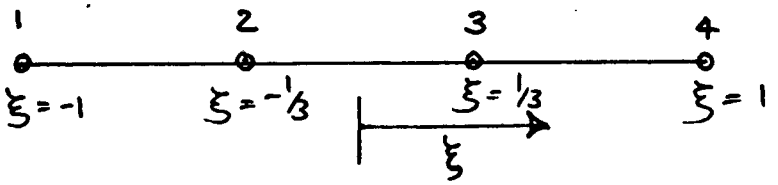

Figure 1

Using these one dimensional shape functions, determine expressions for the two dimensional interpolation functions at the *two* nodes A and B indicated in Figure 2.

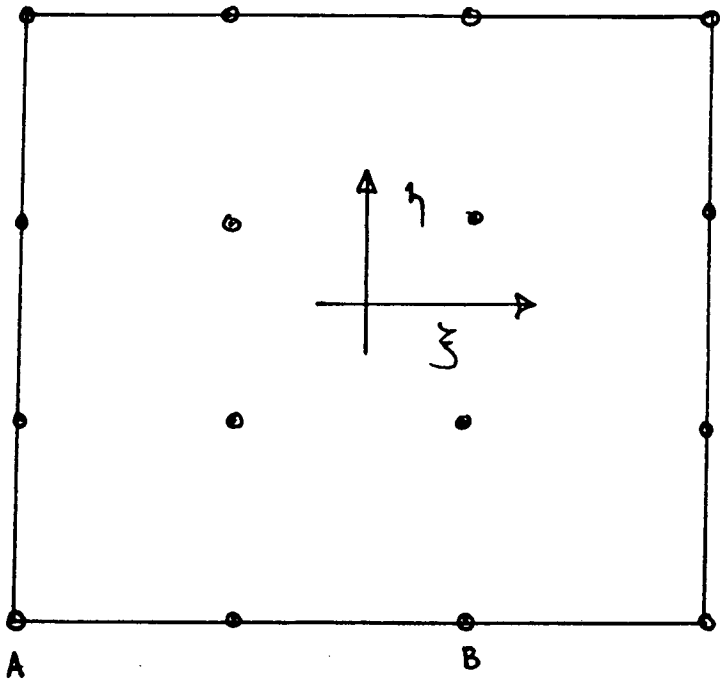

Figure 2

Question 2 [25 marks]

Cubic Hermitian interpolation functions for $C_1(\Omega)$ finite elements are given by:

$$N_1 = \frac{1}{4}(2 - 3\xi + \xi^3)$$

$$\overline{N_1} = \frac{1}{4}(1 - \xi - \xi^2 + \xi^3)$$

$$N_2 = \frac{1}{4}(2 + 3\xi - \xi^3)$$

$$\overline{N_2} = \frac{1}{4}(-1 - \xi + \xi^2 + \xi^3)$$

Show how these are derived by considering the displacement function for an Euler-Bernoulli beam element:

$$w(\xi) = w_1 N_1(\xi) + \theta_1 \overline{N_1}(\xi) + w_2 N_2(\xi) + \theta_2 \overline{N_2}(\xi)$$

where

$$\theta_1 = \frac{dw_1}{dx}$$

and

$$\theta_2 = \frac{dw_2}{dx}$$

Question 3 [15 marks]

The behaviour of a simple (Euler Bernoulli) beam is described by the following 4th order differential equation:

$$\frac{d^2}{dx^2}(EI\frac{d^2w}{dx^2}) + f = 0$$

for $0 < x < L$, subject to the boundary conditions:

$$w(0) = 0$$

$$\frac{dw(0)}{dx} = 0$$

$$EI\frac{d^2w(L)}{dx^2} = M_L$$

$$-\frac{d}{dx}(EI\frac{d^2w(L)}{dx^2}) = S_L$$

(a) Classify the four boundary conditions, i.e are they essential (Dirichlet) or natural (Neumann) BC's.

(b) Determine the weak form of this equation in general terms, i.e do not use approximations for any of the terms.

(c) What are the benefits of expressing the differential equation in its weak form?

Question 4 [25 marks]

NB. Answer either Part A or Part B of this question

Part A

Starting from the potential energy functional,

$$\Pi = \frac{1}{2}\int_\Omega \sigma_{ij}\varepsilon_{ij}d\Omega - \int_\Omega u_i f_i d\Omega - \oint_\Gamma u_i t_i d\Gamma$$

where

$$\begin{aligned}\sigma_{ij} &= D_{ijkl}\varepsilon_{kl} \\ \varepsilon_{ij} &= \frac{1}{2}(\frac{\partial u_i}{\partial x_j} + \frac{\partial u_j}{\partial x_i})\end{aligned}$$

derive the stiffness matrix and load vector for a plane problem. Write out the full strain-displacement matrix for a 4-noded quadrilateral (Note that it is not necessary here to use the full expression for the shape functions, and N_1, etc will suffice).

Part B

The governing differential equation for an aquifer with flow in the xy plane is given by

$$-(a_{11}\frac{\partial^2\phi}{\partial x^2} + a_{22}\frac{\partial^2\phi}{\partial y^2}) + f = 0$$

on the domain Ω. The *natural* boundary condition is given by

$$a_{11}\frac{\partial\phi}{\partial x}n_x + a_{22}\frac{\partial\phi}{\partial y}n_y = \phi_n$$

on part of the boundary Γ_1 and the *essential* boundary condition is

$$\phi = \phi_0$$

the remainder of the boundary Γ_2.

Derive the weak form of this equation and hence give expressions for the "stiffness" matrix and "load" vector for a single generic element.

Question 5 [12 marks]

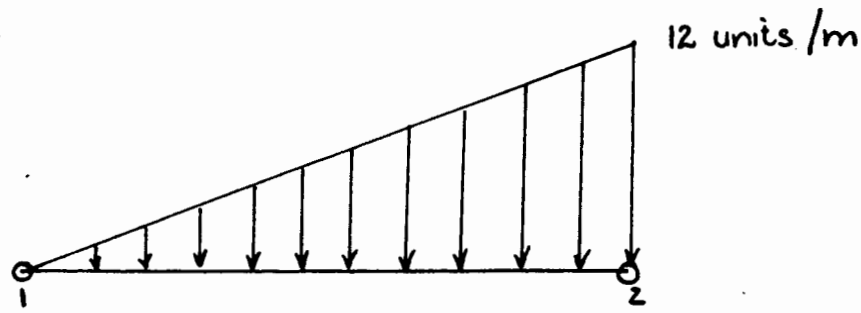

Figure 3

Using typical finite element calculations with Gaussian quadrature and linear interpolation functions to approximate both the spatial variable and the applied load, show that the equivalent nodal loads for the above element are respectively $P_1 = 2$ unit and $P_2 = 4$ units.

$$N_1 = \frac{1}{2}(1 - \xi)$$

$$N_2 = \frac{1}{2}(1 + \xi)$$

ABSCISSAE AND WEIGHT COEFFICIENTS OF THE GAUSSIAN QUADRATURE FORMULA

$$\int_{-1}^{1} f(x)\,dx = \sum_{j=1}^{n} H_i f(a_j).$$

$\pm a$	H
$n = 1$	
0	2·00000 00000 00000
$n = 2$	
0·57735 02691 89626	1·00000 00000 00000
$n = 3$	
0·77459 66692 41483	0·55555 55555 55556
0·00000 00000 00000	0·88888 88888 88889
$n = 4$	
0·86113 63115 94053	0·34785 48451 37454
0·33998 10435 84856	0·65214 51548 62546

Question 6 [10 marks]

a) List three sources of nonlinearities in solid mechanics problems.

b) Write brief notes (maximum of 200 words) on two solution techniques that could be applied to the general nonlinear equation $H(\phi)\phi + f = 0$.

Question 7 [10 marks]

Assuming that you have a solution for the matrix differential equation

$$[A]\{\frac{du}{dt}\} + [B]\{u\} = \{P\}$$

at time $t = t_{n-1}$, determine the solution for $\{u\}_n$ at the end of a generic step Δt_n. Use the θ *family of approximation* i.e

$$\theta\{\dot{u}\}_n + (1-\theta)\{\dot{u}\}_{n-1} = \frac{\{u\}_n - \{u\}_{n-1}}{\Delta t_n}$$

for $0 \leq \theta \leq 1$ and $\dot{u} = \frac{du}{dt}$. *Briefly* comment on the choice of θ.

University of Cape Town

Center for Research in Computational and Applied Mechanics

University Examination: 15-June-1990

END524Z Engineering Software Design and Development

Time: Part A: 1 1/2 hours, Part B: 1 1/2 hours, Total: 3 hours

Open Book

Answer All Questions

Total: 200 marks

Internal Examiner: Mr J Vos
External Examiner: Prof GL Murray

Part A: Theoretical

1. Using DOS

(a) The file CONFIG.SYS contains the following statements:

```
BREAK=ON
BUFFERS=20
FILES=30
DEVICE=C:\DOS\ANSI.SYS
SHELL=C:\DOS\COMMAND.COM /E:1024 /P
```

Discuss the purpose of each of these statements. (5)

(b) Assume that you have to set up a batch file FEAP.BAT in the directory \BAT that can execute the pre-processor program PRE.EXE and analysis program MAIN.EXE in tandem (both these programs reside in the directory \FEAP. The program PRE reads the input data from a file connected to unit 11 and creates a list file on unit 12, assuming both these files to be in the current directory. The program PRE also creates a temporary work file called FEAP.TMP in this directory in which all the data are stored for the analysis program MAIN, which should delete it upon termination. The program MAIN appends its results to the file connected to unit 12. In case of errors during the input phase, PRE sets the environment variable ERRORLEVEL to 1, to indicate that MAIN should not be executed. Assume the input data for the analysis resides in a file DAM1.DAT in directory \PROJ278 and that the results are to be stored in a file called DAM1.LST. Invoke the batch file as follows: (15)

```
> FEAP DAM1
```

[20]

2. Modularity and Information Hiding

An interactive finite element preprocessor program needs to store the information about all nodal points in the finite element mesh of a model. Assume the following information are associated with each nodal point:

```
node id, X-coordinate, Y-coordinate, Z-coordiate
```

The node id for each node is a positive integer value and must be unique, but need not be in sequence. Thus the first three nodes in a mesh could have identifiers 10, 21, and 47. The X,Y,Z-coordinates are real values associated with the node.

Also assume that the total number of nodes is small enough so that they may all be stored in a table in memory rather than on a disk file. The following operations need to be performed on this table:

(a) Store new nodal point values in the table.

(b) Modify the coordinates of an existing node.

(c) Retrieve the coodinates of a given node.

(d) Delete a given node.

It is important that the table be organized in such a way to facilitate the fast retrieval of coordinates for a given node, as this operation will be performed many times over.

Design a module which implements the conceptual model of the nodal point table described above, and its associated operations. Discuss the following aspects of this module:

(a) The data structure for storing the nodal points in and the way it is organized.

(b) The algorithms for storing and retrieving nodal point coordinates.

(c) Error conditions that may occur for each operation and how they may be handled.

(d) The names of the routines that implement these operations and their respective interfaces (arguments).

[40]

3. Decision Matrix Logic

A measuring device which is connected to a computer can transmit readings whenever it is requested to do so. Each reading consists of the current time and a value that is returned to the computer in the following ASCII character format:

Th(h):mmVnnX

where (hh,mm) is the current time in hours and minutes and (vv) is an integer in the range [0,99] that represents the current reading. Thus, a typical sequence of strings from the device would be as follows:

```
T9:23V17X  T10:6V5X  T10:56V88X ...
```

Set up a decision table to parse a given string in order to extract the time and value from it. Describe each of the basic actions to be performed, but do not code them. [20]

Subtotal = [100]

Part B: Practical

1. **Functions in C**

   The file XSORT.C provides the main function of a program that sorts an array of real values using a simple exchange sort. Develop the function *ExchangeSort* that can sort the *actual* values in the given array. [30]

2. **File I/O in C**

   The file FXSORT.C provides the main function of a program that reads the values from any specified file and sorts them. Develop the function *ReadData* that prompts the user for a given text file which contains the values. The values are stored one per record, with the first record containing the number of values to read. See the file FXSORT.DAT for an example of such a file. The function should first read the number of values and then load each of the values into the given array. The function should return the number of values as its result. [40]

3. **DOS Interrupts in C**

   Study the DOS interrupt mechanism in the file GETTIME.C and write a program that uses this function to display the current time in the middle of the screen. Extend the program to also display the current date by writing a similar function. [30] [30]

Subtotal = [100]

Overall Total = [200]